Università degli Studi di Bologna

Facoltà di Scienze Fisiche, Matematiche e Naturali
Dipartimento di Fisica

Dottorato di Ricerca in Geofisica

XVII Ciclo

Stochastical and Mathematical Modeling of Long-term Interaction among Earthquakes and between Earthquakes and Volcanic Eruptions

Candidato:
Dott.
Jacopo Selva

Tutore:
Dott.
Warner Marzocchi

Referente:
Prof.
Paolo Gasperini

Coordinatore:
Prof.
Maurizio Bonafede

Bologna, Marzo 2005

Contents

Chapter 1

Summary

1.1 Introduction

In seismology, the ability of an earthquake to promote other seismic events has been widely accepted for many years. For instance, the term aftershock implies a strong link of such a seismic event with the occurrence of a main shock. A major question, presently a matter of debate, concerns the spatiotemporal scale of the coupling among seismic events [*Kerr*, 1998].

For small spatiotemporal window, interactions have been modeled as the effect of the stress field due to the mainshocks, which perturb the neighbor faults, and induce an higher number of events where the stress is increased, and a lack of events where is decreased [eg., *King and Cocco*, 2000]. Such a scheme has been applied with good results at many real sequences of earthquakes [e.g., *Reasemberg and Simpson*, 1992; *King et al.*, 1994; *Stein et al.*, 1994; *Hardebeck et al.*, 1998], and at real fault systems [e.g., *Nostro et al.*, 1997; *Stein et al.*, 1997; *Harris*, 1998].

Lately, many authors find, or suggest, that such a coupling may involve spatiotemporal distances much larger than previously suspected to be necessary to trigger earthquakes [e.g.,

Romanowicz, 1993; *Hill et al.*, 1993; *Marzocchi et al.*, 1993; *Marzocchi and Mulargia*, 1995; *Pollitz and Sacks*, 1997; *Rydelek and Sacks*, 1999; *Casarotti et al.*, 2001]. Comparable spatiotemporal scales have also been found in the interaction among large earthquakes and volcanic eruptions [e.g., *Linde and Sacks*, 1998; *Marzocchi*, 2002; *Marzocchi et al.*, 2002]. It has been argued that part of such long-term interactions may be explained by the postseismic stress diffusion due to the relaxation of the upper mantle, and/or the lower crust [*Pollitz*, 1992; *Piersanti et al.*, 1995, 1997; *Pollitz et al.*, 1998; *Freed and Lin*, 2001; *Marzocchi et al.*, 2002].

The relative importance of the effect of postseismic relaxation compared to the coseismic effect grows with distance [Pollitz, 1992; Piersanti et al., 1995, 1997]. Coseismic effects are prominent at small distances from the source (the classical aftershock sequences), while delayed effects due to the asthenosphere and/or lower crust relaxation are relatively more important at larger distances.

At the same time, many researchers remain very skeptical regarding long-term coupling between earthquakes. Part of the skepticism about long-term interaction is due to lack of convincing phenomenological evidence. The still growing body of evidence of long-term triggering effects reported in the scientific literature relate only to single local cases [*Pollitz and Sacks*, 1997; *Chéry et al.*, 2001; *Freed and Lin*, 2001]. A formal statistical calculation performed on a representative sample of worldwide earthquakes is still lacking. Another the main objection is that postseismic effects lead to small stress variations, in absolute and relative sense.

As regards the 'small' value in a relative sense, postseismic stress variations are small relative to the other stress fields which act on the seismogenetic faults. In this sense, we argue

that it may be misleading to compare perturbations with the absolute values of other natural fields. It is certainly more useful to compare the amplitude of stress variations with other processes that can perturb the system over a comparable time interval. For instance, it has been proposed that perturbations as large as tenth of bars may reasonably promote earthquakes [e.g., *Reasember and Simpson*, 1992], also at depth where the lithostatic pressure is up to 4 orders of magnitude greater than such a proposed threshold. But the natural fluctuations of the lithostatic pressure are meant to be very small, then much smaller than stress perturbations. Under this perspective, it is remarkable to note the stability of the tectonic loading measured over time intervals of 5 order of magnitude different [tens of years *Sella et al.*, 2002, and millions of years *DeMets et al.*, 1994]. This may be an important evidence of the extreme stability of the tectonic loading; in this case, the tectonic rate has very low natural fluctuations (at least over time intervals of decades) and therefore it may be significantly perturbed also by apparently small postseimsic stress fields.

A discussion about the "small" value in an absolute sense implicitly assumes the existence of a stress threshold needed to trigger an earthquake, whose even the existance requires further validation [e.g., *Rydelek and Sacks*, 1999, *Ziv and Rubin*, 2000]. Others have considered earthquake nucleation to be part of a critical system and thus highly sensitive to very small perturbations [e.g., *Turcotte*, 1997].

In our opinion, part of the problem is the concept of 'triggering', which we consider somewhat misleading. It implies a deterministic relationship between source and triggered event, and therefore can be used, in the most optimistic cases, only retrospectively. We believe that a more appropri-

ate term is "promoting", because it implies a more suitable probabilistic coupling. In forward analysis, in fact, the only relevant aspect of the coupling is to quantify the change in probability of occurrence of an earthquake due to the stress variation induced by a remote seismic event [e.g., *Stein*, 1999; *Parson et al.*, 2000]. From this perspective, the concept of stress threshold would lose any physical meaning. Therefore, it may be more realistic to study seismic rate changes, more than triggered events.

The relationship between seismic rate changes and stress perturbations is still an open issue in seismology. Mainly the problem is that it depends on both i) the perturbation field, and ii) the seismogenetic process of faults, which react to perturbations. In this issue, a possible solution has been proposed with rate-and-state fault models perturbed by external stress fields [*Dieterich*, 1994], and applied to real cases [*Toda et al.*, 1998; *Stein*, 1999], but it still depends on the reliability of such seismogenetic model.

Another open issue in interactions studies is the identification of the main stress field responsible for interactions, i.e., the absolute value of stress, or its temporal derivate. The choice is strongly related to the seismogenetic process of faults. For instance, the Coulomb Failure Function criterion is sensible to variations on the absolute value of stress [e.g., *Reasember and Simpson*, 1992; *King et al.*, 1994; *Stein et al.*, 1994], while rate-and-state criterion is sensible also to variations on stress rates [e.g., *Dieterich*, 1979; *Ruina*, 1983; *Okubo*, 1989; *Marone*, 1998]. This point is particularly crucial for long-term interactions studies, where big spatiotemporal windows are involved; in fact, variations in absolute value and rate of stress are equivalent in small spatiotemporal windows [see chapter 5]. An important point is that,

since there is not a widely accepted failure criterion for earthquakes, it might be better to relate interactions studies to the main field responsible for earthquakes, i.e., the tectonic stress field. Therefore, we argue that it may be more conservative to study stress rates, rather than the absolute value of stress, because of their direct relationship with tectonic stress rates.

1.2 Tasks of the work

At first, we investigate on the physical mechanisms responsible for for long-term interactions. It has been argued that postseismic relaxation field might be responsible of such long-term interactions; then, our first task is understand whether or not the postseismic stress field can produce not negligible perturbations (respect to the tectonic field) and lead to long-term variations on a seismogenetic system.

The second task of this work is to systematically investigate on the effects of long-term interactions in the seismic data. In particular, we focus our attention on the perturbation induced by the greatest earthquakes of the last century, all occurred in the period 1952-1965.

At global scale, we study the distribution of strong earthquakes ($M \geq 7.0$), and specifically we try to understand whether spatial and temporal distribution of $M \geq 7.0$ earthquakes occurred after 1965 is correlated with the perturbation due to the 5 giant earthquakes Kamchatka 1952, Aleutins 1957, Chile 1960, Alaska 1964, and Aleutins 1965.

At local scale, we aim to understand the effects of long-term interactions on moderate seismicity. In particular, we study the effects of the two strongest event of the past century (Chile 1960 and Alaska 1964) in Southern California, where is available a catalog (complete with focal parameters

estimation) for moderate seismicity ($M \geq 4.7$) since 1933.

Finally, we study the effects of long-term stress perturbations on volcanic systems. The interaction between strong tectonic earthquakes and volcanic eruptions has been found through various statistical analysis of catalogs [e.g., *Linde and Sacks*, 1998; *Marzocchi*, 2002; *Marzocchi et al.*, 2002]. Anyway, some authors remain skeptical because of the retrospective approach used in those works. Therefore, here we aim to set an objective tool to accomplish a forward test to quantitatively analyze such a long-term interaction among earthquakes and volcanoes.

1.3 Method

1.3.1 Physical field for long-term interactions

The first issue to be addressed is understand whether the postseismic stress field can be the leading mechanism for long-term interactions. In chapter 2, we set a conceptual experiment to test the significance of postseismic stress perturbations at great distances in space and time. We design a simple source-receiver scheme, where i) the receiver fault is governed by a simple seismogenetic mechanism, and ii) the far natural seismicity can interact with the receiver through the co- and post-seismic stress field. The results show that the stress perturbations induced by far seismicity on the receiver fault are not negligible at all, even as compared with the local tectonic field. Moreover, by analyzing its seismogenetic behavior, we show that the receiver is significantly influenced by strong earthquakes ($M \geq 8.0$) as far as 1000 Km. In fact, such perturbations can significantly change the rate of earthquakes for tens of years; the observed seismic

rate experiences sudden increases (effect of 'cluster') as positive interactions occur, or decreases (effect of 'gap') with negative interactions.

1.3.2 Global scale: strong earthquakes ($M \geq 7.0$) and post-seismic stress changes

The strong earthquakes ($M \geq 7.0$) release a huge amount of energy. Can small stress perturbations significantly influence such strong events? The most energetic earthquakes of last century occurred in a short time period, which spans from 1952 to 1965; these 5 events (Kamchatka 1952, Aleutins 1957, Chile 1960, Alaska 1964, and Aleutins 1965) are source of strong stress perturbations, which might have influenced the following worldwide seismicity with $M \geq 7.0$. In order to test such hypothesis, in chapter 3, we show a procedure to extend the estimation of focal parameters to all worldwide, shallow seismicity with $M \geq 7.0$ since 1900. With this database, in chapter 4 we estimate the stress perturbations induced on all the events occurred after 1965. Then, we compare such perturbations with the ones which would affect the events before 1952, which are surely not influenced by the 5 giant earthquakes. This comparison clearly show that, while the events before 1952 are, as expected, not correlated with perturbations, after 1965 the earthquakes significantly tend to occur where perturbations are positive, i.e., promote other events. In fact, only a few of them occurred where perturbations are negative, i.e., discourage other events, and most of them where they are positive. This clearly shows that the probability of occurrence of even strong earthquakes can be strongly influenced by small perturbations due to far events.

1.3.3 Local scale: long-term variations in moderate seismicity

In chapter 5, we investigate on the effects of long-term interactions on moderate seismicity. A systematic search of nonstationarities in Southern California seismicity shows that a significant change occurs during the sixties. Before 1960, most of the events are right-lateral earthquakes correlated with San Andreas fault system; afterward, the seismic rate significantly decreases, and a not negligible number of dip-slip events occurred (which are not directly linked to the San Andreas fault system). Then, we compute the perturbations induced on the Southern California seismicity by the Chile 1960 and Alaska 1964 giant earthquakes. We find that, in a first order, such perturbations completely agree with the seismicity changes observed. We finally formulate a forward test to validate the hypothesis of causal relationship between the observed nonstationarity and such perturbations.

1.3.4 Tectonic earthquakes and volcanic eruptions: a forward test to analyze interactions

In chapter 6, we set an objective and quantitative procedure to test the interaction between strong tectonic earthquakes and volcanic eruptions. This task is accomplished by forward testing the hypothesis of correlation between the stress field due to an earthquake and the spatio-temporal distribution of the eruptions which follow the earthquake. In chapter 6, we provide an exhaustive description of the rules of the forward test; we also provide two examples of real applications of the forward test: the Denali (Alaska, Nov. 2002) and the Engano (Sumatra, Jun. 2000) earthquakes.

1.4 Results

The results of this work can be summarized as follows:

- Post-seismic stress field can induce interactions at long distances; strong earthquakes ($M \geq 8.0$) can lead to long-term variations on seismogenetic systems at distances up to a thousand of Km for tens of years.
- Giant earthquakes can globally change the worldwide strong seismicity, by promoting or discouraging earthquakes with $M \geq 7.0$ for tens of years; in particular, worldwide seismicity with $M \geq 7.0$ has been significally influenced by stress perturbations due to the 5 giant earthquakes Kamchatka 1952, Aleutins 1957, Chile 1960, Alaska 1964, and Aleutins 1965.
- Giant earthquakes can significantly influence the moderate seismicity observed in a specific area, having a strong effect on seismic rates and types of earthquakes for years at great distances; in particular, Southern California seismicity has been significantly perturbed by stress perturbations due to the giant earthquakes Chile 1960 and Alaska 1964.
- Long-term interactions among earthquakes and volcanoes can be quantitatively tested by a forward test, which is the only objective tool to avoid any unconscious retrospective overfitting of data.

References

Casarotti E., A. Piersanti, F.P. Lucente, and E. Boschi, Global postseismic stress diffusion and fault interaction at long distances, *Earth and Planet. Sci. Lett. 191*, 75-84, 2001.

Chéry J., S. Carretier, and J. Ritz, Postseimsic stress transfer explains time clustering of large earthquakes in Mongolia, *Earth Planet. Sci. Lett. 194*, 277-286, 2001.

DeMets, S., Fordon, R.G., Argus, D.F., and Stein, S., Effect of recent revisions to the geomagnetic reversal time scale on estimates of current plate motions, *Geophys. Res. Let. 21*, No. 20, 2191-2194, 1994.

Dieterich, J.H., A constitutive law for the rate of earthquake production and its application to earthquakes clustering, *J. Geophys. Res., 99*, B2, 2601-2618, 1994.

Dieterich, J.H., Modeling of rock friction. 1, Experimental results and constitutive equations, *J. Geophys. Res., 84*, 2161-2168, 1979.

Freed A.M., and J. Lin, Delayed triggering of the 1999 Hector Mine earthquake by viscoelastic stress transfer, *Nature 411*, 180-183, 2001.

Hardebeck, J.L, Nazareth, J.J., and Hauksson, E., The static stress change triggering model: Constraints from two southern California aftershock sequences. *J. Geophys. Res., 103*, B10, 24,427-24,437, 1998.

Harris, R.A., Introduction to special section: stress triggers, stress shadows, and implication for seismic hazards, *J. Geophys. Res., 103*, B10, 24,347-24,358, 1998.

Hill D.P., *et al.*, Seismicity remotely triggered by the magnitude 7.3 Landers, California, earthquake, *Science 260*, 1617-1623, 1993.

Kerr, R. A., Can great quakes extend their reach?, Science, 280, 1194-1195, 1998.

King, G. C. P., and M. Cocco, Fault interaction by elastic stress changes: New clues from earthquake sequences, *Adv. Geophys. 44*, 1-38, 2000.

King, G. C. P., R. S. Stein, and J. Lin, Static stress changes and the triggering of earthquakes, *Bull. Seismol. Soc. Am., 84*, 935-953, 1994.

Linde, A.T., and I.S. Sacks. *Triggering of volcanic eruptions.* **Nature**, 395, 888-890, 1998.

Marone, C., Laboratory-derived friction laws and their application to seismic faulting. *Ann. Revs. Earth & Plan. Sci., 26*, 643-696, 1998.

Marzocchi, W., *Remote seismic influence on large explosive eruptions.* **J. Geophys. Res.**, VOL. 107, NO. B1, 10.1029/2001JB000307, 2002.

Marzocchi W., R. Scandone, and F. Mulargia, The tectonic setting of Mount Vesuvius and the correlation between its eruptions and the earthquakes of the Southern Apennines. *J. Volcan. and Geoth. Res. 58*, 27-41, 1993.

Marzocchi W., and F. Mulargia, Stress pulses in Southern Italy, *Geophys. Res. Lett. 22*, 29-32, 1995.

Marzocchi, W., E. Casarotti, and A. Piersanti. *Modeling the stress variations induced by great earthquakes on largest volcanic eruptions of the 20th century.* **J. Geophys. Res.**, 107, B11, 2320, doi:10.1029/2001JB001391, 2002.

Nostro C., Stein, R.S., Cocco, M., Belardinelli, M.E., and Marzocchi, W., Two-way coupling betweeen Vesuvius eruptions and southern Apennine earthquakes, Italy, by elastic stress transfer. *J. Geophys. Res., 103*, 24,487-24,504, 1998.

Okubo, P.G., Dynamic rupture modeling with laboratory derived constitutive relations, *J. Geophys. Res., 94*, 12,321-

12,336, 1989.

Parson, T., S. Toda, R. S. Stein, A. Barka, and J. H. Dieterich, Heightened odds of large earthquakes near Istanbul: An interaction-based probability calculation, *Science, 288*, 661-665, 2000.

Piersanti A., G. Spada, R. Sabadini, and M. Bonafede, Global postseismic deformation, *Geophys. J. Int. 120*, 544-566, 1995.

Piersanti A., G. Spada, and R. Sabadini, Global postseismic rebound of a viscoelastic Earth: Theory for finite faults and application to the 1964 Alaska earthquake, *J. Geophys. Res. 102*, 477-492, 1997.

Pollitz F.F., Postseismic relaxation theory on the spherical Earth, *Bull. Seismol. Soc. Am. 82*, 422-453, 1992.

Pollitz F.F., and I.S. Sacks, The 1995 Kobe, Japan, earthquake: a long-delayed aftershock of the offshore 1944 Tonankai and 1946 Nankaido earthquakes, *Bull. Seismol. Soc. Am. 87*, 1-10, 1997.

Reasenberg, P.A., and Simpson, R.W., Response of Regional Seismicity to the Static Stress Change Produced by the Loma Prieta Earthquake, *Science 255*, 1687-1690, 1992.

Romanowicz B., Spatiotemporal patterns in the energy release of great earthquakes, *Science 260*, 1923-1926, 1993.

Ruina, A.L., Slip instability and state variable friction laws, *J. Geophys. Res., 88*, 10,359-10,370, 1983.

Rydelek P.A., and I.S. Sacks, Large earthquake occurrence affected by small stress changes, *Bull. Seismol. Soc. Am. 89*, 822-828, 1999.

Sella, G.F., Dixon, T.H., and Mao, A., REVEL: A model for Recent plate velocities from space geodesy, *J. Geophys. Res. 107*, No. B4, 10.1029/2000JB000033, 2002.

Stein, R. S., The role of stress transfer in earthquake oc-

currence, *Nature, 402*, 605-609, 1999.

Stein, R. S., G. C. P. King, and J. Lin, Stress triggering of the 1994 M = 6.7 Northridge, California, earthquake by its predecessors, *Science, 265*, 1432-1435, 1994.

Stein, R.S., A.A. Barka, and J.H. Dieterich, Progressive failure on the North Anatolian fault since 1939 by earthquake stress triggering, *Geoph. J. Int., 128*, 594-604, 1997.

Toda, S., Stein, R.S., Reasenberg, P.A., Dieterich, J.H., and Yoshida, A., Stress transferred by the 1995 Mw = 6.9 Kobe, Japan, shock: Effect on aftershocks and future earthquake probabilities, *J. Geophys. Res. 103*, B10, 24,543-24,565, 1998.

Ziv, A., and A. M. Rubin, Static stress transfer and earthquake triggering: No lower threshold in sight?, *J. Geophys. Res. 105*, 13,631-13,642, 2000.

Chapter 2

PSV and long-term interaction

In this chapter, we investigate the feasibility of remote earthquake interaction through a model simulation which mimics the co- and post-seismic stress diffusion in realistic cases. In brief, we generate a synthetic catalog of worldwide seismicity with $M_s \geq 7.0$ that has the same statistical distribution of the period 1900-1999 (*Pacheco and Sykes*' [1992] catalog + the CMT catalog [e.g., *Dziewonski et al.*, 1981; *Dziewonski and Woodhouse*, 1983] after 1989), but spans a much longer time period. Then, we check the contribution to stress rate and stress variation from earthquakes occurring worldwide at two selected points on the earth located in two different tectonic regimes, Southern California and Southern Italy.

2.1 The Model

The approach adopted in this chapter consists of simulating the possible interaction between remote earthquakes. It can be summarized in four steps: (1) Definition of the "reference" points (from now on RPs) on the earth surface where the perturbations due to remote earthquakes are calculated;

(2) generation of a synthetic global catalog; (3) calculation of the stress rate variation induced by the remote earthquakes of the synthetic catalog at the RPs; (4) estimation of changes in seismicity rate on a simple seismogenetic fault model located at the RPs, due to the stress induced by the remote earthquakes. The steps 2 and 3 are the most important, because they describe the core of the model, i.e., they contain the idealization of the process of the long-term interaction, and the most important assumptions.

2.1.1 Choice of the RPs

The RPs are located in Southern California (Los Angeles, RP1) and Southern Italy (Calabria region, RP2). The choice of these two sites has been made because they represent two active seismic regions with quite different tectonic settings. We stress that the results of the model are not constrained by the choice of these two specific points. Indeed, the aim of the model described here is to mimic a plausible situation at any point on the Earth's surface, and it does not claim to describe the reality at these two specific sites. In this respect, the two selected RPs can be seen as generic representatives of the Pacific Ring and of the Central Mediterranean tectonic domains, respectively.

2.1.2 The Synthetic Seismic Catalog

In order to set up a plausible model for long-term interactions, we need to define a synthetic seismic catalog with the same statistical features as the real seismicity. Specifically, in our case we need to mimic a realistic distribution of the scalar seismic moment released in space and time. Therefore, the synthetic catalog will contain three variables for each earth-

quake: the time of occurrence, the spatial distance of the epicenter from the RP chosen, and the scalar seismic moment released. Since the spatial distance depends on the RP considered, we generate two synthetic catalogs, one for each RP.

Since the strongest earthquakes are the most influential, we generate synthetic catalogs having the main statistical features of the worldwide seismicity of the last century with $M_s \geq 7.0$ and depth ≤ 70 km. The real data comes from the *Pacheco and Sykes'* [1992] catalog for the period 1900-1989. For the following decade (1990-1999) we use the seismic events with the same characteristics reported by the CMT Harvard catalog [*Dziewonski et al.*, 1981; *Dziewonski and Woodhouse*, 1983]. The total number of events of this dataset (from now on called PSCMT-M7) is 799.

The derivation of the synthetic catalog is a crucial step of the analysis and the assumptions used deserve careful discussion. In general, a synthetic seismic catalog of the type we wish to use is a collection of random events having a joint probability cumulative function $F(\Delta t, d, Mo)$, where Δt is the inter-event time between the earthquake and the previous event, d is the spatial distance between the earthquake and the selected RP, and Mo is the seismic moment of the earthquake. Typically, we do not know $F(\Delta t, d, Mo)$ *a priori*; in such cases, the usual procedure is to estimate its functional form and the parameters of this functional form, by using past observations and some assumptions concerning the process.

Our synthetic catalogs are built by assuming that the process is memoryless, and a complete spatio-temporal independence among the remote earthquakes. In this case, the joint

cumulative probability function of the synthetic catalogs is

$$F(\Delta t, d, Mo) = F(\Delta t, d, Mo|[H]) = F_1(\Delta t) \cdot F_2(d) \cdot F_3(Mo) \tag{2.1}$$

where $[H]$ represents the past history of the process, and F_1, F_2, and F_3 represent three distinct cumulative probability functions for each single variable. Since the theoretical form of the distributions F_1, F_2, and F_3 is unknown, we estimate them by fitting the data of a filtered version of the PSCMT-M7 catalog (see below), by using a nonparametric density estimation technique [*Gershenfeld*, 1999]. The details are reported in the Appendix A. The estimated empirical cumulatives are $\hat{F}_1$, $\hat{F}_2$, and $\hat{F}_3$. The synthetic catalog is then obtained by

$$\Delta t_i = \hat{F}_1^{-1}(\xi_{1i}); \quad d_i = \hat{F}_2^{-1}(\xi_{2i}); \quad Mo_i = \hat{F}_3^{-1}(\xi_{3i}) \qquad i = 1, \ldots, N_e \tag{2.2}$$

where $\hat{F}_1^{-1}$, $\hat{F}_2^{-1}$, and $\hat{F}_3^{-1}$ are, respectively, the inverse of the fitted empirical cumulative distributions of the inter-event times, spatial distances, and seismic moment, and ξ_{1i}, ξ_{2i}, and ξ_{3i} are independent random numbers that follow a $[0, 1]$ uniform distribution. In other words, a synthetic catalog is produced by generating three sets of N_e random numbers uniformly distributed between 0 and 1 (ξ_{1i}, ξ_{2i}, and ξ_{3i}), and then by inverting the marginal empirical cumulative distributions of the variables ($\hat{F}_1$, $\hat{F}_2$, and $\hat{F}_3$) [see e.g. *Ripley*, 1987]. In this way, each synthetic catalog generated has the same marginal distributions as the PSCMT-M7 catalog for the inter-event times, the spatial distances, and the seismic moment released. Note that one effect of this procedure is to set the largest earthquake of the synthetic catalog not greater than the largest earthquake in the observed catalog.

As mentioned before, the empirical cumulative distribu-

tions $\hat{F}_1$, $\hat{F}_2$, and $\hat{F}_3$ are built from a filtered version of the PSCMT-M7 catalog. In particular, we remove from PSCMT-M7 catalog the seismic events that occur at distances $> 5 \times 10^3$ km, and $< 3 \times 10^2$ km from the selected RPs. The filtered catalogs contain 115 earthquakes for RP1 and 56 earthquakes for RP2. These events are used to fit the empirical statistical distributions (see Figure 2.1 and the Appendix A). Note that the number of data is sufficient in both cases to obtain reliable estimate of the parent distributions F_1, F_2, and F_3.

The filtering of the real catalog is performed before calculating $\hat{F}_1$, $\hat{F}_2$, and $\hat{F}_3$. The first threshold (5×10^3 km) has been chosen to rule out possible biases in the spatial distribution of the seismic moment. In practice, this means that giant earthquakes with seismic moment of the Alaska (1964) event are possible only for the synthetic catalogs of the RP located at Los Angeles (and for most of possible reference points in the Pacific Ring), while they are excluded from the synthetic catalogs of the RP located in Southern Italy. At the same time, seismic events with a seismic moment comparable to the Chile earthquake (1960) are excluded from both synthetic catalogs because the epicentral distance of the Chile earthquake (1960) from both RPs is larger than 5×10^3 km. From a physical point of view this implies that only earthquakes with distances $\leq 5 \times 10^3$ km from the RP are considered representative of the remote seismicity. Note that this choice is conservative for our purpose because we cannot exclude that giant earthquakes (like Chile, 1960) can influence significantly remote regions at distances larger than 5000 km. In fact, as we will show in the next section, the remote stress perturbation depends on both distance and seismic moment.

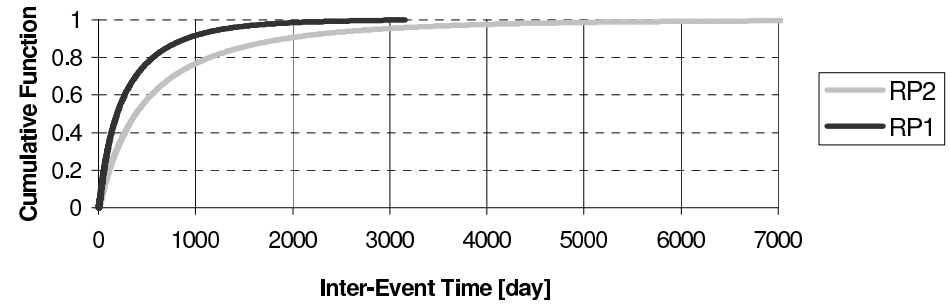

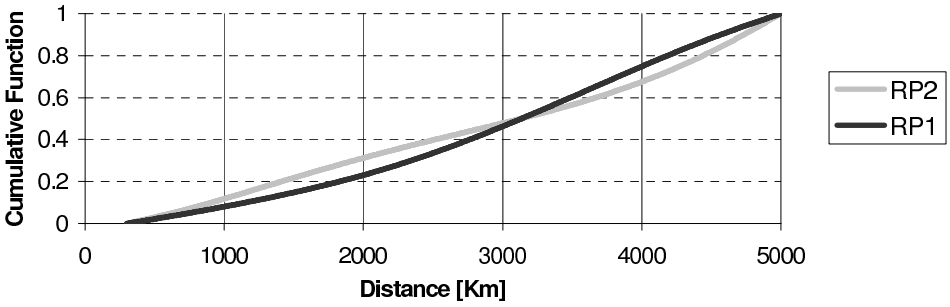

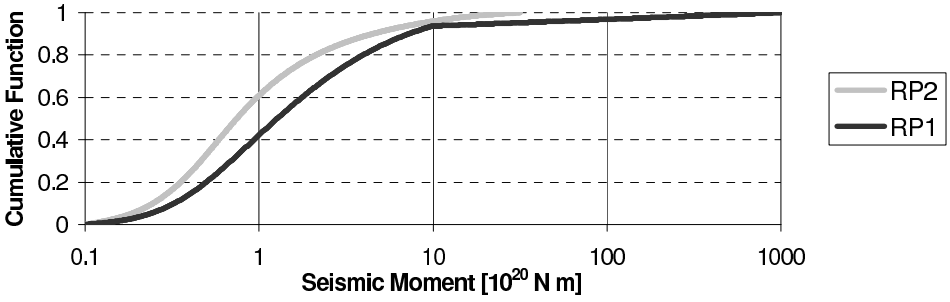

Figure 2.1: Empirical cumulative functions for the inter-event time, distance, and seismic moment from the PSCMT-M7 catalog (see text), calculated as reported in the Appendix A. The two curves of each graphs correspond to the two RPs (see text).

The effects of the first threshold will be discussed later.

The second threshold (300 km) allows us to highlight the long-term interaction by removing the obvious effects of earthquakes occurring too close to the RPs. This induces an underestimation of the perturbations induced by earthquakes at the RPs, but it allows us to consider only the contribution of distant earthquakes, eliminating, for example, the well-known and well-studied phenomenon of aftershocks. In practice, this also implies that the RPs are located in seismic regions where the rate of occurrence of "local" very large earthquakes is negligible compared to the rate of occurrence of very large remote earthquakes (see in chapter 5 the case of Southern California). Obviously, if a seismic region experiences a significant number of such a strong earthquakes (for instance in part of Japan), the effects of large remote earthquakes can be blurred by the effects of the closer seismic events. The value of 300 km is chosen because it is larger than almost all the fault lengths of big earthquakes (except the giant ones). In other words, we consider "remote" all the earthquakes occurred at distances larger than this dimension. As a final consideration, it is worth noting that the global effect of both thresholds is to make the results of our analysis conservative. The removal of such a filtering, in fact, would lead to higher stress perturbations induced by earthquakes at the RPs.

In order to have a large number of seismic events, we extend the synthetic catalogs to 5×10^5 years. This extrapolation, as well as the assumption of no memory of the past configurations (see equation 2.1), deserves further discussion. Such a long extrapolation (compared to 100 years of real seismicity) neglects all possible long-term nonstationarities; the hypothesis of no memory neglects all possible correlation

in time and space between events. We stress that this is not critical for the aim of this chapter, because the important aspects concern the spatial distribution of the seismic moment released. The temporal distribution of the events acts only to guarantee that the synthetic catalog has a frequency of large events comparable to the value observed in the past century. Possible long-term variations with or without time-space memory of this frequency would not significantly change the implications derived from the results of the model. Finally, we remark that we have to caution about very long extrapolations only when we use them to make some "real forecasting" of the future seismic activity. Here, instead, we only want to study the statistical distribution of the long-term seismic interactions for a realistic scenario of the global seismicity, i.e., having the same characteristics of the seismicity observed in the last century.

2.1.3 Calculation of the Stress Rate Variations

The occurrence of any earthquake induces a perturbation in the stress field at any point on the earth's surface. Generally speaking, there are three different types of perturbations: the dynamical stress variations (DSV) due to the passage of the seismic waves, the co-seismic stress variations (CSV) due to the elastic residual deformation of the lithosphere, and the post-seismic stress variations (PSV) due to the visco-elastic readjustment of the lower-crust and/or asthenosphere and mantle. From an observational point of view, these three perturbations are characterized by different attenuation of the effects as a function of distance from the epicenter, and different characteristic times. The DSV lasts only few minutes (at maximum), and its maximum amplitude attenuates

with distance slowly, compared to the CSV and PSV [e.g. *Gomberg et al.*, 1998]. The CSV is approximately instantaneous (being due to the elastic rebound) and it does not vary with time; its maximum perturbation decreases drastically with distance [see e.g. *Stein et al.*, 1992; *King et al.*, 1994; *Stein et al.*, 1994]. The PSV reaches its maximum effect after a few decades or centuries [e.g. *Thatcher*, 1983, *Piersanti et al.*, 1997; *Pollitz et al.*, 1998; *Piersanti*, 1999; *Kenner and Segall*, 2000), depending on the viscosity of the lower crust and mantle, and it decays with distance less rapidly than the CSV.

In this study, we are mainly interested in estimating possible long-term interactions (in terms of distances and overall times), therefore we model only the CSV and the PSV. The stress field at the RPs is calculated numerically as the effect of stress redistribution in a spherical, viscoelastic, layered earth. This is accomplished by using the model proposed by *Piersanti et al.* [1995, 1997]. Numerical estimation is used because a direct computation of the stress field through the *Piersanti et al.*'s [1995, 1997] model would have required the focal mechanisms of all the earthquakes and a prohibitive amount of CPU time. In the present simulation the computation of the time dependent stress field of about one million of earthquakes is involved; for each event the time required would be about one minute on the fastest CPUs available [*Casarotti et al.*, 2001]. Instead, the stress perturbation at time t due to the i-th earthquake is written, for each RP, as

$$\sigma(t) = G_i Mo_i[\Delta_{co}(d_i)H(t-t_i) + \Delta_{post}(d_i)\Omega(t-t_i)] \quad (2.3)$$

where G_i is a geometric factor that will be discussed later, Mo_i and t_i are the seismic moment and the time of occurrence of the i-th earthquake, $\Delta_{co}(d)$ and $\Delta_{post}(d)$ describe

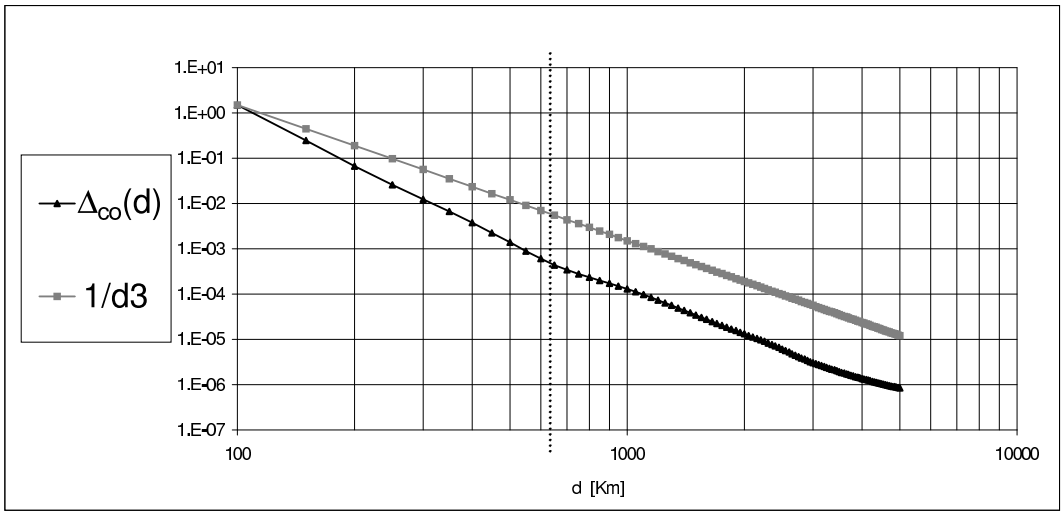

Figure 2.2: $\Delta_{\rm co}(d)$ (see equation 2.3) compared to the function $1/d^3$.

how CSV and PSV decay with distance between the epicenter and the RP, $\Omega(t - t_i)$ is a time function that takes into account the relaxation of the viscous layers in the earth, and $H(t - t_i)$ is the Heaviside function. Mo is in 10^{20} Nm, d in km, Δ_{co} and Δ_{post} in MPa/10^{20} Nm.

Numerical simulations using the earth model proposed by *Piersanti et al.* [1995, 1997] allow us to estimate realistic averaged forms for the functions $\Delta_{co}(d)$, $\Delta_{post}(d)$, and $\Omega(t - t_i)$. In particular, $\Delta_{co}(d)$ is reported in Figure 2.2. The same numerical simulations show that the relation between $\Delta_{co}(d)$ and $\Delta_{post}(d)$ can be approximated as

$$\Delta_{post}(d) = \Delta_{co}(d)(0.012\delta + 1) \tag{2.4}$$

where δ is a dimensionless number which coincides numerically with distance in km. Equation 2.4 shows that the relative importance of the PSV compared to the CSV increases with distance [e.g. *Pollitz*, 1992; *Piersanti et al.*, 1995, 1997].

In Figure 2.2, we show the function $\Delta_{co}(d)$ together with the function d^{-3} that describes stress perturbation decreases

with distance in the far field of elastic planar models [e.g. *Lay and Wallace*, 1995]. Note that the amplitude of $\Delta_{co}(d)$ attenuates faster than d^{-3} in the first $600 - 700$ km, and decreases as d^{-3} in the range $700 - 5000$ km. Thus, the model proposes less interaction than d^{-3}.

The temporal evolution of PSV is given by $\Omega(t)$, and is approximated as

$$\Omega(t) = \begin{cases} 1 - \exp[-t/\tau] & \text{if } t \geq 0 \\ 0 & \text{if } t < 0 \end{cases} \tag{2.5}$$

where t is the elapsed time from the occurrence of the earthquake that generates the PSV variations. This is a simplification of *Piersanti et al.*'s [1995, 1997] model, where $\Omega(t)$ consists of a sum of functions similar to equation 2.5, each one representing distinct modes of relaxation of the viscous layers. Our simplification assumes that one mode prevails over the others. The relaxation time τ mainly depends on the viscosity of the mantle. Indirect estimations of the asthenosphere viscosity provide quite different values, ranging from 5×10^{17} Pa s [e.g., *Pollitz et al.*, 1998] to 10^{20} Pa s [e.g., *Piersanti*, 1999]. Since τ is not well constrained, calculations are performed for two different values, $\tau_1 = 10$ yr (corresponding to a viscosity of the asthenosphere of $5 - 10 \times 10^{17}$ Pa s) and $\tau_2 = 100$ yr (that corresponds to a viscosity of the asthenosphere of $5 - 10 \times 10^{18}$ Pa s). With τ_1 and τ_2 , the PSV reaches 95% of its maximum value after 30 years and 300 years, respectively. We will refer hereafter to the two cases with PSV (30 yr) and PSV (300 yr).

The geometric factor G_i expresses the geometric coupling between the i-th remote earthquake and a possible fault located at the RPs [e.g., *Stein et al.*, 1992; *King et al.*, 1994; *Stein et al.*, 1994]. Each G_i is randomly selected from a

[-1,1] continuous uniform random distribution. A negative value for G_i means that the stress induced at RP tends to reduce the stress on a possible fault; a positive value tends to increase the stress at RP. Obviously, the closer G_i is to 0, the less the effect of the i-th remote earthquake at RP is. We remark that the choice of a random uniform distribution is probably conservative because in real cases the coupling might depend on distance. Indeed, the earthquakes closer to RP might have potentially a positive coupling because of a similar tectonic setting.

The choice of a uniform [-1,1] distribution implies that the remote stress tends to zero if averaged over long periods of time, because $< G_i >= 0$. In this case, a long period of time is an interval that includes the occurrence of a large number of earthquakes. From a physical point of view this also means that the stress does not accumulate indefinitely. On the other hand, the remote stress can have large fluctuations around zero if averaged over short periods of time. In this case, a short period of time (for instance, comparable or shorter than the average inter-event times) does not contain a sufficient number of earthquakes to guarantee that the average of the stress tends to zero.

2.1.4 Effects on the Characteristic Earthquake Model

In order to further evaluate the effect of the stress induced by remote earthquakes on the RPs, we simulate the effects on the simplest fault model, i.e., the Characteristic Earthquake Model (from now on CEM; see *Schwartz and Coppersmith*, [1984]). The CEM is based on the concept of stick-slip on a fault where the elastic strain energy is accumulated at constant rate and released through identical seismic

events that occur periodically in time. In such a model the stress accumulated σ depends only on the tectonic rate c and on the elapsed time from the last earthquake $(t - t_0)$, i.e., $\sigma = c(t - t_0)$. An earthquake occurs when $\sigma = \sigma_{crit}$, and the stress drop $\Delta\sigma$ is always the same. Here, we have used $\sigma_{crit} = \Delta\sigma = 3$ MPa. The inter-event times in the absence of remote interactions are exactly the same, $\Delta t_0 = \Delta\sigma/c$. The interactions with the remote earthquakes are considered by adding to the stress accumulated linearly through tectonic rate, the stress given by equation 2.3.

Note that the choice of the CEM has been made only to better highlight the effects of the remote earthquakes. This model has not been chosen for its intrinsic physical reliability (which is probably very low), but because the CEM allows us to assess long-term perturbations.

2.2 Results of the Model and Discussion

In Figure 2.3 we present the probability distribution of the yearly absolute stress rate ($|\dot{\sigma}| = |\frac{d\sigma}{dt}|$) due to the CSV and PSV induced by remote earthquakes at the two RPs considered. The rate is calculated numerically by using a sampling time interval of 1 year, and subtracting the values of stress calculated at the end and at the beginning of each year. The resulting time series $|\dot{\sigma}|_i$ consists of 500,000 data $(i = 1, ..., 500,000)$, one for each year of the synthetic catalog. Note that while $< \dot{\sigma} >= 0$ because $< G >= 0$ (see above), this is not true for $< |\dot{\sigma}| >$. The choice of the sampling time interval (1 year) has been made by taking into account two opposite requirements: the need to have a sampling time interval as short as possible to capture the variability of the time series, but large enough to have a tractable number of

data points. These requirements are the same usually encountered in sampling a continuous time series. A sampling time interval of 1 year fulfills these requirements. The number of data (500,000) is not excessive, and the probability of more than one influential remote earthquake in 1 year is negligible. Moreover, this period of time allows an easy comparison with the annual stress rate due to tectonics. The results reported in Figure 2.3 are stable for sampling intervals of few decades.

The ordinate of each point of the curve represents the fraction of time covered by the synthetic catalog for which the annual stress rate is lower than or equal to the value reported in the abscissa. We report the absolute values because we are interested only in estimating the generic influence, not a specific influence (i.e., if the CSV and PSV are in concordance or opposite to the tectonic stress rate). In the same figure we note also the tectonic stress rate for the two RPs as reported in the literature. For RP1 (Los Angeles) we use $c = 9.45 \times 10^{-3}$ MPa/y [*Stacey*, 1977]. For RP2 (Calabria region), we use $c_1 = 0.19 \times 10^{-3}$ extrapolated from the strain rate reported by *Viti et al.* [1997] for the Mediterranean region, and $c_2 = 3 \times 10^{-3}$ in order to have a "recurrence" time for earthquakes in the CEM of about 10^3 years [e.g., *Pantosti et al.*, 1993]. These two values probably represent a maximum and a minimum estimate of the real tectonic stress rate. In Figure 2.3, for the sake of clarity, we report only c_2, i.e., the highest rate (and therefore the most conservative for remote influences).

From the plots we see that about 50% for RP1 and 30% for RP2 of the stress rates due to the PSV induced by remote earthquakes ($|\dot{\sigma}|$) are non-negligible compared to the tectonic stress rates, i.e., $|\dot{\sigma}| \geq 0.1c$. If we use the lower tec-

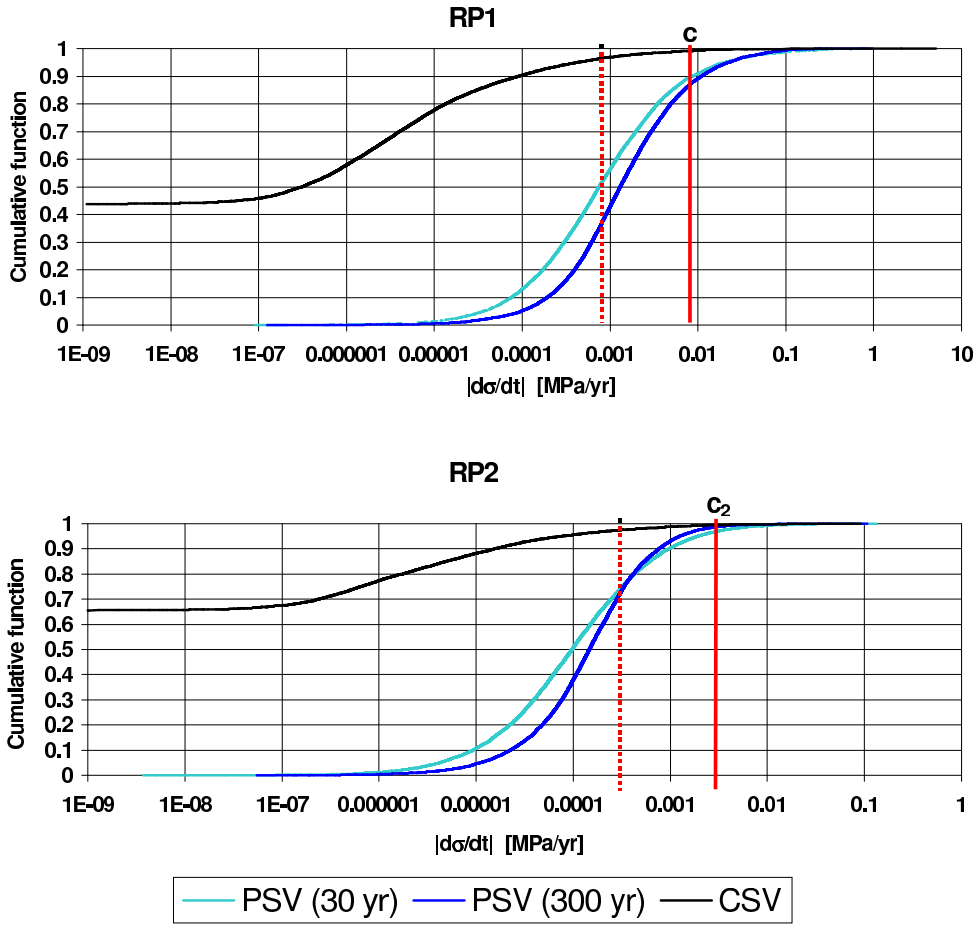

Figure 2.3: Cumulative functions for the stress rates induced by remote earthquakes of the synthetic catalog for RP1 (top) and RP2 (bottom). The black curve corresponds to the CSV. The light and dark blue lines correspond to the PSV with different relaxation times. The vertical red solid line is the tectonic stress rate c observed at the RP. The vertical dotted red line is $o(c)$, i.e., $0.1 \times c$, taken as a threshold stress rate. All stress rates under this threshold are considered negligible compared to the tectonic stress rate.

tonic stress rate at RP2 (c_1; not reported in the graph), more than 70% of the stress rates due to the remote earthquakes are non-negligible compared to the tectonic rate. From the same figure, we also observe two other interesting features. First, the CSVs are negligible compared to both the tectonic stress rate and the PSVs; 40% of the time at RP1 and 60% of the time at RP2 the CSV is less than the minimum abscissa value. This may be due to the use of a threshold in the minimum distance considered (300 km). Second, the PSVs are not particularly sensitive to a wide range of possible relaxation times. The slight departure found for intermediate stress rates is due to the effect that the longer the relaxation time, the higher the number of years perturbed by remote earthquakes.

In Figure 2.4 we show results for the length of the inter-event times obtained by the CEM. Specifically, we show the cumulative function of the inter-event times for the unperturbed CEM, and for the CEM perturbed by CSV and PSV. As for the previous figure, we see that the CSV have a very low impact on the CEM. On the other hand, the PSV strongly influences the CEM, particularly for RP1 (note the different scale of the x-axes). Again, the relaxation time for the PSV plays a minor role. Note that for RP2 we have used the most conservative tectonic stress rate, i.e., c_2.

The departures for the perturbed CEM from the Heaviside function that characterizes the unperturbed CEM indicates "clusters" and "gaps" in seismicity, i.e., periods of larger and smaller seismic rates. The duration of these gaps and clusters depend on the relaxation time, i.e., they can last from few decades to few centuries. Over the whole period of time considered (500,000 years) the gaps and clusters tend to balance producing a null overall effect. This is a direct consequence

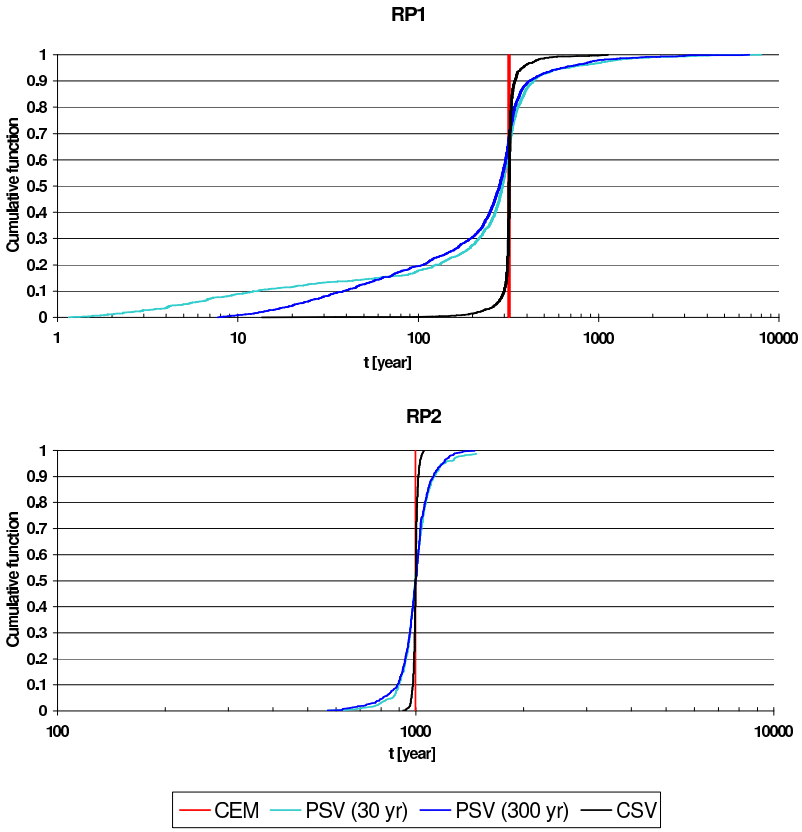

Figure 2.4: Observed cumulative functions for the inter-event times of the unperturbed and perturbed CEM (see text). The vertical red line corresponds to the unperturbed CEM. The black line corresponds to the inter-event time obtained by a CEM perturbed only by CSVs. The light and dark blue lines are the inter-event times obtained by the CEM perturbed by the PSVs.

of the fact that $< G >= 0$ as mentioned before. It is worth noting that these nonstationarities are overwhelmingly due to the influence of remote earthquakes by means of the relaxation modes of the viscous layers (i.e., PSV). This can be seen from the time derivative of equation 2.3 (including also equation 2.5) that reads

$$\dot{\sigma}(t) = G_i Mo_i[\Delta_{co}(d_i)\delta(t-t_i) + H(t-t_i)\frac{\Delta_{post}(d_i)}{\tau}\exp(-t/\tau)] \tag{2.6}$$

where δ is the Dirac's function.

While the CSV effects induced on a fault by a remote earthquake vanish after the occurrence of an earthquake on the fault, the PSVs induce time dependent effects whose duration is a function of the viscosity of the layers. This might be one possible explanation of the long-term space-time clustering of earthquakes [e.g., *Kagan and Jackson*, 1991a], and of the failure of the "gap" hypothesis to predict the occurrence of the earthquakes [*Sykes and Nishenko*, 1984; *Nishenko and Sykes*, 1993; *Kagan and Jackson*, 1991b; *Kagan and Jackson*, 1995]. In our analysis, a gap of seismicity reflects a remote influence that lowers the stress accumulated in a fault, not the signal of an impending earthquake, and clusters are due to a remote influence that increases the stress.

In order to quantify the influence of a remote earthquake relative to the unperturbed CEM we define, for each inter-event time Δt_i,

$$\alpha_i = \left|\ln\left(\frac{\Delta t_i}{\Delta t_0}\right)\right| \tag{2.7}$$

For instance, a value $\alpha = 0.4$ represents an inter-event time which is increased or decreased about a factor of two of Δt_0.

In Figure 2.5 we show the distance and magnitude of the remote earthquakes as a function of α for RP1. We plot the

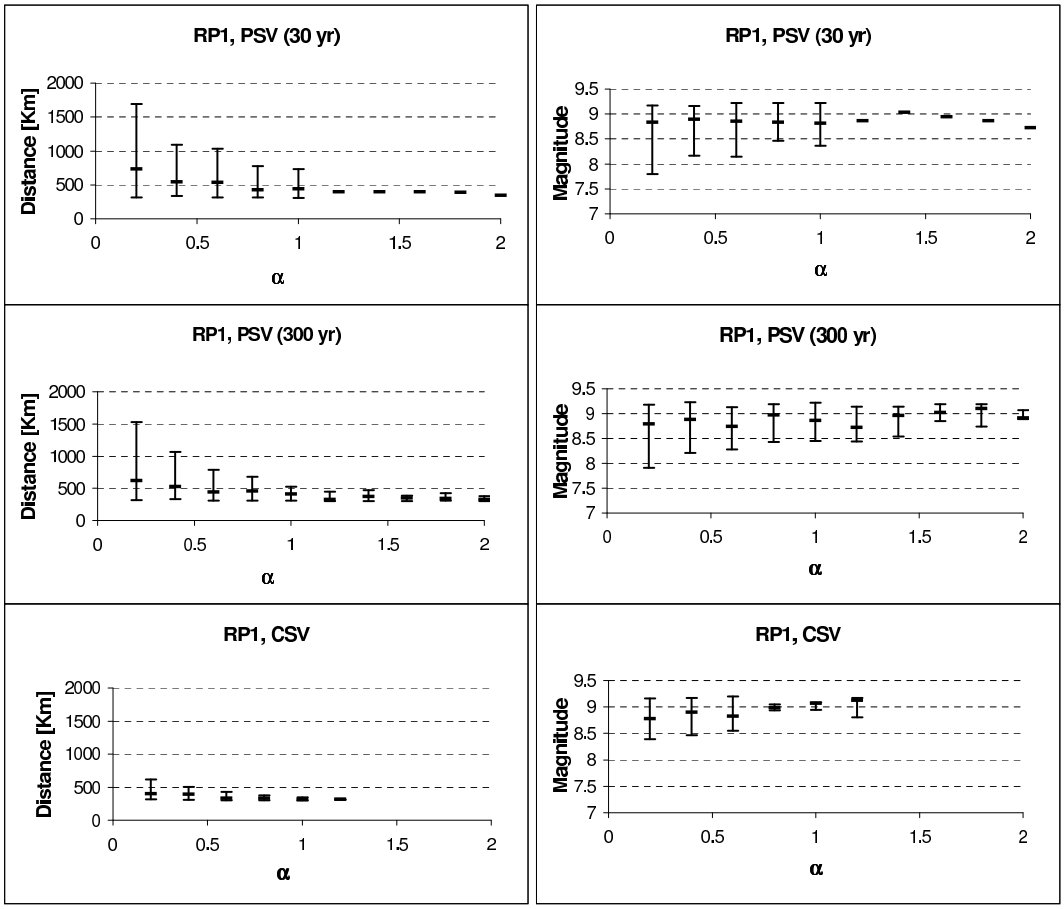

Figure 2.5: The graphs on the left show the distances of the remote earthquakes as a function of binned α values at RP1. The range for the binning is 0.2. For each α, the 5, 50 (median) and 95 percentile of the distances is reported. The three graphs are the perturbations obtained by using a relaxation time of 30 years, 300 years, and by using only the coseismic effects. The graphs on the right are the same but for the magnitudes as a function of binned α.

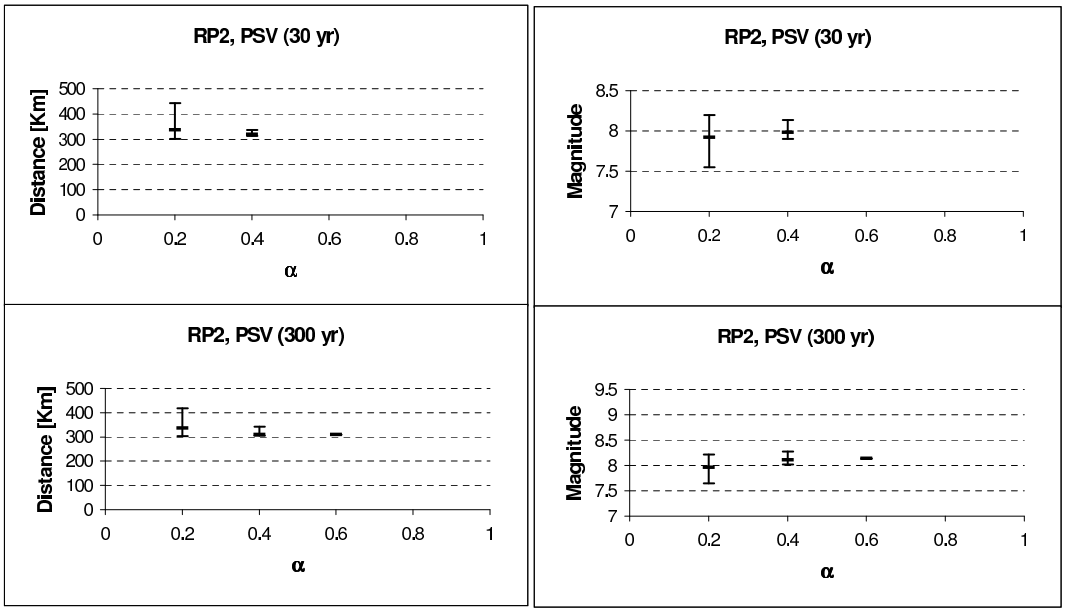

Figure 2.6: The same as for Figure 2.5, but for RP2.

5, 50 (the median) and 95 percentiles of the distances (left panel of Figure 2.5) and magnitudes (right panel of Figure 2.5) of the remote earthquakes that influence the CEM for α in a particular range. From the plot shown in the left part of Figure 2.5 we see that remote earthquakes that occurred beyond one thousand kilometers from RP1 can significantly perturb the CEM ($\alpha \sim 0.2 - 0.5$). Also in this case, the CSV are negligible compared to the PSV. From the right part of Figure 2.5, we see that almost all the significant perturbations are due to remote earthquakes with $M \geq 8.0 - 8.5$.

Figure 2.6 reports the same calculations for RP2. In this case, the distances are smaller than for RP1. Most of the influence is from distances $\leq$ 400 km and for magnitudes $\geq 7.5 - 8.0$. This lower range of distances compared to the RP1 case (see Figure 2.5) is because the highest magnitudes of the remote earthquakes for RP2 are smaller, lacking giant

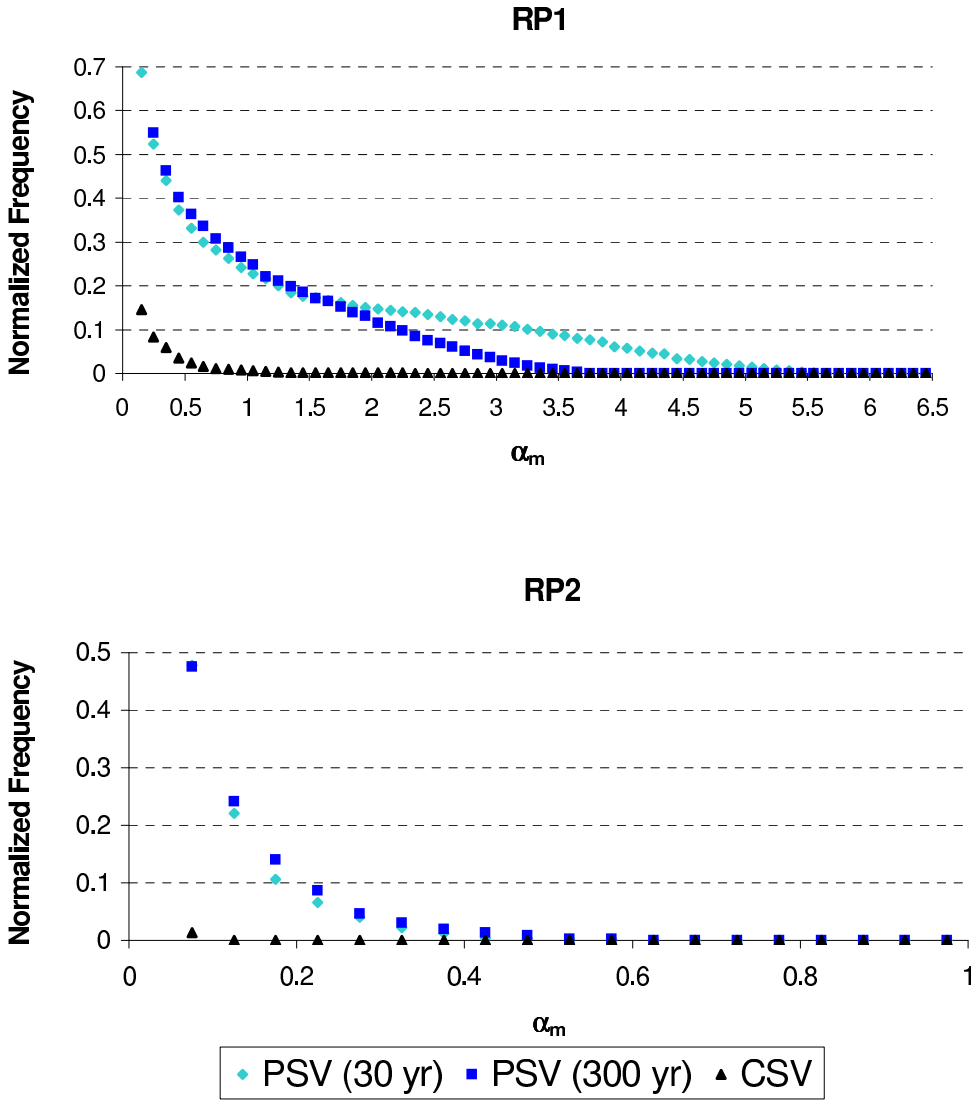

Figure 2.7: Probability to observe a random inter-event time with $\alpha \geq \alpha_m$ for RP1 (upper panel) and RP2 (lower panel). The colors indicate different types of remote perturbations as shown in the legend.

events, and the average distance of remote earthquakes at RP2 is smaller than at RP1 (see Figure 2.1). We do not show the CSV results in Figure 2.6 because this effect is always negligible for RP2. Note that the results shown in Figures 2.5 and 2.6 justify in retrospect the use of the 5×10^3 km threshold for the catalog.

A final aspect concerns the time frequency of the perturbing remote earthquakes. In order to estimate the probability of having a particular perturbation at the two RPs, we report in Figure 2.7 the normalized frequency (i.e., the probability) of an inter-event time Δt_i with $\alpha_i \geq \alpha_m$. From Figure 2.7 we see that the probability that an observed inter-event time at RP1 is strongly influenced by remote earthquakes is high. For instance, there is a probability of about 40% that an observed inter-event time has $\alpha \geq 0.4$. At RP2 the effects are less strong. Specifically, we have a probability $\simeq 0.10$ to have an observed inter-event time with $\alpha \geq 0.2$.

2.3 Summary and Conclusions

To summarize, the main results of this study are:

1. The post-seismic stress variations induced by remote earthquakes at both RPs are not negligible compared to the tectonic loading rates measured at the two sites. On the other hand, the co-seismic stress variations are almost negligible at the distances considered (≥ 300 km). The effects for Southern California, as well as for most of sites in the Pacific Ring, are stronger than the effects calculated for Southern Italy. This is due to the higher magnitudes of the remote earthquakes and to the smaller average distances.

2. The time dependent post-seismic stress variations are able to explain clusters and gaps of seismicity. Note that in this picture, a gap does not represent a possible precursory feature for an impending earthquake, but rather a time period in which the influence of remote earthquakes has worked against the tectonics, lowering the stress accumulated in a fault. Clusters of seismicity are explained by a strong positive influence of remote earthquakes. The general scheme is the same as for aftershock sequences, but the physical mechanism of the stress diffusion, the distances, and times involved, are different.

3. Remote earthquakes with $M \geq 8.0 - 8.5$ occurring at distances up to one thousand kilometers can significantly perturb a seismic zone. These distances are larger than what was commonly believed in the past [e.g., *Pollitz et al.*, 1998; *Casarotti et al.*, 2001].

4. The probability that a random sampled inter-event time observed in a particular seismic zone is significantly perturbed by a remote earthquake is not negligible.

The most important consequence is that seismic regions, as well as single tectonic structures, cannot be considered as "closed" systems, but are able to interact significantly with other remote regions. Independently from the physical mechanism that generates earthquakes, the parameters that control the system can be modulated by earthquakes that occur at large distance and decades before. Time features observed in many seismic catalogs, such as time clustering, seismic gaps, and nonstationary behavior, that are usually explained by evoking the complex (tectonic) nature of the seismic source, might also be due to the influence of a large

remote earthquake. This would shed a new light in hazard assessment studies, because it would imply that a reliable estimate of the probability of earthquake occurrence has to take into account the strain diffusion from past large earthquakes, distant from the region considered [e.g. *Rydelek and Sacks*, 1999]. This issue, to be effective, needs a lot of further work. In this respect, the most important aspect consists of converting the coupling found into a well defined change in probability of earthquake occurrence.

As a final consideration, we remark that the reliability of the remote interaction hypothesis is still far from being definitely proven. The results reported here, and the reliability of the model proposed, are mainly supported by the simple and realistic (often conservative) physical assumptions made, and by some empirical evidence reported in recently published papers, as well as in *Chapter 4* and *Chapter 5*. In this respect, notable support is provided by the finding of statistically significant interactions in different datasets, i.e., between large earthquakes and volcanic eruptions [*Marzocchi*, 2002; *Marzocchi et al.*, 2002]. The time-distance scales found and the physical model proposed for such coupling are similar to the ones reported here. Moreover, other papers reported phenomenological (retrospective) evidence of different kind of remote earthquake interactions [e.g., *Romanowicz*, 1993; *Hill et al.*, 1993; *Marzocchi et al.*, 1993; *Marzocchi and Mulargia*, 1995; *Pollitz and Sacks*, 1997; *Freed and Lin*, 2001; *Chéry et al.*, 2001; *Casarotti et al.*, 2001; *Jacques et al.*, 2001], and of the long-term effects of large earthquakes on ground deformation [e.g., *Kenner and Segall*, 2000; *Klotz et al.*, 2001].

We think, however, that the technical difficulty of identifying the effects of remote coupling in real earthquake datasets

(that are too short; see discussion above) suggests checking the validation of the long-term interaction hypothesis through a forward analysis. This strategy rules out *a priori* any possible overfit of the data due to unconscious choice of parameters of the model adopted (a kind of *retrospective realism*). Our results suggest, for instance, that a viable way might consist of identifying, immediately after the occurrence of the next very large earthquakes, the surrounding remote regions (excluding the closer aftershock area) where the model predicts the future occurrence of clusters and gaps. In this way, the future seismicity in such areas will provide a robust test to validate or discard the long-term interaction hypothesis.

References

Casarotti E., A. Piersanti, F.P. Lucente, and E. Boschi, Global postseismic stress diffusion and fault interaction at long distances, *Earth and Planet. Sci. Lett. 191*, 75-84, 2001.

Chéry J., S. Carretier, and J. Ritz, Postseimsic stress transfer explains time clustering of large earthquakes in Mongolia, *Earth Planet. Sci. Lett. 194*, 277-286, 2001.

Dziewonski A.M., T.A. Chou, and J.H. Woodhouse, Determination of earthquake source parameters from waveform data for studies of global and regional seismicity. *J. Geophys. Res. 86*, 2825-2852, 1981.

Dziewonski A.M., and J.H. Woodhouse, An experiment in systematic study of global seismicity: Centroid-moment tensor solutions for 201 moderate and large earthquakes of 1981. *J. Geophys. Res. 88*, 3247-3271, 1983.

Freed A.M., and J. Lin, Delayed triggering of the 1999 Hector Mine earthquake by viscoelastic stress transfer, *Nature 411*, 180-183, 2001.

Gershenfeld N., *The nature of mathematical modeling*, Cambridge University Press, Cambridge, 1999.

Gomberg, J., N. M. Beeler, M. L. Blanpied and P. Bodin, Earthquake triggering by transient and static deformations, *J. Geophys. Res. 103*, 24,411-24,426, 1998.

Hill D.P., *et al.*, Seismicity remotely triggered by the magnitude 7.3 Landers, California, earthquake, *Science 260*, 1617-1623, 1993.

Jacques E., C. Monaco, P. Tapponier, L. Tortorici, and T. Winter, Faulting and earthquake triggering during the 1783 Calabria seismic sequence. *Geophys. J. Int. 147*, 499-516, 2001.

Kagan Y.Y., and D.D. Jackson, Long-term earthquake clustering. *Geophys. J. Int. 104*, 117-133, 1991a.

Kagan Y.Y., and D.D. Jackson, Seismic gap hypothesis: ten years after. *J. Geophys. Res. 96*, 21419-21431, 1991b.

Kagan Y.Y., and D.D. Jackson, New seismic gap hypothesis: five years after. *J. Geophys. Res. 100*, 3943-3959, 1995.

Kenner S.J., and P. Segall, Postseismic deformation following the 1906 San Francisco earthquake, *J. Geophys. Res. 105*, 13195-13209, 2000.

King G.C.P., R.S. Stein, and J. Lin, Static stress changes and the triggering of earthquakes, *Bull. Seismol. Soc. Am. 84*, 935-953, 1994.

Klotz J., G. Khazaradze, D. Angermann, C. Reigber, R. Perdomo, O. Cifuentes, Earthquake cycle dominates contemporary crustal deformation in central and Southern Andes. *Earth Plan. Sci. Lett 193*, 437-446, 2001.

Lay T., and T.C. Wallace, *Modern global seismology*, Academic Press, San Diego, 1995.

Marzocchi, W., Remote seismic influence on the large explosive eruptions, *J. Geophys. Res. 107(B1)*, 10.1029/2001JB000307, 2002.

Marzocchi W., R. Scandone, and F. Mulargia, The tectonic setting of Mount Vesuvius and the correlation between its eruptions and the earthquakes of the Southern Apennines. *J. Volcan. and Geoth. Res. 58*, 27-41, 1993.

Marzocchi W., and F. Mulargia, Stress pulses in Southern Italy, *Geophys. Res. Lett. 22*, 29-32, 1995.

Marzocchi W., E. Casarotti, A. Piersanti, Modeling the stress variations induced by great earthquakes on the largest volcanic eruptions of the 20^{th} Century, *J. Geophys. Res. 107(B11)*, 2320, doi:10.1029/2001JB001391, 2002.

Nishenko S.P., and L.R. Sykes, Comment on "Seismic gap

hypothesis: ten years after" by Y.Y. Kagan and D.D. Jackson, *J. Geophys. Res. 98*, 9909-9916, 1993.

Pacheco J.F., and L.R. Sykes, Seismic moment catalog of large shallow earthquakes, 1900 to 1989, *Bull. Seismol. Soc. Am. 82*, 1306-1349, 1992.

Pantosti D., D.P. Schwartz, and G. Valensise, Paleoseismology along the 1980 surface rupture of the Irpinia fault; implications for earthquake recurrence in Southern Apennines, Italy. *J. Geophys. Res. 98*, 6561-6577, 1993.

Piersanti A., Postseismic deformation in Chile: constraints on the asthenospheric viscosity, *Geophys. Res. Lett. 26*, 3157-3160, 1999.

Piersanti A., G. Spada, R. Sabadini, and M. Bonafede, Global postseismic deformation, *Geophys. J. Int. 120*, 544-566, 1995.

Piersanti A., G. Spada, and R. Sabadini, Global postseismic rebound of a viscoelastic Earth: Theory for finite faults and application to the 1964 Alaska earthquake, *J. Geophys. Res. 102*, 477-492, 1997.

Pollitz F.F., Postseismic relaxation theory on the spherical Earth, *Bull. Seismol. Soc. Am. 82*, 422-453, 1992.

Pollitz F.F., and I.S. Sacks, The 1995 Kobe, Japan, earthquake: a long-delayed aftershock of the offshore 1944 Tonankai and 1946 Nankaido earthquakes, *Bull. Seismol. Soc. Am. 87*, 1-10, 1997.

Pollitz F.F., R. Bürgmann, and B. Romanowicz, Viscosity of oceanic asthenosphere inferred from remote triggering of earthquakes, *Science 280*, 1245-1249, 1998.

Ripley B.D., *Stochastic simulations*, John Wiley and Sons, New York, 1987.

Romanowicz B., Spatiotemporal patterns in the energy release of great earthquakes, *Science 260*, 1923-1926, 1993.

Rydelek P.A., and I.S. Sacks, Large earthquake occurrence affected by small stress changes, *Bull. Seismol. Soc. Am. 89*, 822-828, 1999.

Schwartz D.P., and K.J. Coppersmith, Fault behavior and characteristic earthquakes: examples from the Wasatch and San Andreas fault zones. *J. Geophys. Res., 89*, 5681-5698, 1984.

Stacey F.D., *Physics of the Earth*, John Wiley, New York, 1977.

Stein R.S., G.C.P. King, and J. Lin, Change in failure stress on the southern San Andreas fault system caused by the 1992 magnitude=7.4 Landers earthquake, *Science 258*, 1328-1332, 1992.

Stein R.S., G.C.P. King, and J. Lin, Stress triggering of the 1994 M=6.7 Northridge, California, earthquake by its predecessors, *Science 265*, 1432-1435, 1994.

Sykes L.R:, and S.P. Nishenko, Probabilities of occurrence of large plate rupturing earthquakes for the San Andreas, San Jacinto, and Imperial faults, California, 1983-2003. *J. Geophys. Res. 89*, 5905-5927, 1984.

Thatcher W., Non linear buildup and earthquake cycle on the San Andreas fault. *J. Geophys. Res. 88*, 5893-5902, 1983.

Viti M., D. Albarello, and E. Mantovani, Rheological profiles in the Central-Eastern Mediterranean. *Ann. Geophys. 15*, 849-864, 1997.

Chapter 3

FM0076 and FM7789 catalogs

A worldwide seismic catalog of source parameters is an important tool in many geophysical studies. Such a kind of database is available only since 1977 with the CMT catalog. The main goal of this chapter is to compile a similar catalog for the time period 1900-1976 estimating the focal parameters of shallow seismicity (depth $\leq$ 70 Km) with $M_s \geq 7.0$ (607 events). In particular, this new catalog (FM0076) contains strike, dip, rake, and depth estimations for 588 earthquakes in the period 1900-1976. At each estimate two reliability flags are assigned. The first is linked with the availability of data, and the second is given by comparing focal mechanism estimations and the tectonics of the epicentral area. The estimation procedure is based on the knowledge of the moment tensor of shallow earthquakes after 1977. From these data, the new concept of Weighted Cumulative Moment Tensor (WCMT), which represents such a kind of moment tensor for a mean earthquake in the epicentral area, leads to estimate the focal parameters. The estimation method is also tested by comparing out our dataset for the period 1977-1989 (FM7789) with the CMT one (91 events). This comparison reveals a good agreement between the two meth-

ods and confirms the reliability of the catalog FM0076.

3.1 Introduction

The knowledge of focal mechanism of the earthquakes is of fundamental importance in many geophysical research fields. For instance, all studies about earthquake-earthquake and earthquake-volcano interactions [*King and Cocco*, 2000 and references therein; *Nostro et al.*, 1998; *Marzocchi et al.*, 2002], tectonic evolution of plate boundaries [*Pollitz and Sacks*, 1997], and so on, are based on this knowledge.

The CMT catalog [*Dziewonski and Anderson*, 1981; *Dziewonski and Woodhouse*, 1983] supplies such a kind of information, giving a systematic estimate of focal parameters of the worldwide seismicity since 1977 (complete for $M \geq 5.5$).

Before 1977, only some sporadic focal mechanism estimations are available, overall for very large earthquakes [*Ben-Menahem and Toksoz*, 1963; *Kanamori*, 1970; *Wu and Kanamori*, 1973; *Kanamori and Cipar*, 1974; *Kanamori*, 1977; *Beck and Christensen*, 1991; *Johnson et al.*, 1994], or for such particularly well known regions, as California, Japan, or Italy [e.g., *Working Group CPTI*, 1999; *Deng and Sykes*, 1997; *Ando*, 1975]. In any case, a complete worldwide data set for focal mechanisms before 1977 is still lacking.

The aim of this study is to try to fill this gap providing a focal mechanism estimation for shallow (depth $\leq$ 70 Km) earthquakes occurred since 1900 with $M_S \geq 7.0$. The database of the epicenter of these events is the Pacheco and Sykes worldwide catalog [hereinafter PSC; *Pacheco and Sykes*,1992] which covers the period 1900-1989.

The estimation method is based on the computation of a mean seismic moment tensor of neighboring earthquakes

close to each event of PSC. The mean moment tensor is computed by using the source parameters of neighboring earthquakes occurred after 1977 for which a seismic moment tensor estimation exists [*Dziewonski and Anderson*, 1981; *Dziewonski and Woodhouse*, 1983; *CMT Catalog*, http://www.seismology.harvard.edu/projects/CMT/]. Then, the best double couple is estimated from the mean moment tensor relative to each event contained in PSC. In the same way, also a characteristic depth is defined.

Finally, a new catalog (FM0076) is compiled, which adds hypocenter, depth, and source planes solutions to PSC information, i.e., location, origin time, magnitude, and scalar seismic moment to 588 events. FM0076 contains also the choice of the fault plane between the two focal planes of the mechanism. Every estimate is also accompanied by two reliability indexes. The first (H, or L) is linked to the availability of data for the estimation (see paragraph *Test of accuracy*), and it is independent from the plane selection. The second (A, B, C, or D) is, instead, assigned after the comparison between the focal mechanism estimation and the tectonics of the epicentral area (see paragraph *Plane selection*).

The focal mechanisms estimated for the earthquakes after 1977 (catalog FM7789) are used to check the goodness of FM0076 estimates. The check is performed by comparing our estimations with the ones provided by the CMT catalog. The overlapping of the two catalogs CMT and PSC covers the years 1977-1989 and it consists of 91 events. In order to make an unbiased comparison, these 91 CMT estimates (and their sequences) are not used in calculating our estimations (see below).

As a further check for the reliability of the FM0076 source estimations, we compare our estimations of the focal mechanisms relative to the six greatest earthquakes before 1976

with the ones reported in previous works.

3.2 Dataset

The *Pacheco and Sykes* catalog [1992] contains 698 $M_s \geq 7.0$ shallow (depth ≤ 70 Km) earthquakes, worldwide distributed, occurred in the period 1900-1989 (whose 607 before 1977 and 91 after). Specifically, the catalog reports for each event the epicentral coordinates, origin time, estimates of the magnitude and of the seismic moment and, sometimes, depth.

The CMT catalog [e.g., *Dziewonski et al.*, 1981; *Dziewonski and Woodhouse*, 1983] contains seismic events worldwide distributed occurred after 1977. The CMT dataset for each event gives epicenter coordinates, origin time, depth, seismic scalar moment, the moment tensor, and the focal mechanism described in term of strike, dip and rake angles, relative to the best double couple solution for the moment tensor observed.

3.3 Cumulative Weighted Tensor Method

The goal of this study is to estimate the focal parameters and depth for $M_S \geq 7.0$ shallow events (depth ≤ 70 Km) between 1900 and 1976. The basic idea behind the method is that the focal parameters of earthquakes are similar for events occurred in the same region, even though in different time period [*Kagan*, 1992; 2000]. In other words, we assume that in a small area the tectonic stress field is roughly constant on space and time (at least for about one century) and it is the main responsible for the faults geometrical orientation (at least for high magnitude earthquakes).

In this study, the capital letters C,P, and E are added to all symbols which represent the parameters and indicate the origin of the data. In particular C,P, and E refer, respectively, to CMT catalog, to PSC, and to our estimates, collected in FM0076. For the generic k-th event, we define the origin time with t_k, epicentral coordinates with $\vec{x}_k$, depth with d_k, and, finally, the seismic moment tensor with $\mathbf{M}_k$.

The method can be summarized in 4 steps.

1. *Definition of the area*

   We set a specific area A_k for each k-th PSC earthquake, which is defined as

   $$A_k = S_{\vec{x}_k^{(P)}}(R) \tag{3.1}$$

   where $S_{\vec{\nu}}(R)$ is a circle centered in $\vec{\nu}$ with radius R. The circle radius R has been set up to 200 Km. We will discuss later this choice (see paragraph *Test of accuracy*).

2. *Data extraction*

   We select from the CMT catalog all the earthquakes occurred in each area A_k.

3. *Data filtering*

   - To avoid a systematic bias of the estimations in the overlapping period 1977-1989, i.e., in catalog FM7789, we do not consider the events of the CMT catalog occurred close in time to the origin time $t_k^{(P)}$ of each PSC event. So the m-th CMT earthquake is not taken into account, even though $\in A_k$, when

     $$|t_m^{(C)} - t_k^{(P)}| \leq 90 \qquad \text{days} \tag{3.2}$$

     In this way, to estimate the parameters of an earthquake occurred in the period 1977-1989, i.e., in the

FM7789 catalog, (the time interval used to check the validity of the method), we do not use the event itself and its seismic sequence.

- Since PSC contains only the shallow seismicity (depth ≤ 70 Km) we do not consider the CMT events when

$$d_m^{(C)} > 70 \qquad \text{Km} \tag{3.3}$$

After these first three steps, the number of selected earthquakes of the CMT catalog for the k-th PSC earthquake is N_k.

4. *Estimation method*

The focal mechanism of each PSC earthquake is computed by using the concept of Weighted Cumulative Moment Tensor, (from now on WCMT) $\mathcal{M}_k^{(E)}$. The WCMT is a modification of the Cumulative Moment Tensor introduced by Kostrov [1974] to estimate tectonic motion in seismically deforming areas. This method consists of summing the moment tensor for all the earthquakes in a given area, and then to extract the best double couple for such a cumulative tensor.

The WCMT is a modification of this method. Here, in fact, we are interested in estimating the focal mechanism of an earthquake occurred in a given point, not to provide a mean focal mechanism of a specific area. For this reason, we compute the WCMT weighting also for the spatial distances of neighbors to the point we are interested in. In particular, we have

$$\mathcal{M}_k^{(E)} = \frac{\sum_{m=1}^{N_k} \mathbf{M}_m^{(C)} \omega_{mk}}{\sum_{m=1}^{N_k} \omega_{mk}} \tag{3.4}$$

where ω_{mk} is

$$\omega_{mk} = \frac{1}{\Delta_{mk}^2} \tag{3.5}$$

and Δ_{mk} is the distance between the m-th (from CMT) and the k-th (from PSC) epicenters.

In this way, $\mathcal{M}_k^{(E)}$ takes properly into account the seismic energy and the distance of nearest neighbors. Then, it is possible to compute the best double couple planes for the source, i.e., strike $\phi^{(E)}$, dip $\delta^{(E)}$ and rake $\rho^{(E)}$ for both planes, from $\mathcal{M}_k^{(E)}$ [*Dziewonski et al.*, 1987].

We apply a similar method to estimate the depth, computing for each PSC event the weighted (with the distance) average of the CMT nearest neighbors. With the same symbols defined before, we write the estimated depth of the k-th PSC earthquake

$$d_k^{(E)} = \frac{\sum_{m=1}^{N_k} d_m^{(C)} \omega_{mk}}{\sum_{m=1}^{N_k} \omega_{mk}} \tag{3.6}$$

where the sum is restricted to only CMT events occurred in the area A_k.

The accuracy of the estimate of focal parameters and depths will be shown in the next sections.

3.4 Plane selection

The greatest earthquakes are generally closely linked to the tectonic setting and known fault features of each area. This coupling is the base of the WCMT method, but it is also relevant to discriminate between the two planes of the best double couple solution.

In the following description, we refer to the concept of thrust, normal and strike slip faults. In this chapter we define:

- thrust fault (TF): when $110 \geq \rho_{1,2} \geq 70$
- normal fault (NF): when $-70 \geq \rho_{1,2} \geq -110$
- strike slip fault (SSF): when $\mid \rho_i \mid \leq 20$ or $\mid \rho_i \mid \geq 160$, $i = 1, 2$

where $\rho_{1,2}$ represents the rake angles of the two solutions.

In the following, we summarize the criteria used to choice the preferred focal plane.

1. *Automatic step*
   - When TFs have one fault plane with a dip angle $\delta <$ 45 and the second fault plane has a dip $>$ 45, the former plane is considered the correct one.
   - When NFs have one fault plane with a dip angle $\delta <$ 45 and the second fault plane has a dip $>$ 45, the second plane is considered the correct one.
2. *Manual step and final selection*

   This step is based on the comparison between each nodal solution and the active known features in the hypocenter area. We analyze all focal solutions, also the ones selected in the previous step.

   The rules for the comparison can be summarized as follows.
   - For SSF: we compare the strike alignment with the local features and compatibility with the tectonic field.
   - For TF: we consider that the strike has to be coherent with the slab. When both strike directions are aligned, the smallest dip angle has been selected.

- For NF: we consider the strike alignment with pre-existing features. When both strike directions are aligned, the biggest dip angle is selected.

- For intermediate faults: the alignment between strike estimates and known active faults on each area is considered.

When there is ambiguity, we do not select any preferred plane to the earthquake.

In order to describe the accuracy of the selection, at each preferred solution is assigned a flag. This flag does not depend on the estimation accuracy, but only on the alignment between preferred fault plane and pre-existent fault features. The flag is assigned by the following criterion:

- A: good alignment between the focal mechanism chosen and the pre-existing faults.

- B: good alignment between the focal mechanism chosen and the pre-existing faults, but one angle has a significant discrepancy from what expected (i.e., ≥ 40 degree)

- C: both planes do not exactly fit the active faults, but one of them is coherent with the local tectonic field (i.e., compressive, distensive, and transcurrent)

- D: the selection has not been possible

Another flag, linked to the reliability of each estimation, will be assigned in the following. This second flag follows the observation of the results of the test of accuracy and is not plane selection dependent (see paragraph *Test of Accuracy*).

3.5 Accuracy of the estimates

3.5.1 Angle transformations

We transform the strike and dip angles in order to avoid definition problems. In particular, we set

$$\begin{cases} S = \phi \\ D = \delta \end{cases} \quad \text{for} \quad 0 \leq \phi < 180 \tag{3.7}$$

$$\begin{cases} S = \phi - 180 \\ D = 180 - \delta \end{cases} \quad \text{for} \quad 180 \leq \phi < 360 \tag{3.8}$$

where ϕ and δ are the strike and dip angles respectively.

The change in variables is through a 1-1 transformation, therefore it is invertible; moreover, this change solves a verse definition problem linked to the choice of the dip angle. In fact the strike is defined to make the dip ≤ 90. This definition sets an effective coupling between these independent angles. The transformation in 7 and 8 breaks such a coupling.

Let us consider, for instance, two fault planes defined by

$$\text{Plane} \quad 1 \rightarrow \begin{cases} \phi = \overline{\phi} \\ \delta = 90 - \epsilon \end{cases} \tag{3.9}$$

$$\text{Plane} \quad 2 \rightarrow \begin{cases} \phi = \overline{\phi} + 180 \\ \delta = 90 - \epsilon \end{cases} \tag{3.10}$$

The angle between Plane 1 and Plane 2 is exactly 2ϵ. Although for small ϵ the two planes are almost the same, $\Delta\phi$ is always equal to 180. Instead, using the change of angles defined in 7 and 8, we can see that

$$\begin{cases} S_1 - S_2 = 0 \\ |D_1 - D_2| = 2\ \epsilon \end{cases} \tag{3.11}$$

Therefore differences on angles are small when planes are close.

Equations 3.7 and 3.8 lead to change the definition domain of strike and dip. In fact, the new domains of S and D are

$$\begin{cases} S \in [0, 180[\\ D \in [0, 180[\end{cases} \tag{3.12}$$

3.5.2 Test of accuracy

In the previous sections, we describe the procedure to estimate the focal mechanism for almost all the earthquakes contained in PSC. Part of this catalog overlaps the CMT catalog, i.e., in the period 1977-1989. The data in this time interval are used to test the accuracy of our method. This dataset is composed by 91 earthquakes.

Note that the parameters of these earthquakes contained in the CMT catalog are not used in the estimation procedure (see equation 3.2). This avoids a circular logic which could bias the results of the test.

We define the estimation errors ε_S, ε_D, and ε_ρ on stike S, dip D, and rake ρ as

$$\begin{cases} \varepsilon_S = \text{Min}(|S^{(C)} - S^{(E)}|, 180 - |S^{(C)} - S^{(E)}|) \\ \varepsilon_D = |D^{(C)} - D^{(E)}| \\ \varepsilon_\rho = \text{Min}(|\rho^{(C)} - \rho^{(E)}|, 360 - |\rho^{(C)} - \rho^{(E)}|) \end{cases} \tag{3.13}$$

For the depth, the estimation error ε_d is

$$\varepsilon_d = |d^{(C)} - d^{(E)}| \tag{3.14}$$

Since both CMT and our estimates contain two focal planes, we have to decide which solution of both sets should be compared. We assume that the correct couples to be compared are the ones for which the angle between the fault planes is

minimum. Specifically, let us denote with α_{ij} the angle between the i-th estimated plane, labeled with "E", and j-th CMT plane, labeled with "C". In this way we define a 2x2 tensor, $\{\alpha_{kl}\}_{k,l=1,2}$.

Let us call n,m the position of the minimum angle; that is

$$\alpha_{nm} = \mathrm{Min}(\alpha_{ij}; i, j = 1, 2) \tag{3.15}$$

Therefore the n-th estimated plane has to be compared with the m-th CMT plane. By this way, the other couple of planes to compare is set.

In Figure 3.1 and Figure 3.2 the angular errors distributions are reported. The numbers 1 and 2 are referred to the two focal planes of the best double couple in CMT data. Figure 3.3 shows the errors of the depth estimate.

The relevant results are reported in Table 3.1. Since the angles and depth distributions are not symmetrical, the median and the 10th, 20th, 80th and 90th percentiles are computed from data.

The errors are generally small. The 90th percentiles in the distributions are not steady because the dataset is composed by 91 events; for this reason, it has been reported the 80th percentiles too. Nevertheless, the most important value is the median. In Table 3.1, it is possible to see that this value is generally less than 15 degrees. Our estimates show a good agreement with CMT solutions and the discrepancies are close to the CMT estimation errors, which have been estimated to be a 10 degrees cone around eigenvectors of the moment tensor [*Dzienwonski and Woodhouse*, 1983; *Vannucci and Gasperini*, 2003].

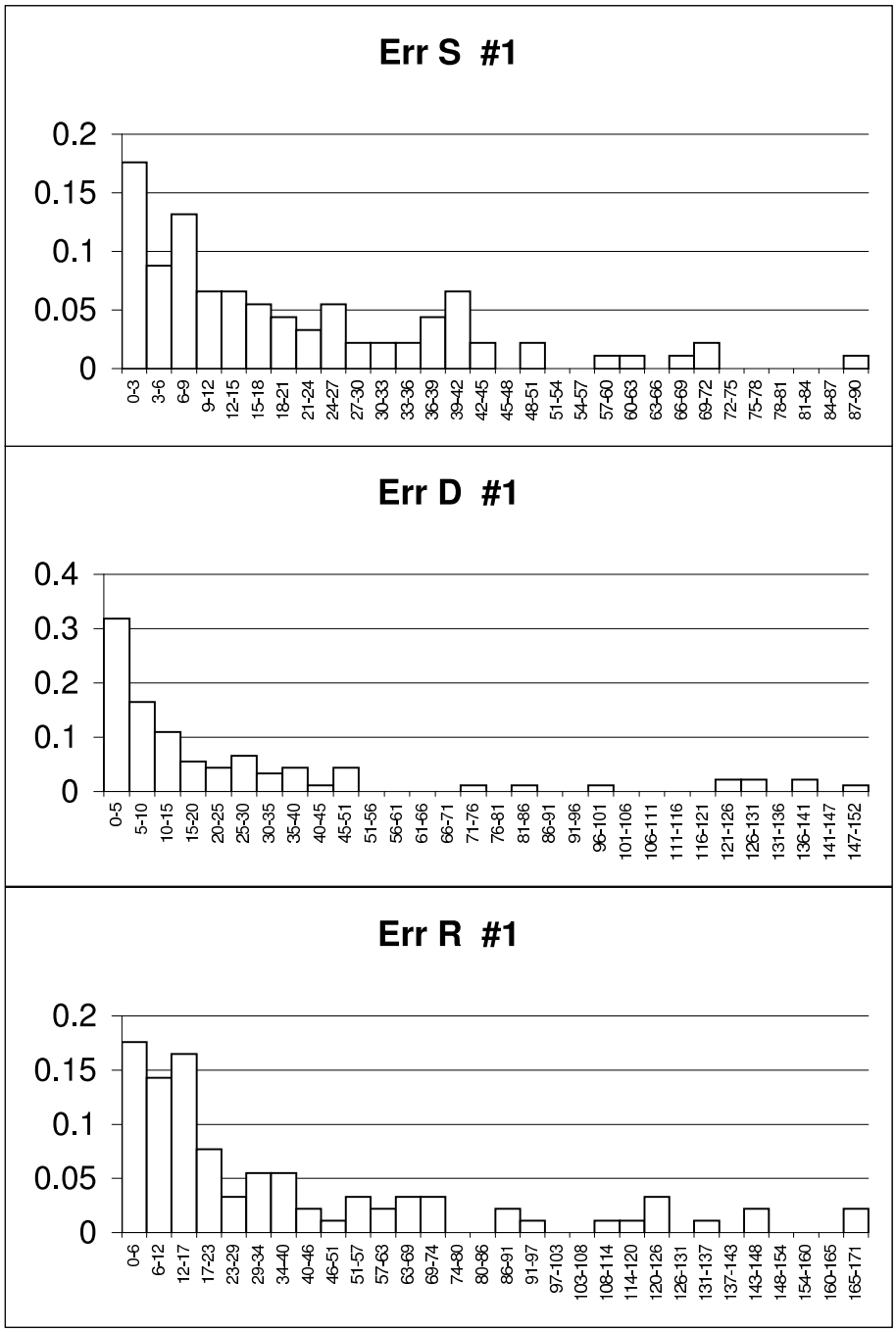

Figure 3.1: Error distributions of strike, dip and rake estimates [degree] for the first solution plane (#1).

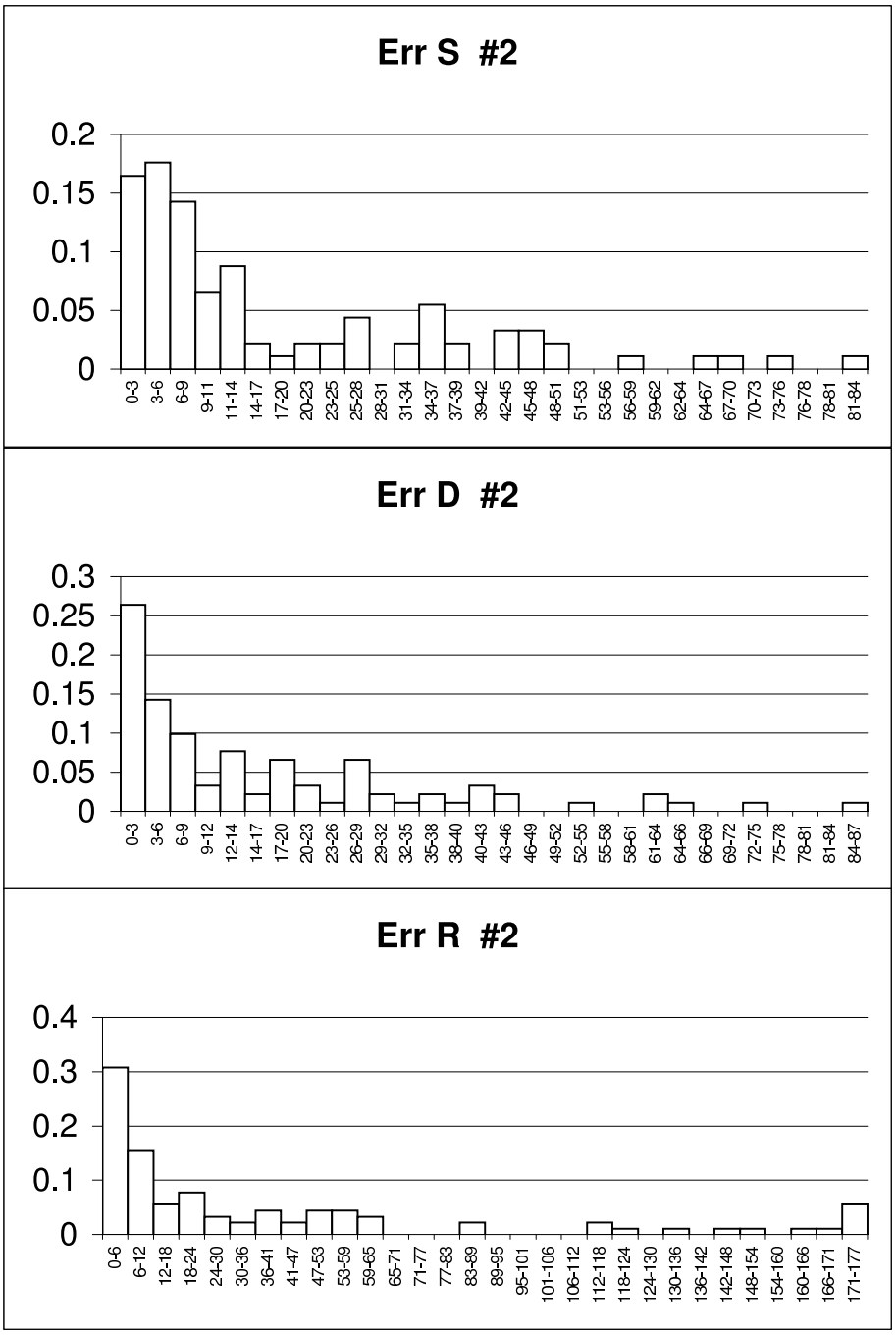

Figure 3.2: Error distributions of strike, dip and rake estimates [degree] for the second solution plane (#2).

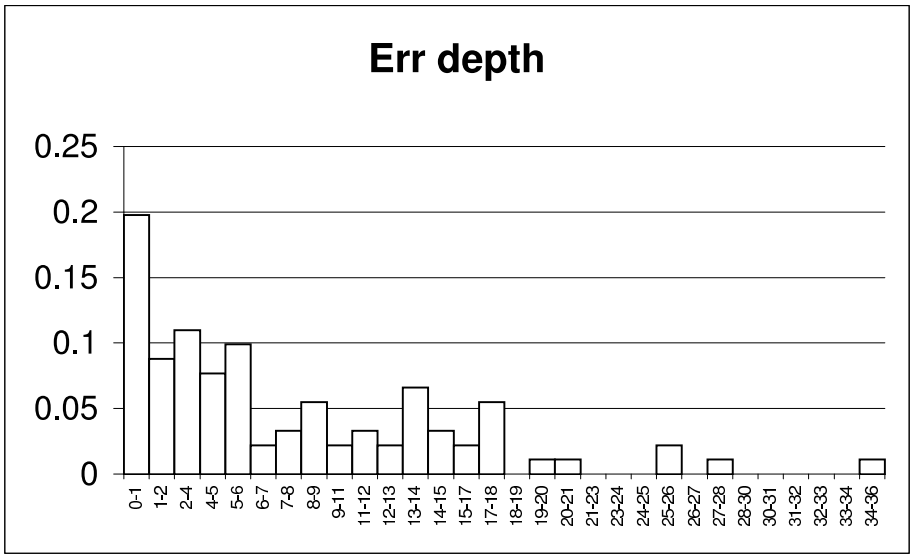

Figure 3.3: Error distribution of depth estimates [Km].

Table 3.1: Estimation errors; angles are written in degree, and depth in Km.

VARIABLE	10th PERC	20th PERC	MEDIAN	80th PERC	90th PERC
PLANE 1					
Err S	2	4	14	38	42
Err D	1	3	11	36	72
Err R	3	7	18	64	114
PLANE 2					
Err S	2	4	9	34	45
Err D	1	2	9	28	41
Err R	2	3	14	57	135
DEPTH	1	1	5	14	17

In Figure 3.3 the distribution of depth estimates is plotted. Also in this case a good agreement is observed.

As a further check, we compare our estimates of the focal mechanisms relative to the greatest earthquakes of the period 1900-1976 with estimations reported in literature.

In Table 3.2 we report our estimates of focal parameters and the ones from literature. This comparison shows that differences are generally small, inside the error bars previously

reported. The only exception is the Alaska 1964 earthquake estimation, where the errors on the dip and rake angles are large. We argue that such a discrepancy is due to the peculiar tectonic setting where the Alaska earthquake occurred. In fact, the epicenter of the event (61.10,-147.60) is located at the north-east end of its fault, in a complicated and multi-fractured area. This area represents the transition between the megatrust fault of Aleutian and the trascurrent faults of eastern Alaska, such as Farewell, Denali and Queen Charlotte faults. In this kind of transition area, the main assumption of this work (similarity of sources for near events) probably does not hold.

Table 3.2: Comparison of our estimates with sources estimated in previous works of the greatest events occurred in the period 1900-1976.

EVENT	FM0076	PREVIOUS ESTIMATES	SOURCE
KAMCHATKA 1952	(214,29,86) d = 40.52 Km	(214,30,90) d = 30 Km	Ben-Menahem and Toksoz, 1963
ALEUTIAN 1957	(245,22,85) d = 37.70 Km	(260,30,90) d = 40 Km	Johnson et al, 1994
CHILE 1960	subev 1 (350,16,83) d = 32.00 Km subev 2 (11,15,103) d = 32.00 Km	(7,20,90) d = 40 Km	Kanamori and Cipar, 1974
SOUTH KURILI 1963	(224,13,94) d = 40.00 Km	(223,22,90) d = 40 Km	Kanamori, 1977
ALASKA 1964	(227,57,-71) d = 30.00 Km	(245,20,90) d = 70 Km	Kanamori, 1970
ALEUTIAN 1965	(272,20,111) d = 35.00 Km	(289,18,142) d = 35 Km	Kanamori, 1977

Let us now introduce an important parameter that characterize each estimate. This parameter is the distance between each PSC earthquake epicenter and the nearest CMT event used.

In other words, we define $\overline{\Delta}_k$ as

$$\overline{\Delta}_k = \mathrm{Min}(\Delta_{kn}, n = 1, ..., N_k) \tag{3.16}$$

Although we use an average weighted with distance, it is clear that, when there are only far events, i.e., for great $\overline{\Delta}_k$, the estimates quality should worse quickly. In equation 3.1

the value of R, which has been fixed at 200 Km, represents an higher threshold in $\overline{\Delta}_k$. When this threshold is exceeded, the estimate is not computed. This choice is necessary in order to avoid an estimate based only on far earthquakes. Such a threshold does not allow estimating the focal parameters for 19 earthquakes.

In Figure 3.4 and 3.5 we report the median of angular errors of each plane, which are grouped into binned intervals, versus N_k (the number of CMT events used in each estimation), and $\overline{\Delta}_k$ respectively.

In Figure 3.4, we can see that the errors do not depend on N_k. On the other hand, in Figure 3.5 we can see that the estimates are better for small $\overline{\Delta}_k$. In particular, when $\overline{\Delta}_k < 60$ Km, errors greater than 30 degrees are not observed. The greater $\overline{\Delta}_k$ is, the worse the estimates are.

The behavior is in agreement with the assumption of our method. Indeed, figure 3.5 confirms that in a first approximation the parameters relative to an earthquake are similar for close events.

A flag "L" or "H" is then reported in FM0076 to indicate Low or High quality, respectively: "H" is reported for estimates with $\overline{\Delta}_k < 60$ Km; "L" is reported for 60 Km $\leq \overline{\Delta}_k \leq 200$ Km.

3.6 Catalogs FM0076 and FM7789

In this section the catalogs FM0076 and FM7789 are reported.

FM0076 contains all $M_s \geq 7.0$ shallow (depth $\leq 70Km$) earthquakes (607 events). The focal planes have been estimated for 588 of them. The fault plane has been selected in

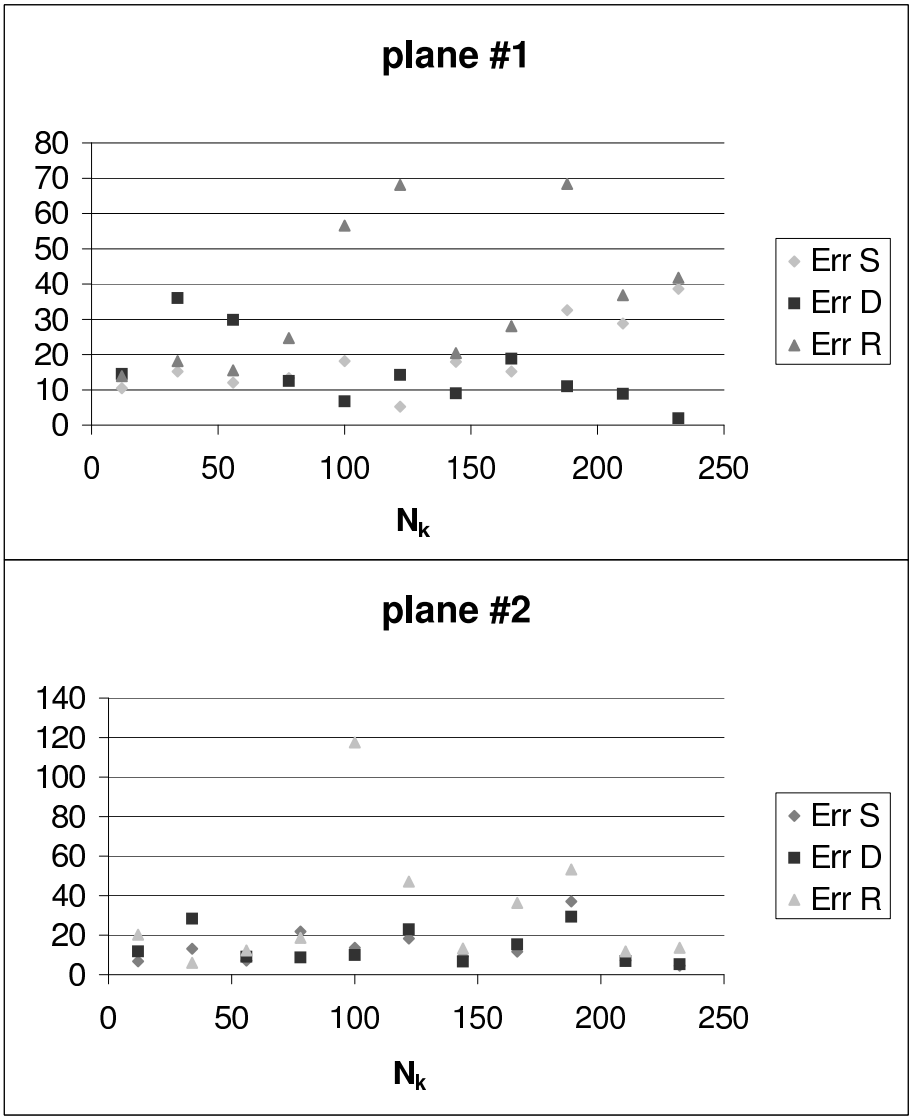

Figure 3.4: Angular errors versus the number of CMT events used in the computation. For each interval the median of data is plotted.

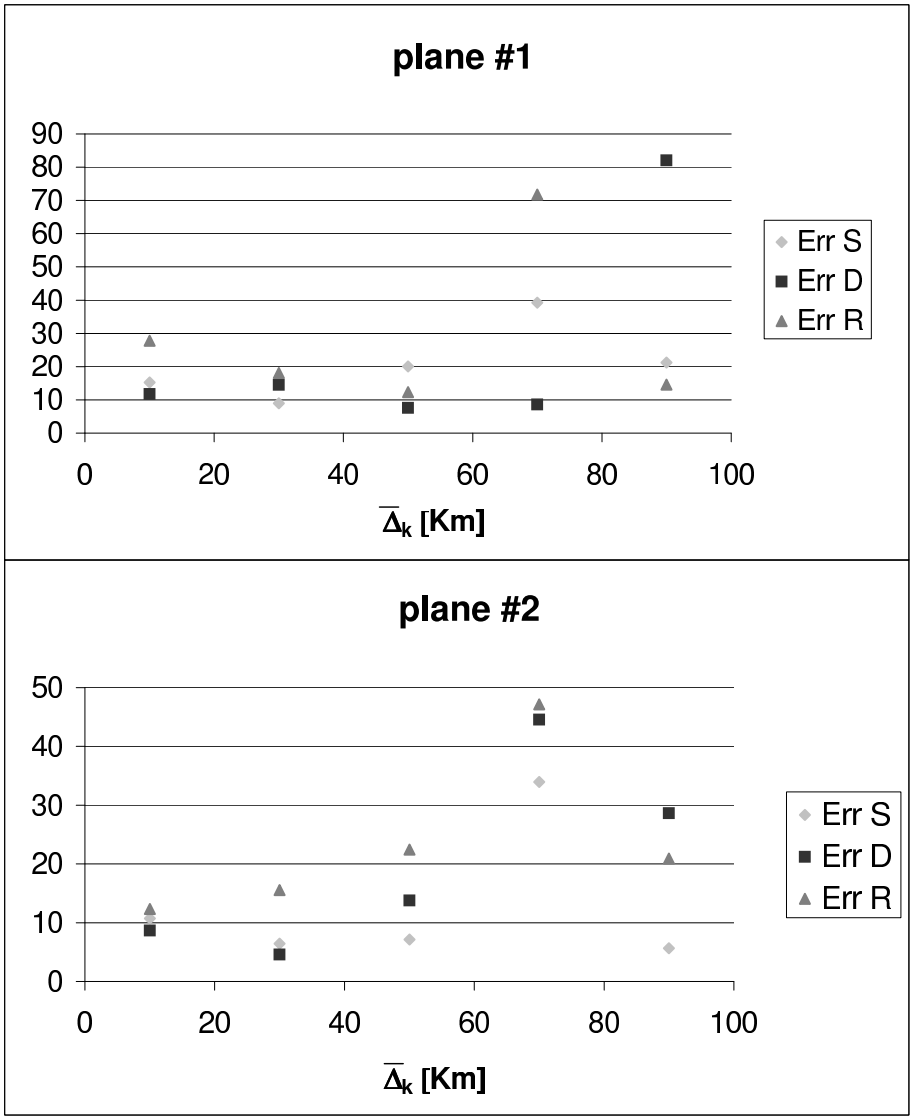

Figure 3.5: Angular errors versus the parameter $\overline{\Delta}_k$, representing distance of the nearest earthquake. For each interval the median of data is plotted.

537 events. The statistics relative to the estimation performances ad the accuracy flags are reported in Table 3.3.

In Table 3.4 the description of formats used in the catalogs are summarized.

The FM0076 catalog can be found in Appendix B, or on the web site http://www.bo.ingv.it/∼jacopo/EC0076/. In this website, it is also available the catalog FM7789, equivalent of FM0076 for the years 1977-1989.

Table 3.3: Estimations summary.

n events with estimation	n events without estimation	n high accuracy events (H)	n low accuracy events (L)	n high corrispondence planes (A)	n medium corrispondence planes (B)	n low corrispondence planes (C)	n of selection not done (D)
588	19	470	118	263	169	105	51

Table 3.4: Description of the FM0076 and FM7789 format.

VARIABLE NAME	SOURCE
EARTHQUAKES WITH ESTIMATION	
year, month, day, time	PSC
latitude, longitude	PSC
depth (Km)	PSC when available, WCMT otherwise
scalar moment($*10^{20} N\ m$)	PSC
location	PSC
flag of accuracy	H → High L → Low
strike, dip and rake # 1	estimated with WCMT
strike, dip and rake # 2	estimated with WCMT
plane selection	
flag of selection	A → Good agreement (Next selected plane) B → Sufficient agreement (Next selected plane) C → Selectable (Next selected plane) D → Not selectable
EARTHQUAKES WITHOUT ESTIMATION	
year, month, day, time	PSC
latitude, longitude	PSC
depth (Km)	PSC
scalar moment($*10^{20}$ Nm)	PSC
location	PSC
Message	
R (Km)	see paragraph 'Weighted Cumulative Moment Tensor Method'

3.7 Final remarks

The goal of this study has been to estimate the focal parameters of shallow (depth ≤ 70 Km) earthquakes with $M_s \geq 7.0$ occurred in the period 1900-1976 (607 events). In particular, we have provided strike, dip, rake and depth for most of the earthquakes contained in the *Pacheco and Sykes* [1992] catalog by means of a new estimation method.

The main assumption of the model is that close events have similar focal parameters and depth, even though occurred at different times. Using the data from CMT catalog (collected after 1977), we have computed, for each event from 1900 to 1977, a Weighted (with distance) Cumulative Moment Tensor, which represents a characteristic moment tensor for the each epicentral area. Then, the focal parameters have been computed from this moment tensor.

Through this new method, we have estimated the focal parameters and depth of 588 events and we have failed to provide an estimation only in 19 cases, for which there are not CMT events occurred within a distance of 200 Km from the epicenter. We have also selected the fault plane for 537 earthquakes, through comparison with known faults in the hypocentral area.

The goodness of the model has been checked by comparing our estimations for the 91 $M_s \geq 7.0$ shallow earthquakes occurred in the period 1977-1989 (FM7789 catalog) with the focal mechanism estimations reported in the CMT catalog. The results of the check confirm the goodness of the estimation model and the reliability of estimates.

The results obtained have been reported in a new worldwide catalog, called FM0076, which contain locations, time origins, scalar seismic moment and the new estimates of fo-

cal parameters, depth, and plane selection, of the $M_s \geq 7$ shallow (depth $\leq$ 70 Km) earthquakes occurred since 1900 to 1976.

References

Ando, M.. Source mechanisms and tectonic significance of historical earthquakes along the Nankai Trough, Japan. *Tectonophysics, 27,* 119-140, 1975.

Ben-Menahem, A., and M.N. Toksoz. Source mechanism from spectrums of long period surface waves, 2, The Kamchatka earthquake of November 4, 1952. *J. Geophys. Res., 68*, 5207-5222, 1963.

Beck, S.L., and Christensen, D.H.. Rupture Process of the February 4, 1965, Rat Islands Earthquake. *J. Geophys. Res., 96*, No B2, 2205-2221, 1991.

Deng, J., and L.R. Sykes. Evolution of the stress field in southern California and triggering of moderate-size earthquakes: A 200-year perspective. *J. Geophys. Res., 102*, No B5, 9859-9886, 1997.

Dziewonski, A.M., and D.L. Anderson. Preliminary reference Earth model (PREM). *Phys. Earth Plan. Int., 25*, 297-356, 1981.

Dziewonski, A.M., and J.H. Woodhouse. An experiment in systematic study of global seismicity: Centroid-moment tensor solutions for 201 moderate and large earthquakes of 1981. *J. Geophys. Res., 88*, 3247-3271, 1983.

Dziewonski, A.M., Ekström, G., Franzen, J.E., and J.H. Woodhouse. Centoid-moment tensor solutions for January-March 1986. *Phys. Earth Plan. Int. 45*, 1-10, 1987.

Johnson, J.M., Y. Tanioka, L.J. Ruff, K. Satake, H. Kanamori, and L.R. Sykes. The 1957 great Aleutian earthquake. *Pure Appl. Geoph.*, 142, 3-28, 1994.

Kagan, Y.Y., Correlations of earthquake focal mecanisms. *Geophys. J. Int., 110*, 305-320, 1994.

Kagan, Y.Y., "Temporal correlations of earthquake focal

mecanisms". *Geophys. J. Int., 143*, 881-897, 2000.

Kanamori, H., Alaska earthquake of 1964: radiation of long-period surface waves and source mechanism. *J. Geophys. Res., 75*, 5029-5040, 1970.

Kanamori, H., and J.J. Cipar. Focal process of the great Chilean earthquake My 22, 1960. *Phyis. Eearth Planet. Interiors, 9*, 128-136, 1974.

Kanamori, H., The energy release in great earthquakes. *J. Geophys. Res., 82*, 2981-2987, 1977.

King, G. C. P., and M. Cocco, Fault interaction by elastic stress changes: New clues from earthquake sequences, *Adv. Geophys. 44*, 1-38, 2000.

Kostrov, V.V., Seismic moment and energy of earthquakes, and seismic flow of rock. *Izv. Acad. Sci. USSR, Phys. Solid earth,* 13-21, 1974.

Marzocchi, W., Casarotti, E. and Piersanti, W., Modeling the stress variations induced by the great earthquakes on the largest volcanic eruptions of the 20th century. *J. Geophys. Res., 107*, B11, 2320, doi:10.1029/2001JB001391, 2002.

Nostro C., Stein, R.S., Cocco, M., Belardinelli, M.E., and Marzocchi, W., Two-way coupling betweeen Vesuvius eruptions and southern Apennine earthquakes, Itlay, by elastic stress transfer. *J. Geophys. Res., 103*, 24,487-24,504, 1998.

Pacheco, J.F., and L.R. Sykes. Seismic moment catalog of large shallow earthquakes, 1900 to 1989. *Bull. Seismol. Soc. Am., 82*, 1306-1349, 1992.

Pollitz, F.F. and Sacks, I.S., The 1995 Kobe, Japan, Earthquake: A Long-Delayed Aftershock of the Offshore 1944 Tononkai and 1946 Naikaido Earthquakes. *Bull. Seismol. Soc. Am., 87*, No 1, 1-10, 1997.

Vannucci, G., and Gasperini, P., A database of revised fault plane solutions for Italy and surrounding regions. *Com-*

puter & Geosciences, 29, 903-909, 2003.

Working Group CPTI. Catalogo Parametrico dei terremoti Italiani. ING,GNDT,SGA,SNN, Bologna, 99pp, 1999.

Wu, F.T., and Kanamori, H., Source Mechanism of February 4, 1965, Rat Island Earthquake. *J. Geophys. Res., 78*, No 26, 6082-6092, 1973.

Chapter 4

PVS on global scale

The strongest earthquakes of the last century were able to influence the seismicity at large spatio-temporal distances, extending their reach also at thousand of kilometers and decades later. We find differences between worldwide seismicity before and after the occurrence of such strongest earthquakes that have a low probability to be observed by chance. This behavior is discussed and interpreted in terms of co and post seismic stress transfer in a planet lying in a critical state. This result provides new insights which could be profitably used in seismic risk mitigation of many area of the world.

4.1 Method

The aim of this study is to analyze the worldwide seismicity in order to check if and how giant earthquakes modify the spatio-temporal occurrence of earthquakes, also at large distances and times. At this purpose, we consider a seismic datset composed by FM0076 + FM7789 [see *Chapter 3*], which contain the worldwide shallow (depth < 70 km) earthquakes with $M_s \geq 7$ occurred in the time interval 1900-1989 [*Pacheco and Sykes*, 1992] for which the focal mechanism

has been estimated [see *Chapter 3* and *Selva and Marzocchi*, 2004]. The catalogs contain the epicentral coordinates, the time origin, the estimates of magnitude and seismic moment, and the estimates of focal mechanisms for 628 seismic events. Note that this selection implies that we are assuming that the perturbation relative to the events removed from the catalog are a random sampling of the perturbations related to the whole seismic dataset. After 1977, it is also available the CMT catalog, but we choose to use FM7789 instead, in order to have an homogeneous dataset.

The analysis consists of the numerical modeling of ΔCFF and ΔCFF rate ($\Delta\dot{\text{C}}$FF) induced by the 5 largest earthquakes of the century (Kamchatka 1952, Aleutins 1957, Chile 1960, Alaska 1964, and Aleutins 1965) on earthquakes that occurred after and before them, and to check if these values are significantly different. The main rationale of the comparison is that if giant earthquakes have a significant influence on the occurrence of the worldwide earthquakes, we should find a statistical difference between ΔCFF and $\Delta\dot{\text{C}}$FF calculated before and after the occurrence of such giant earthquakes.

We calculate ΔCFF and $\Delta\dot{\text{C}}$FF by means of a spherical, viscoelastic, stratified and self-gravitating earth model [*Piersanti et al.* (1995), see Table 4.1], for the earthquakes occurred in the time period I that spans from 1928-1951, and in the time period II that ranges from 1966 to 1989. The two time intervals have the same length, and are before and after the giant earthquakes that occurred all between 1952 and 1965. The values of ΔCFF and $\Delta\dot{\text{C}}$FF for the events that occurred before the giant earthquakes establish the reference distribution for ΔCFF and $\Delta\dot{\text{C}}$FF in an unperturbed case, because obviously giant earthquakes cannot influence events occurred before. Since the time between source and receiving

earthquakes has to be positive in the model, at each event occurred before the giant earthquakes is attributed a fictitious time $t^\star = t_i + T_0$, where t_i is the real time of occurrence of the i-th earthquake and T_0 is the time interval between 1/1/1928 and 1/1/1965.

Table 4.1: Earth model parameters.

Model parameters	set values
Core radius	3471 Km
Mantle thickness	2620 Km
Mantle Maxwell viscosity	10^{21} Pa s
Asthenosphere thickness	200 Km
Asthenosphere Maxwell viscosity	5 10^{18} Pa s
Lithosphere thickness	80 Km

4.2 Results and preliminary discussion

We check the influence of giant earthquakes by means of 2 statistical tests relative to two different null hypothesis. The first null hypothesis ($H_0^{(1)}$) is that the probability to have positive values of the variable considered (ΔCFF and/or $\Delta\dot{\text{C}}$FF) for time periods I and II is equal to 0.5 (i.e., negative and positive values have the same probability); we use a binomial test to calculate the significance level at which we can reject $H_0^{(1)}$. The second null hypothesis ($H_0^{(2)}$) is that the median of ΔCFF and $\Delta\dot{\text{C}}$FF calculated in period I and II are equal; we use the Wilcoxon test to calculate the significance level at which we reject $H_0^{(2)}$.

The results of the binomial tests for the different datasets by using a viscosity of 5×10^{18} Pa s are reported in Table 4.2. From the table we can see that ΔCFF distributions do not show any significant difference before and after giant earthquakes, while $\Delta\dot{\text{C}}$FF shows a statistically increase after the

giant earthquakes; in other words, earthquakes occurred in period II are characterized by more positive values of $\Delta\dot{C}FF$ than the events occurred in period I. The second null hypothesis ($H_0^{(2)}$) of equivalence of the medians for the two periods can be rejected with a s.l. 0.07. We verify the stability of the results by using different viscosities (10^{18} and 10^{19} Pa s) and subsets of the seismic catalog where the focal mechanism are better constrained (A and B in FM0076 and FM7789, see *Chapter 3*). Notably, the use of the latter leads to an even more clear distinction between periods I and II.

Table 4.2: The results of the tests for the different datasets.

Dataset	# ΔCFF > 0	# $\Delta\dot{C}FF > 0$	total # of events	Binomial test, $H_0^{(1)}$	Wilcoxon test, $H_0^{(2)}$
I	83	92	176	0.27	0.07
II	79	113	173	< 0.01	

The results reported above stand for a significant perturbation of the giant earthquakes on the worldwide seismicity. The perturbation consists of variation of CFF rate that significantly increases (or decreases) the tectonic loading of a seismogenic fault. Remarkably, we do not find any difference in ΔCFF values, implying that the stress induced may be not the most relevant parameter in promoting changes in seismicity, at least over a large time-distance domain (see the discussion of the physical implications of this in section 5.3 *Modeling the seismicity changes* in *Chapter 5*). We argue that this influence of giant earthquakes can explain worldwide nonstationarities over time intervals of decades (see figure 4.1, *Chapter 2* and *5*). Despite this statistically significant relationship, we note that the postseismic stress rates have small values, in relative and absolute sense.

For what concern the small value in a relative sense, we

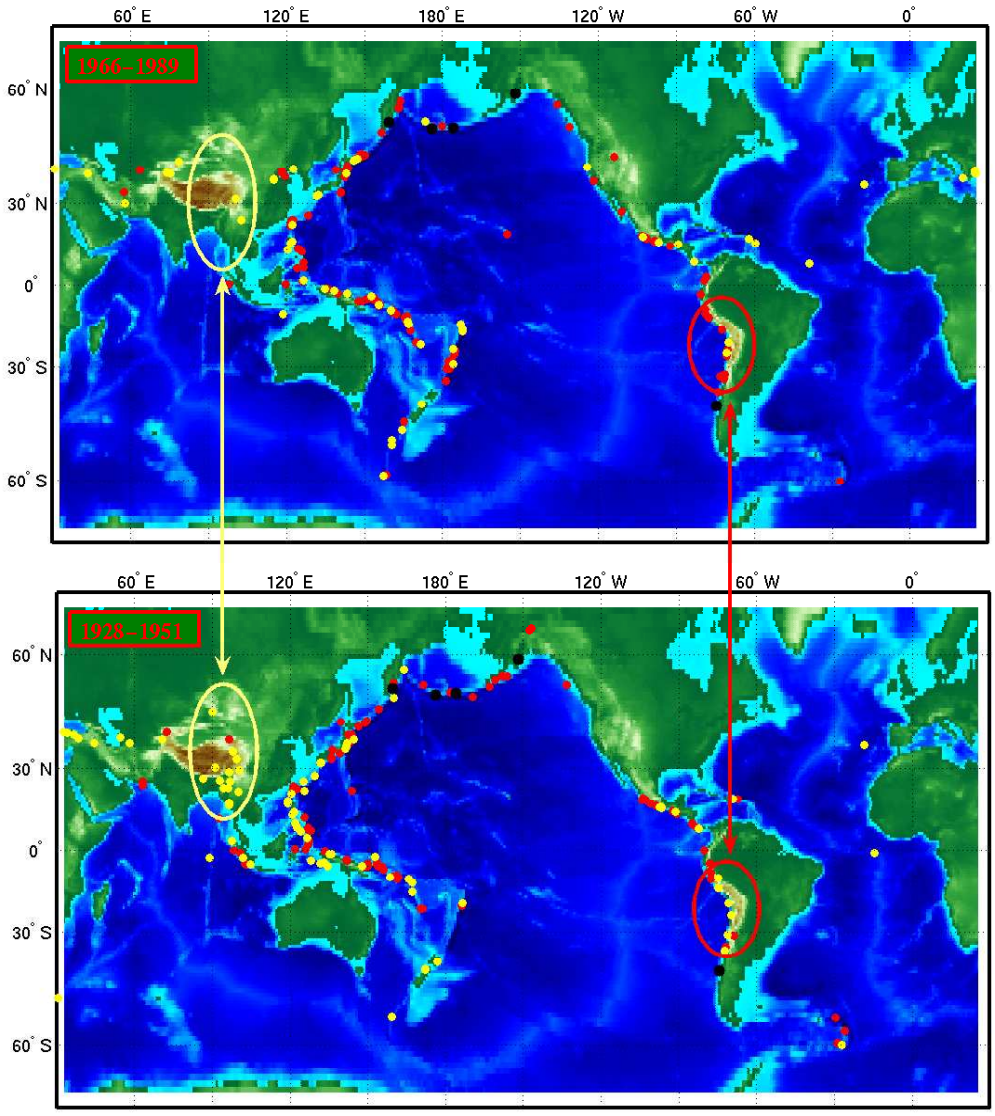

Figure 4.1: Comparison between Period I and Period II. Red dots indicate epicenters of events which experienced positive perturbation, i.e.,$\Delta\dot{\text{C}}\text{FF} > 0$, while yellow dots events with negative perturbation, i.e., $\Delta\dot{\text{C}}\text{FF} < 0$. In the map are highlighted areas which experienced nonstationarities.

argue that it may be misleading to compare $\Delta\dot{C}FF$ directly with the tectonic rate. At first, for a meaningful comparison we need to project the tectonic rate on the seismogenic structures; this operation may reduce the stress variation of one order of magnitude or more [cf. *King and Cocco*, 2000]. Then, it is certainly more useful to compare the amplitude of $\Delta\dot{C}FF$ with other processes that can perturb the system over a comparable time interval, rather than to the tectonic rate directly. Under this perspective, it is worth noting that the stability of the tectonic loading rate measured over time intervals of 5 order of magnitude different [tens to millions of years; e.g., *Sella et al.*, 2000; *De Mets et al.*, 1994]. This may be an important evidence of the extreme stability of the tectonic loading; in this case, the tectonic rate has very low natural fluctuations (at least over time intervals of decades), and, therefore, it may be significantly perturbed also by apparently small postseismic stress rates. Note that the same point may be valid also for static stress changes ΔCFF; in this case, it has been proposed that perturbations as large as tenth of bars may reasonably promote earthquakes [e.g., *Reasemberg and Simpson*, 1992], also at depth where the lithostatic pressure is also 4 orders of magnitude greater than such a proposed threshold.

Another relevant aspect involves the dimension of the area postseismically perturbed by the giant earthquakes; these areas are usually much larger than the one involved by perturbations induced by smaller local earthquakes; in other terms, local earthquakes may yield even higher local stress variations, but have a smaller average effect over a large area.

A discussion about the small value in an absolute sense implicitly assumes the existence of a stress threshold needed

to trigger an earthquake, whose even the existence requires further validation [e.g., *Rydelek and Sacks*, 1999, *Ziv and Rubin*, 2000]. Others have considered earthquake nucleation to be part of a critical system and thus highly sensitive to very small perturbations [e.g., *Turcotte*, 1997]. Under this perspective, we suggest that the only relevant aspect of the stress coupling is to quantify the change in probability of occurrence of an earthquake due to the stress perturbation induced by a remote seismic event [e.g., *Stein*, 1999; *Parson et al.*, 2000; *Marzocchi et al.*, 2003]. Here, the concept of stress threshold would lose any physical meaning; in general, we can surmise that the larger the stress induced, the more significant the change in probability of a seismic event.

For what concerns the practical aspect, we want to highlight that the presence of a systematic behavior in the data due to long-term interaction among earthquakes could have a significant impact in seismic risk mitigation, improving earthquake long-term forecasting.

References

DeMets, S., Fordon, R.G., Argus, D.F., and Stein, S., Effect of recent revisions to the geomagnetic reversal time scale on estimates of current plate motions, *Geophys. Res. Let. 21*, No. 20, 2191-2194, 1994.

King, G. C. P., and M. Cocco, Fault interaction by elastic stress changes: New clues from earthquake sequences, *Adv. Geophys. 44*, 1-38, 2000.

Marzocchi, W., J. Selva, A. Piersanti, and E. Boschi, On the long-term interaction among earthquakes: Some insight from a model simulation, *J. Geophys. Res. 108*, B11, 2538, doi:10.1029/2003JB002390, 2003.

Pacheco, J.F., and L.R. Sykes. Seismic moment catalog of large shallow earthquakes, 1900 to 1989. *Bull. Seismol. Soc. Am., 82*, 1306-1349, 1992.

Parson, T., S. Toda, R. S. Stein, A. Barka, and J. H. Dieterich, Heightened odds of large earthquakes near Istanbul: An interaction-based probability calculation, *Science, 288*, 661-665, 2000.

Piersanti, A., G. Spada, R. Sabadini, and M. Bonafede, Global postseismic deformation, *Geophys. J. Int. 120*, 544-566, 1995.

Reasenberg, P.A., and Simpson, R.W., Response of Regional Seismicity to the Static Stress Change Produced by the Loma Prieta Earthquake, *Science 255*, 1687-1690, 1992.

Rydelek, P. A., and I. S. Sacks, Large earthquake occurrence affected by small stress changes, *Bull. Seismol. Soc. Am. 89*, 822-828, 1999.

Sella, G.F., Dixon, T.H., and Mao, A., REVEL: A model for Recent plate velocities from space geodesy, *J. Geophys. Res. 107*, No. B4, 10.1029/2000JB000033, 2002.

Selva, J., and W. Marzocchi, Focal parameters, depth estimation, and plane selection of the worldwide shallow seismicity with $M_s \geq 7.0$ for the period 1900-1976, *Geochem. Geophys. Geosyst. 5*, Q05005, doi:10.1029/2003GC000669, 2004.

Stein, R. S., The role of stress transfer in earthquake occurrence, *Nature, 402*, 605-609, 1999.

Turcotte, D. L., *Fractals and Chaos in Geology and Geophysics*, Cambridge University Press, Cambridge, 1997.

Ziv, A., and A. M. Rubin, Static stress transfer and earthquake triggering: No lower threshold in sight?, *J. Geophys. Res. 105*, 13,631-13,642, 2000.

Chapter 5

PSV on local scale: Southern California

We investigate on the Southern California seismicity in order to characterize its time evolution during the last decades. We analyze the time series composed of the number of events per year, and the focal mechanisms of the earthquakes. The results show a statistically significant nonstationarity, with a change that occurred in the sixties in both time series. The seismicity before the change point is strictly linked to the San Andreas fault system; after the sixties, the seismicity appears to be more scattered in terms of focal mechanisms, and has a lower seismic rate. We provide a possible physical explanation of the significant nonstationarity by modeling the postseismic stress perturbation field induced by two giant earthquakes that occurred in the sixties, the Chile (1960) and Alaska (1964) earthquakes. At a first order, the postseismic stress rate seems to be in agreement with the changes in seismicity observed, supporting a causality hypothesis. The model also foretells the future behavior of the trend of Southern California seismicity; this (forward) prediction provides an important opportunity to validate the causal hypothesis of remote (and long-term) coupling between earthquakes.

5.1 Introduction

The stationarity of seismic activity is a basic fundamental assumption of seismic hazard assessments [e.g., *Cornell*, 1968], and, in general, of the models of the spatio-temporal distribution of earthquakes [e.g., *Kagan and Jackson*, 2000]. From a practical point of view, stationarity means that the average and natural variability of the rate of seismicity are constant over time intervals of decades, centuries, and in some cases up to thousands of years as in paleoseismicity studies [*Hanks and Schwartz*, 1987; *Pantosti et al.*, 1993]; in other terms, the seismicity over these time intervals is considered representative of what can happen in the future.

This paradigm implicitly requires that the seismicity of a specific zone may experience significant changes only over larger time intervals (i.e., million of years), on the scale of plate motion processes. The only significant departure from this picture on short time scale are aftershock sequences; such variations are usually removed through a declustering technique in order to make the seismic catalog stationary.

Remarkably, in spite of commonly assumed stationarity of seismicity over decades or centuries, some seismic areas show apparent variations over those time ranges. Some studies found that Southern California seismicity may have experienced significant changes in long-term activity, even though there is no agreement on the type of variations [cf. *Press and Allen*, 1995; *Jones and Hauksson*, 1997; *Marzocchi et al.*, 2003].

Here, we provide some new insights on this topic, by analyzing the Southern California seismic catalog of the last century, which is one of the most detailed and complete catalogs for small to moderate magnitudes. The specific goal

is to find and characterize possible nonstationarities from a phenomenological and physical point of view. We analyze the time evolution of the seismic rate, and of the focal mechanism of the earthquakes that occurred in Southern California since 1933, looking for statistically significant changes, and quantifying them to provide empirical constrains to physical modeling.

Since we are investigating variations over a time scale of decades, the physical model used to describe them has to act over comparable time scales. A possible candidate is the postseismic relaxation of viscoelastic layers beneath the crust [e.g., *Piersanti et al.*, 1997; *Pollitz et al.*, 1998], which has been suggested to be responsible for long-term coupling between earthquakes [e.g., *Romanowicz*, 1993; *Pollitz and Sacks*, 1997; *Freed and Lin*, 2001; *Chéry et al.*, 2001; *Casarotti et al.*, 2001; *Marzocchi et al.*, 2003], and earthquakes and volcanic eruptions [e.g., *Marzocchi*, 2002; *Marzocchi et al.*, 2002, 2004].

Here, we model the postseismic effects using a layered, stratified, self-gravitating and viscoelastic Earth model [*Piersanti et al.*, 1995, 1997]. In particular, we estimate the Coulomb Failure Function [ΔCFF; see *Stein et al.*, 1994; *King et al.*, 1994; *King and Cocco*, 2000] rate due to giant remote earthquakes that increase or decrease the tectonic stress loading applied to the faults located in Southern California. Note that this approach differs from the one usually followed in studies devoted to stress triggering, where the ΔCFF is used; our approach assumes that the overall rate of Southern California seismicity may be mostly perturbed by the ΔCFF rate evolution rather than its value. We discuss in depth this point in section 5.3.

Finally, we anticipate that a relevant aspect of the model

is the possibility to validate it in forward analysis since the future evolution of the rate of seismicity in Southern California may be forcast.

5.2 Searching for significant changes in seismicity

The seismic database used is the "small box" of the *s_cal* catalog, available in the Y. Kagan's web page (http://moho.ess.ucla.edu/~kagan/s_cal.dat). The catalog reports, for each event, the origin time, the hypocenter location, the magnitude, the focal plane, and the probability P_m that the event can be considered a mainshock. The catalog is considered complete since 1933 for magnitude ≥ 4.7 [*Field et al.*, 1999]. The declustering of the catalog is accomplished by removing all the events for which $P_m < 0.5$. Then we analyze the sequence of mainshocks that occurred in the "small box" from 1933 to 2003. The analysis consists of searching for and characterizing statistically significant changes in seismicity.

The search for possible change points in seismicity is performed by analyzing the annual rate of seismicity (R_t, $t = 1, ..., T$, where T is the number of years of the catalog), and the sequence of the rake angles of the events ($\rho_i = |\sin(Rake_i)|, i = 1, ..., N$, where N is the number of mainshocks in the catalog). The change point search is a still unsolved problem in statistics. A detailed discussion on this technical issue can be found in *Mulargia and Tinti* [1985]. In practice, a reasonable strategy to find possible change points has been proposed by *Mulargia and Tinti* [1985], who applied it successfully in many real and synthetic cases, where no assumptions on the type of statistical distributions of the random variables could be made [see also *Mulargia et al.*, 1987].

In brief, assuming a given significance level $\tilde{\alpha}$ in discriminating the different regimes, the method determines the change point according to a sequential scanning which, making use of Kolmogorov-Smirnov two-sample statistics, identifies the principal change point. We refer to this method as CPKS. Here, we also use a modification of the method by using the Wilcoxon test (CPW) rather than the Kolmogorov-Smirnov test, because we want to check specifically differences in the central values. Technical details on the CPKS and CPW methods can be found in *Appendix C* and *Appendix D*.

The results of CPKS and CPW methods applied to R_t and ρ_i are shown in Figure 5.1. We find a significant decrease ($\tilde{\alpha} < 0.01$) of R_t after the year 1959; this change is consistent with the independent results of an analogous test performed over the SCSN catalog in a slightly different region of Southern California [see *Marzocchi et al.*, 2003]. For ρ_i, we find a significant change point ($\tilde{\alpha} < 0.01$) in 1969. Both analysis lead to the identification of changes in the sixties, and the period 1959-1969 might be taken as a confidence interval of the change.

In order to characterize the changes found, we divide the seismic dataset into two sets, one containing the earthquakes in the periods 1933-1959 (C3359), and the other with earthquakes in the period 1965-2003 (C6503). Then, we perform a hierarchical cluster analysis with Euclidean distances (CLA) on the sets of focal mechanisms, i.e., strike, dip, and rake angles, of all earthquakes reported in C3359 and C6503. The details of the method can be found in *Anderberg* [1973] and *Hartigan* [1975]. To avoid the coupling between strike and dip angles given by the Aki convention [*Aki and Richards*, 1980], we apply a 1-1 transformation which make them in-

a)

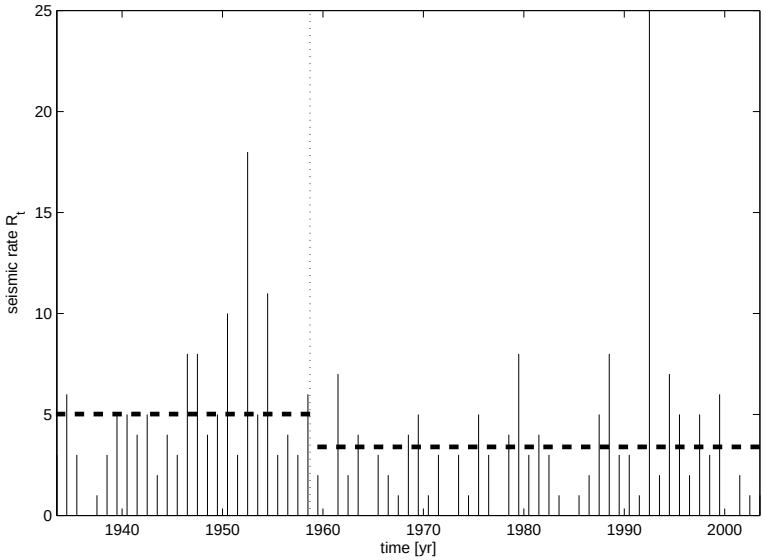

b)

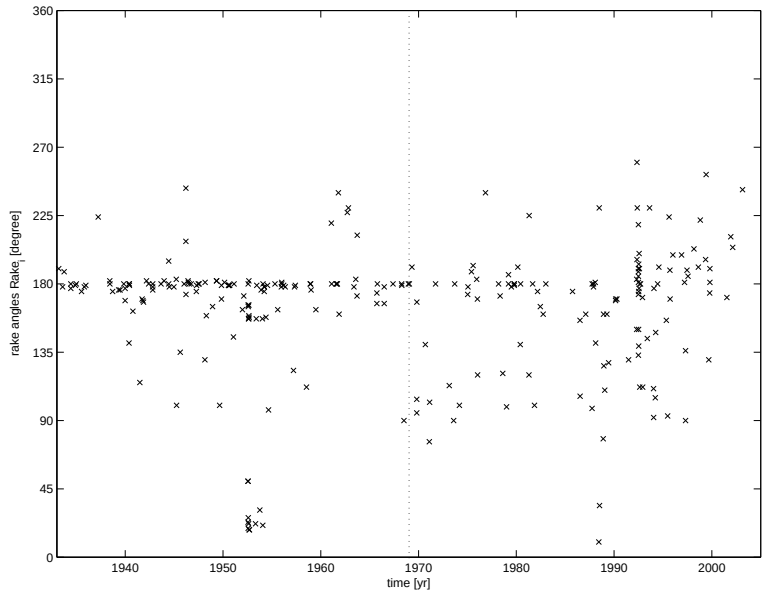

Figure 5.1: Time series of a) seismic rate R_t (the horizontal dashed line indicate the medians of R_t before and after the change point), and b) rake angles $Rake_i$. The vertical dashed lines indicate the timing of the found change points.

dependent [see, *Chapter 3*]. To prevent overfitting, we apply the Beale test [see, i.e., *Davis*, 2002] to chose the correct number of clusters in both periods.

The mean focal mechanism of each cluster (with at least $\geq 5\%$ of events) is reported in Table 5.1. In C3359 three clusters are observed. The clusters #2 and #3 cover 91% of the data and are composed by right-lateral events, with almost vertical fault planes and striking around 138 degrees. Their average mechanisms are compatible with San Andreas (SA) seismicity [*Jones*, 1988]. Cluster #1 contains left-lateral strike-slip events, striking almost perpendicularly to SA and can be interpreted as the conjugate mechanism of SA faults system. In summary, all the events that occurred in C3359 are linked to SA system.

Table 5.1: CLA results over the periods 1933-1959 and 1965-2001.

cluster	relative number of events	average strike	average dip	average rake
PERIOD 1933-1959				
cluster #1	8 %	62±6	72±3	27±12
cluster #2	78 %	138±17	93±14	170±18
cluster #3	13 %	138±8	96±12	-170±17
PERIOD 1965-2001				
cluster #1	13 %	113±16	49±9	109±14
cluster #2	48 %	140±18	95±17	169±14
cluster #3	7 %	105±15	142±13	98±16
cluster #4	28 %	149±16	94±19	-161±17

The CLA applied to C6503 shows that a significant part (about 20%) of the earthquakes have mechanisms which differ from the previous seismicity. In particular, while clusters #2 and #4 contain the SA system seismicity, clusters #1 and #3 are composed by dip-slip events that are not observed in the preceding period. Both inverse fault clusters contain about 45 dipping events, with a thrust rake. These

events are "not SA" earthquakes (NSA) which give a pattern to the period 1965-2003, that significantly differs from the preceding seismicity. This pattern confirms the results of *Press and Allen* [1995] that, through a pattern recognition method applied to a different dataset, found that after the sixties the earthquakes began to occur on structures not activated in the previous period.

Remarkably, the clusters show a small variance; this means that the average mechanism of each cluster represents well the cluster itself, and it could be considered as a "characteristic" event for the cluster.

5.3 Modeling the seismicity changes

The change point analysis points out that Southern California seismicity experienced major changes on the annual rate of earthquakes and on the type of earthquakes during the sixties. Such a change is linked to long-term variations of decades. Consequently, we argue that their cause has to have a comparable time behavior. Postseismic stress changes have characteristic times of several tens of years [*Piersanti et al.*, 1995, 1997; *Pollitz et al.*, 1998; *Kenner and Segall*, 2000], so that, in principle, they may provide a possible explanation of the long-term seismicity changes observed.

Here, we check the plausibility of this causality hypothesis by calculating the stress perturbations due to the Chile (1960) and Alaska (1964) earthquakes on the fault systems of Southern California activated during the past decades. We consider these two events because of two reasons: they occurred at the time of the change points found, and no very big earthquakes (i.e., with $M \geq 8.0$) occurred inside the region that can blur possible effects of these remote earth-

quakes. The perturbation field is studied in term of annual rates of the variations of the Coulomb Failure Function, i.e., $\Gamma = [\Delta\mathrm{CFF}(t) - \Delta\mathrm{CFF}(t - 1\mathrm{yr})]/1\mathrm{yr}$. In other words, Γ represents the numerical evaluation of the temporal derivative of ΔCFF, averaged over one year.

An implicit assumption of this choice is that variations of Γ are more important than the widely used ΔCFF [see, i.e., *King and Cocco*, 2000] to describe remote long-term coupling between earthquakes. Such an assumption deserves a careful discussion. As a general principle, we argue that Γ may be more effective to study the long-term coupling among earthquakes, because it can increase or decrease the tectonic stress loading rate [see *Marzocchi et al.*, 2003], that is ultimately strictly related to the seismic activity. In other words, we assume that temporal variations in the seismicity rate of a specific type of earthquakes (for instance, SA) is directly related to the time evolution of Γ.

The use of Γ instead of ΔCFF also accounts for the temporal evolution of stress loading of faults in a proper way. For the sake of example, let us consider a hypothetical case, in which the coseismic (elastic) stress change is positive, while the postseismic effect has a negative temporal trend which unloads the fault, i.e., see Figure 5.2, case 1. In this case, ΔCFF shows positive values for any time $t > 0$, i.e., earthquakes occurring at $t > 0$ are always "promoted" by the perturbation field. Instead, if we consider Γ, we have a positive value only for very short times, which characterize the coseismic effects (in practice few months; see *Dieterich*, 1994), while for longer times the postseismic stress rate Γ is negative, i.e., discourages other earthquakes, accounting for the fact that the perturbation works against tectonics loading. Similar discussions can be done for other cases (e.g., see Fig-

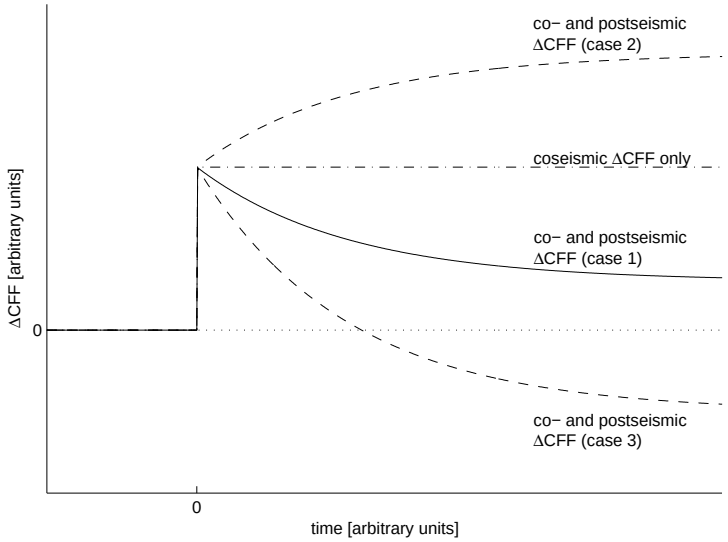

Figure 5.2: Different combinations of coseismic and postseimic stress variations. See the text for the discussion.

ure 5.2, cases 2 and 3), where the relative effects of co- and postseismic fields are different.

Another aspect of Γ worth noting is its time evolution. Just after the earthquake, Γ reproduces the prevision of ΔCFF, as it depends only on the coseismic stress step; the absolute value of Γ for short times is much higher than values achieved later, reproducing the high level of interactions observed in the aftershock sequences. At longer times Γ tends to 0, implying that the perturbation lasts for a finite time length, i.e., tens of years up to few centuries, depending on the viscosity of the relaxing layers.

Finally, note that the use of Γ is still more important if the nucleation process depends on the rate of increasing stress, such as the rate-and-state models show [e.g. *Dieterich*, 1994, and references therein].

5.3.1 Chile '60 and Alaska '64 stress perturbations

The model used to estimate the stress perturbation consists of a spherical, stratified, self-gravitating, and viscoelastic earth model [e.g., *Piersanti et al.*, 1995; 1997]. The parameters of the model are reported in Table 5.2. Figure 5.3 shows the variations of Γ induced by Chile '60 and Alaska '64 earthquakes on the characteristic faults defined through CLA and reported in Table 5.1. Both x and y axes are reported in arbitrary units. The reason is that both values, i.e., time and size of the perturbation, are strongly dependent on the chosen value of viscosity of the asthenosphere, while the general trend is not; in fact, the behavior versus time of Γ is identical in shape for all possible values of viscosity. The time behavior of Γ can be described by 4 consecutive phases: 1) Γ promotes NSA events and discourages SA events; 2) Γ discourages NSA events and promotes SA events; 3) Γ promotes NSA events and discourages SA events; 4) Γ promotes both NSA and SA events.

Table 5.2: Earth model parameters.

Model parameters	set values
Core radius	3471 Km
Mantle thickness	2620 Km
Mantle Maxwell viscosity	10^{21} Pa s
Asthenosphere thickness	200 Km
Asthenosphere Maxwell viscosity	10^{18} - 10^{19} Pa s
Lithosphere thickness	80 Km

Note that the first effect detected by the model is the decrease of the number of events along SA and an increase of NSA events. This behavior is observed in the data, where after 1965 the number of events decreases significantly and NSA events begin occurring. Figure 5.4 reports Γ, Γ^N (nor-

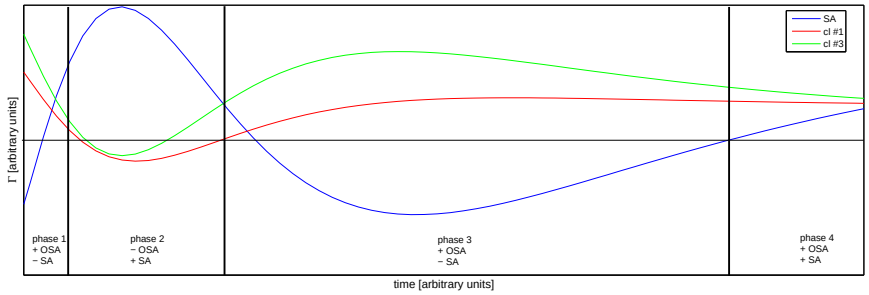

Figure 5.3: Γ changes due to Chile '60 and Alaska '64 earthquakes in arbitrary units.

mal component), and Γ^S (shear component) versus time with an asthenospheric viscosity η of $5 \cdot 10^{18}$ Pa s, which is a mean value given by previous works [e.g., *Piersanti et al.*, 1995; 1997]. This value sets the transition between phases 1 and 2 in the late nineties, when the last NSA event occurred. In Figure 5.4 we can see that both SA and NSA faults are locked by the stress perturbation induced by Chile (1960) and Alaska (1964) earthquakes; in practice, the earthquakes in Southern California were discouraged on average, at least until the end of phase 1, that is what observed in the past decades (i.e., a decrease of the overall seismic rate). In the same period (phase 1), NSA faults undergo greater shear variations than SA; this may explain the increase of NSA events observed after the sixties. Remarkably, the model (assuming a viscosity of $5 \cdot 10^{18}$ Pa s) foresees, in absence of other significant perturbations, the earthquakes of the next few decades should be mostly of SA type (phase 2), like before the sixties.

5.4 Discussion and Remarks

The main finding of the present chapter is the statistically significant variation of Southern California seismicity occurred

a)

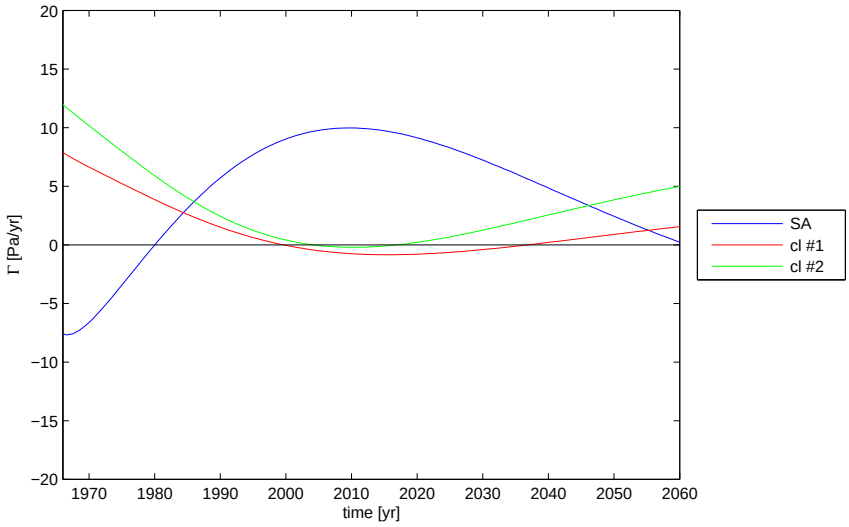

b)

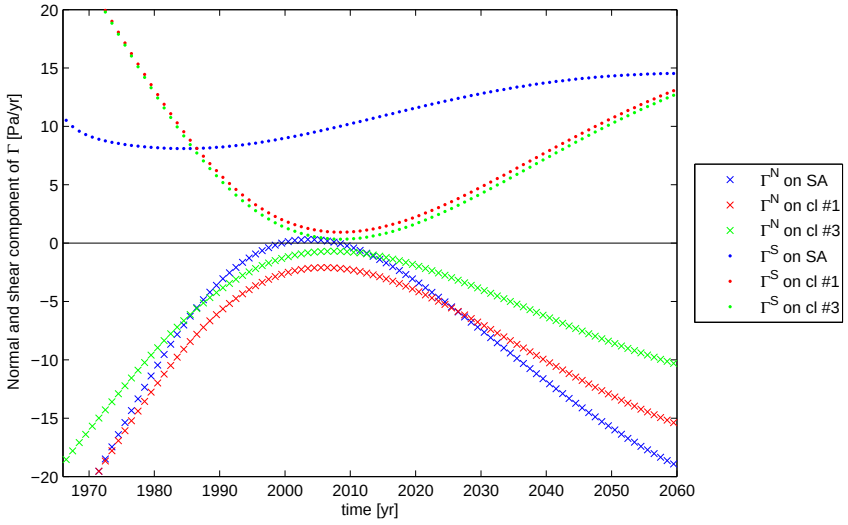

Figure 5.4: Changes of a) Γ, and b) normal and shear components of Γ, due to Chile '60 and Alaska '64 earthquakes, with an asthenospheric viscosity $\eta = 5 \cdot 10^{18} Pa\ s$.

in the sixties. This change consists of a decrease of the overall seismic rate together with the occurrence of earthquakes not related to San Andreas fault, that are not observed in the previous period. We suggest that a possible physical explanation of such a change is the remote effect of the giant Chile (1960) and Alaska (1964) earthquakes. The stress field perturbation due to these two remote events is consistent with the trend in the Southern California seismicity observed since then. The model is predictive and, therefore it implicitly provides a tool to validate it through forward analysis.

In spite of the agreement in the overall trend, other aspects deserve more investigation. The most important is related to the amplitude of the postseismic stress perturbations; neglecting all the possible biases introduced by our calculations, the stress rate induced by Chile (1960) and Alaska (1964) earthquakes Γ is three orders of magnitude less than the tectonic rate in Southern California (about 10 and 10^4 Pa/yr, respectively); for the discussion of this point see section 4.3 *Results and preliminary discussion* in *Chapter 4*.

Finally, we emphasize that the model can be applied predictively to forecast foretells the future trend of Southern California seismicity. In particular, assuming $\eta = 5 \cdot 10^{18}$ Pa s, the earthquakes of the next decades should be predominantly of "San Andreas type", and the rate should increase at a value comparable to the one observed before the sixties. This forward prediction gives an important opportunity to validate the causal hypothesis of remote (and long-term) coupling between earthquakes.

References

Aki, K., and P.G. Richards, *Quantitative Seismology: Theory and Methods*, Freemann & Co, San Francisco, 1980.

Anderberg, M.R., *Cluster Analysis for Applications*, Academic Press, New York, 1973.

Casarotti E., A. Piersanti, F.P. Lucente, and E. Boschi, Global postseismic stress diffusion and fault interaction at long distances, *Earth and Planet. Sci. Lett. 191*, 75-84, 2001.

Chéry J., S. Carretier, and J. Ritz, Postseimsic stress transfer explains time clustering of large earthquakes in Mongolia, *Earth Planet. Sci. Lett. 194*, 277-286, 2001.

Cornell, A., Engineering seismic risk analysis, *Bull. Seism. Soc. Am. 58*, 1583-1606, 1968.

Davis, C. D., *Statistics and Data Analysis in Geology*, John Wiley & Sons, New York, 2002.

Dieterich, J., A constitutive law for the rate of earthquake production and its application to earthquakes clustering, *J. Geophys. Res., 99*, B2, 2601-2618, 1994.

Field, E. H., D. D. Jackson, and J. F. Dolan, A mutually consistent seismic-hazard source model for southern California, *Bull. Seism. Soc. Am. 89*, 559-578, 1999.

Freed, A. M., and J. Lin, Delayed triggering of the 1999 Hector Mine earthquake by viscoelastic stress transfer, *Nature 411*, 180-183, 2001.

Gibbons, J.D., *Non–parametric Statistical Inference*, McGraw–Hill, New York, 306 pp, 1971.

Hanks, T.C., and D.P. Schwartz, Morphologic dating of the pre-1983 fault scarp on the Lost River fault at Doublespring Pass Road, Custer County, Idaho, *Bull. Seismol. Soc. Am. 77*, 837-846, 1987.

Hartigan, J.A., *Clustering Algorithms*, John Wiley & Sons, New York, 1975.

Jones, LM, Focal Mechanisms and the State of Stress on the San Andreas Fault in Southern California, *J. Geophys. Res., 93*, 8869-8891, 1988.

Jones, L. M., and E. Hauksson, The seismic cycle in southern California: Precursor or response?, *Geophys. Res. Lett. 24*, 469-472, 1997.

Kagan, Y.Y., and Jackson, D.D., Probabilistic forecasting of earthquakes, *Geophys. J. Int., 143*, 438-453, 2000.

Kenner S.J., and P. Segall, Postseismic deformation following the 1906 San Francisco earthquake, *J. Geophys. Res. 105*, 13195-13209, 2000.

King, G. C. P., R. S. Stein, and J. Lin, Static stress changes and the triggering of earthquakes, *Bull. Seismol. Soc. Am., 84*, 935-953, 1994.

King, G. C. P., and M. Cocco, Fault interaction by elastic stress changes: New clues from earthquake sequences, *Adv. Geophys. 44*, 1-38, 2000.

Marzocchi W., Remote seismic influence on large explosive eruptions. *J. Geophys. Res. 107(B1)*, doi:10.1029/2001JB000307, 2002.

Marzocchi W., E. Casarotti, A. Piersanti, Modeling the stress variations induced by great earthquakes on the largest volcanic eruptions of the 20th century. *J. Geophys. Res. 107(B11)*, 2320, doi:10.1029/2001JB001391, 2002.

Marzocchi, W., J. Selva, A. Piersanti, and E. Boschi, On the long-term interaction among earthquakes: Some insight from a model simulation, *J. Geophys. Res. 108*, B11, 2538, doi:10.1029/2003JB002390, 2003.

Marzocchi W., L. Zaccarelli, E. Boschi, Phenomenological evidence in favor of a remote seismic coupling for large vol-

canic eruptions. *Geophys. Res. Lett. 31*, L04601, doi:10.1029/2003GL018709, 2004.

Mulargia, F., and S. Tinti, Seismic sample areas defined from incomplete catalogs: an application to the italian territory, *Phys. Earth. Planet. Int. 40*, 273-300, 1985.

Mulargia, F., P. Gasperini, and S. Tinti, Identifying different regimes in eruptive activity: an application to Etna volcano, *J. Volanol. Geotherm. Res. 34*, 89-106, 1987.

Pantosti D., D.P. Schwartz, and G. Valensise, Paleoseismology along the 1980 surface rupture of the Irpinia fault; implications for earthquake recurrence in Southern Apennines, Italy, *J. Geophys. Res. 98*, 6561-6577, 1993.

Piersanti, A., G. Spada, R. Sabadini, and M. Bonafede, Global postseismic deformation, *Geophys. J. Int. 120*, 544-566, 1995.

Piersanti, A., G. Spada, and R. Sabadini, Global postseismic rebound of a viscoelastic Earth: Theory for finite faults and application to the 1964 Alaska earthquake, *J. Geophys. Res. 102*, 477-492, 1997.

Pollitz, F. F., and I. S. Sacks, The 1995 Kobe, Japan, earthquake: A long-delayed aftershock of the offshore 1944 Tonankai and 1946 Nankaido earthquakes, *Bull. Seismol. Soc. Am. 87*, 1-10, 1997.

Pollitz, F. F., R. Bürgmann, and B. Romanowicz, Viscosity of oceanic asthenosphere inferred from remote triggering of earthquakes, *Science 280*, 1245-1249, 1998.

Press F. and Allen, C.R., Patterns of seismic release in the southern California region, *J. Geophys. Res. 100*, 1995.

Romanowicz, B., Spatiotemporal patterns in the energy release of great earthquakes, *Science 260*, 1923-1926, 1993.

Stein, R. S., G. C. P. King, and J. Lin, Stress triggering of the 1994 M = 6.7 Northridge, California, earthquake by

its predecessors, *Science, 265*, 1432-1435, 1994.

Chapter 6

Testing the earthquake-eruption interaction

In this chapter, we propose a formal procedure to validate the hypothesis of a causal relationship between great tectonic earthquakes and volcanic eruptions through a forward statistical test. This approach allows such a hypothesis to be evaluated in an objective way, ruling out any possible unconscious overfitting of the past data. The procedure consists of two steps: a) the computation of the stress perturbation in a volcanic area due to some selected seismic event, by means of a spherical, layered, viscoelastic and self-gravitating earth model; and b) the application of a statistical test to check the differences in the spatio- temporal distribution of eruptions before and after the earthquake, weighting each eruption with the stress perturbation induced at the volcano at the time of the eruption. Finally, for the sake of example, we apply the method to the case of the recent Engano earthquake in Sumatra (Jun. 2000) and the Denali earthquake in Alaska (Nov. 2002).

6.1 Introduction

It has been proposed that one of the most relevant parameters to promote volcanic unrest and/or eruptions may be the interaction with great tectonic earthquakes [*Yokoyama*, 1971; *Nakamura*, 1975; *Marzocchi et al.*, 1993; *Hill et al.*, 1993; *Linde and Sacks*, 1998; *Nostro et al.*, 1998; *Hill et al.*, 2002; *Marzocchi*, 2002; *Marzocchi et al.*, 2002; *Marzocchi et al.*, 2004]. In particular, the stress perturbation due to earthquakes seems to have triggered unrest in volcanic systems, at different spatio-temporal scales.

Some papers have tested the coupling between earthquake and eruptions by using different retrospective correlation analysis [*Marzocchi et al.*, 1993; *Linde and Sacks*, 1998; *Marzocchi*, 2002; *Marzocchi et al.*, 2004]. Here, we investigate this issue by following a different philosophy. In particular, we provide quantitative rules for a forward test. We remark that this approach is the most objective way to verify the hypothesis of a causal relationship between large tectonic earthquakes and following volcanic eruptions, because it rules out any unconscious overfitting of the data (the so-called retrospective realism).

The procedure consists of two steps: a) the computation of the stress perturbation in a volcanic area due to some selected seismic event, by means of a spherical, layered, viscoelastic and self-gravitating earth model; and b) the application of a statistical test (the validation test, VT), that consists of comparing the spatio- temporal distribution of eruptions in the volcanic area, before and after the earthquake, weighting each volcanic event with the stress perturbation induced at the volcano at the time of the eruption.

For the sake of example, we apply the method to two recent

great tectonic earthquakes, which occurred close to volcanic systems: the Engano earthquake (Sumatra, Jun. 2000) and the Denali earthquake (Alaska, Nov. 2002).

6.2 Stress field computation

The stress field computation can be described in three sequential steps: i) definition of the Earth model; ii) definition of the source process of the earthquake; iii) quantification of the stress perturbation.

6.2.1 Earth Model

Here we use the layered, spherical, viscoelastic and self-gravitating Earth model proposed by *Piersanti et al.* (1995). This model has been previously used to test (retrospectively) the long-term interactions among earthquakes (e.g., [*Casarotti et al.*, 2001; *Melini et al.*, 2002]), and between earthquakes and volcanoes [*Marzocchi et al.*, 2002].

The density and the shear modulus of each layer are obtained by volume-averaging the PREM reference model corresponding values [*Dziewonsky and Anderson*, 1981]. The value of the Maxwell viscosity of the two intermediate layers have been fixed to 10^{18} and 10^{21} Pa s [*Pollitz et al.*, 1998; *Casarotti et al.*, 2001]. They control the time delay of the post-seismic stress far from the event source. These values lead to an increase of the stress with a characteristic time of tens of years, that is a time behavior is compatible with previous independent studies [*Piersanti et al.*, 1995; *Piersanti et al.*, 1997; *Pollitz et al.*, 1998; *Kenner and Segall*, 2000].

6.2.2 Source process

The stress field induced by an earthquake obviously depends on its source process. In our physical model, each source is modeled as a one-dimensional dislocation, characterized by a finite length L. The total stress field due to this finite source (with seismic moment M_0) is given by the linear superposition of stress field due to n identical, equally spaced elementary dislocations with seismic moment $\frac{M_0}{n}$ [*Piersanti et al.*, 1997]. The parameters of each seismic source are taken from CMT solutions [*Dziewonsky and Anderson*, 1981; *Dziewonski and Woodhouse*, 1983; *CMT Catalog*]. Other source models, available in scientific literature, are used to check qualitatively the sensitivity of the results from source model uncertainties.

6.2.3 Quantifying the stress perturbation

Usually volcanic areas are strongly heterogeneous and multifractured. In general, magmatic intrusions can have a large variety of possible shapes and orientations. This situation very often prevents the choice of a single or a few planes on which to project the stress tensor (e.g., the Coulomb stress). Furthermore, it is conceivable that different physical mechanisms can promote volcanic unrest, such as compression or dilatation in the magma chamber, or shear stress along the conduit which opens the way toward the surface.

For these reasons we choose to analyze the general behavior of the stress in each volcanic area through the first and the second invariant of the stress tensor [*Marzocchi et al.*, 2002]. The first invariant I_1 is defined as

$$I_1 = \sigma_{ii} \tag{6.1}$$

I_1 can be positive or negative and it indicates positive or negative pressure variation, i.e., volume variations in the rock. I_1 has the dimension of the stress ($[Pa]$).

The second invariant of the deviatoric stress tensor is defined as (e.g., [*Fung*, 1965])

$$J_2 = \frac{I_1^2}{3} - \frac{\sigma_{ii}\sigma_{kk} - \sigma_{ij}\sigma_{ij}}{2} \tag{6.2}$$

J_2 means variation on shear stress and its dimension is $[Pa^2]$. Therefore, in order to have homogeneous variables, we use $\sqrt{J_2}$.

The physical meaning of I_1 and J_2 can be easily explained through the deformation energy (cf. [*Sokolnikoff*, 1956])

$$W = \frac{1}{2}\lambda\epsilon_{ii}\epsilon_{jj} + \mu\epsilon_{ij}\epsilon_{ij} \tag{6.3}$$

where λ and μ are the Lamé constants and $\{\epsilon_{mn}\}_{m,n=1,2,3}$ is the strain tensor. With a little algebra, W can be written

$$W = \frac{I_1^2}{18K} + \frac{J_2}{2\mu} \tag{6.4}$$

where K and μ are respectively the bulk and shear modulus.

I_1 and J_2 fields can be estimated at different depths and times after each earthquake. Since they generally do not vary strongly with depth, in particular far from the earthquake source, we calculate the stress perturbation at an intermediate depth, i.e., at 10 Km.

6.3 The validation test (VT)

Our primary goal is to test the reliability of a causal relationship between strong earthquakes and following volcanic eruptions. We accomplish this task through the validation test VT.

VT is based on an earthquake-eruption correlation parameter Θ, associated with each eruption, defined as

$$\Theta(\vec{x}, \Delta t) = |I_1(\vec{x}, \Delta t)| + \sqrt{J_2(\vec{x}, \Delta t)} \tag{6.5}$$

where $\vec{x}$ is the coordinates vector which define the position of the volcano and Δt is the time lag between earthquake and eruption. In other words, in equation 6.5 we weight each eruption with the stress perturbation observed under the volcano at the time of the eruption.

The same procedure can be applied backward in time by considering the absolute value of Δt. In this way, we can compute the correlation parameter also for the eruptions before the earthquake.

In order to limit the analysis at a reasonable spatial scale, we define a perturbed area (PA) characterized by a correlation parameter threshold, i.e.,

$$\Theta_{t=\infty}(\vec{x}) \geq 0.1 \quad \text{bar} \tag{6.6}$$

where $\Theta_{t=\infty}(\vec{x})$ is the correlation parameter calculated for $\vec{x}$, and $t \to \infty$. In practice, PA contains the volcanoes which experience the largest stress perturbation.

Then, we define two different sets of correlation parameters

$$\Theta^b_1, \Theta^b_2, ..., \Theta^b_{N_b} \tag{6.7}$$

for the eruptions that occurred in PA in the 30 years before the earthquake (N_b is the number of these eruptions), and

$$\Theta^a_1, \Theta^a_2, ..., \Theta^a_{N_a} \tag{6.8}$$

for the eruptions that will occur in PA in the 30 years after the earthquake (N_a is the number of these eruptions). We use a 30 years time windows because it seems a reasonable characteristic time scale for the post-seismic stress evolution

[see *Marzocchi*, 2002; *Kenner and Segall*, 2000]. With this choice we implicitly assume that most of seismic effects on a volcanic area occur in this time window.

The comparison between these two sets shows whether or not earthquakes significantly interact with the volcanic systems. In fact, if the eruptions following the earthquake tend to occur in volcanoes that are more perturbed by the co- and post-seismic stress field, the values of Θ^a will be larger (on average) than the values of Θ^b. In this case, the central value Θ^a will be statistically different from the central value of Θ^b, indicating that a causal coupling between the space and time distribution of eruptions and the seismic stress field exists. We test such an hypothesis by using a nonparameteric test, that is insensitive to strong nongaussian distributions of the data, and to the presence of few data with very high values. In particular, we test the hypothesis of equal medians by applying the non-parametric statistical test Mann-Whitney [*Gibbons*, 1971], by using a significance level of 0.01.

The capability of VT to test efficiently the interaction hypothesis depends on the validity of some implicit assumptions of the procedure: first, the central value of Θ^a tend to be larger then the central value of Θ^b if the 30 years time window before the earthquake does not follow another previous large earthquake in the same region. In this case in fact both Θ^a and Θ^b could reflect the post-seismic effects of similar earthquakes. Second, from a physical point of view, the use of all volcanoes in the PA region, regardless their past activity and present status, implicitly means that we are assuming a random spatial distribution of the volcanoes that are more "sensitive" to seismic perturbations. The possibility to estimate the present status of a volcano, for instance by means of a probability of eruption occurrence $p(\tau)$ (τ is

the time window considered), may lead to a more powerful test for the seismic-volcanic interaction. In this case, in fact, we may carry out the test by selecting the volcanoes that are potentially more influenced by stress perturbations. Presently, however, there is not a commonly accepted model to define the status of each volcano (i.e., $p(\tau)$), and opposite models are often used (e.g., [*Bebbington and Lai*, 1996; *Gusev et al.*, 2003]). For this reason, we decide to consider all volcanoes together. Third, another implicit assumption of VT is that the energy of the triggered eruptions (i.e., the VEI) is independent from the magnitude of the stress perturbation.

6.4 The case of Engano and Denali earthquakes

In order to illustrate the practical application of the procedure, we report the cases relative to two recent large earthquakes occurred in the proximity of important volcanic areas: the Engano (Indonesia) and Denali (Alaska, USA) earthquakes. These two cases are reported for the sake of example. Actually the feasibility of a causal relationship between large earthquakes and eruptions can be jugged (in a satisfactory way) only by considering a larger number of case studies.

We compute the stress field of the Denali earthquake with the CMT source estimation (e.g., [*Dziewonsky and Anderson*, 1981; *Dziewonski and Woodhouse*, 1983; *CMT Catalog*]). In order to evaluate the potential instabilities of the results due to the use of the CMT estimation, we also model the stress field by using a different source model for the earthquake. The Denali earthquake source process is actually well constrained. It is composed by 3 sub-events [*Eberhart-Phillips et al.*, 2003]. The third, along the Totshunda fault, has a significantly smaller moment release, therefore it may be ne-

glected for our purposes. Therefore, we model the stress field by considering the thrust sub- event along the Susitna Glacier fault and the main sub-event along the Denali fault. The focal mechanisms of these events are reported in Table 6.1 [*Kikuchi and Yamanaka*, 2002; *Eberhart-Phillips et al.*, 2003].

Table 6.1: Denali earthquake's source process

Event	Strike	Dip	Rake	Depth (Km)	Moment Release (10^{20} N m)
Model A	296	71	171	15	7.48
sub-event 1 Model B	227	40	99	15	0.46
sub-event 2 Model B	294	86	161	15	7.8

Model A: CMT catalog [*CMT Catalog*]
Model B: *Kikuchi and Yamanaka* [2002]

The comparison between these two source models shows a good agreement. In particular, the spatial distributions of I_1 at a depth of 10 Km, and just after the Denali event, are reported in Figure 6.1 for both source models. Note that the shapes of the perturbations are almost equal. The reason lies on the similarity between the CMT model with the main subevent (the 2nd) of the *Kikuchi and Yamanaka* [2002] source estimation (see Table 6.1). In figures 6.2 and 6.3, we show the stress field I_1 and J_2 for the Denali earthquake calculated at different times and at a 10 km depth for the CMT source.

The source process of most earthquakes is usually less known than the Denali one, in particular for deep and off-shore events. The Engano earthquake, for instance, occurred under the ocean at a depth of 40-50 Km. Therefore its source process is not well known. The epicentral area has a complicated tectonic setting where a great thrust fault, the Sumatran Subduction Zone, is really close to the right-

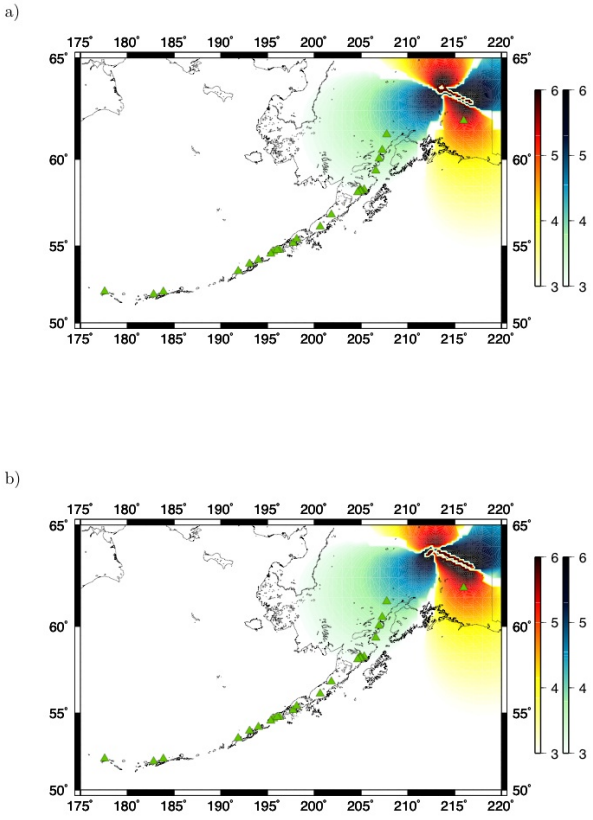

Figure 6.1: I_1 for the Denali earthquake just after the earthquake (t = 1 hr) at the depth of 10 Km; a) with the CMT source model, b) with the *Kikuchi and Yamanaka* (2002) source model. The scales report the Log(I_1), where I_1 is measured in [Pa]. Hot colors mean positive values, while cold colors mean negative values.

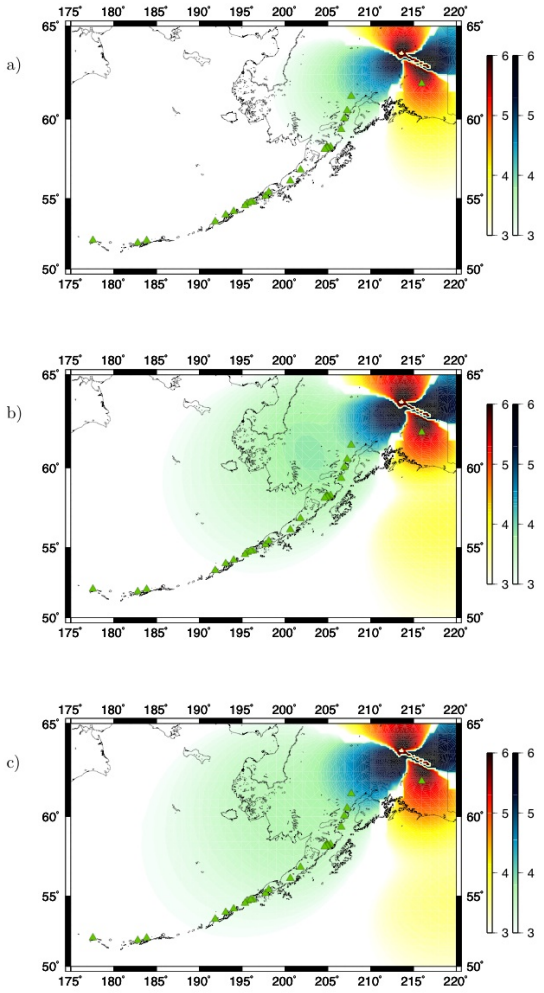

Figure 6.2: I_1 (depth of 10 Km) for the Denali earthquake at different times: a) just after the earthquake (t = 1 hr), b) 10 yr after, and c) 50 yr after. The scales report the Log(I_1), where I_1 is measured in [Pa]. Hot colors mean positive values, while cold colors mean negative values.

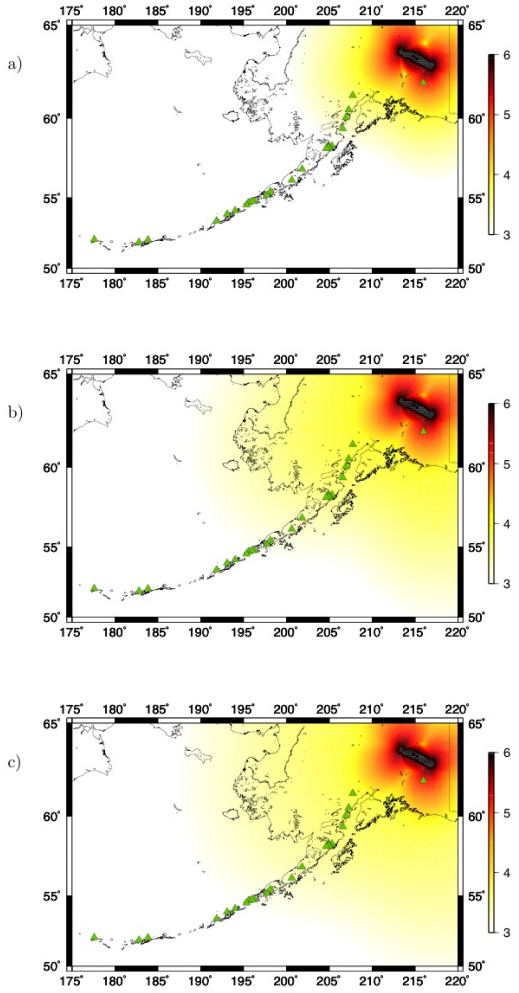

Figure 6.3: As for figure 6.2 but relative to J_2. The scale reports the Log($\sqrt{J_2}$), where $\sqrt{J_2}$ is measured in [Pa].

lateral Great Sumatran Fault. The aftershocks of the Engano earthquake occurred along both fault systems [e.g., *Zhou et al.*, 2002].

Also in this case, we use the CMT solution, and we compare the results with other source mechanisms taken from scientific literature [*Zhou et al.*, 2002; *Abercrombie et al.*, 2003; *CMT Catalog*], in order to check visually the stability of the stress field computation. The focal parameters are reported in Table 6.2. In figure 6.4 we show the comparison between the stress fields obtained by the different source models; in this case, even though the parameters of the three estimations are different (see Table 6.2), the shapes of the perturbations and their polarity are similar to each other. All of them are characterized by a decompressional axis along the volcanic chain and a compressional axis perpendicular to that. Only the *Zhou et al.* model [2002] leads to a different sign of the perturbations on the volcanoes south east of the earthquake source. Anyway, since we consider the absolute value of the perturbations (see equation 6.5), this difference can be considered negligible. The distances involved in each perturbation, and then the volcanoes involved, are quite similar in the different models. Therefore, the differences between the three source models can be considered relatively small and probably within the modeling errors. In figures 6.5 and 6.6 we show the stress field I_1 and J_2 for the Engano earthquake calculated at different times and at a 10 km depth for the CTM source.

Table 6.2: Engano earthquake's source process

Event	Strike	Dip	Rake	Depth (Km)	Moment Release (10^{20} N m)
Model A	199	67	38	43.9	7.46
sub-event 1 Model B	194	82	-1	57	8.04
sub-event 2 Model B	330	37	72	41	4.26
Model C	199	82	5	40	15.0

Model A: CMT catalog [*CMT Catalog*]
Model B: *Abercrombie et al.*, 2003
Model C: *Zhou et al.*, 2002

In Table 6.3 we report the list of the volcanoes in the PAs of the Denali and the Engano earthquakes; the underlined volcanoes are the ones which already erupted after each earthquake. The location and time of eruptions are taken from [*Miller et al.*, 1998; *Simkin and Siebert*, 2003; *V.O.T.W. catalog*]. In figure 6.7 we report the cumulative of Θ^b for both earthquakes, that represent the spatio-temporal distribution of the eruptions occurred inside PA in a time window of 30 years before the earthquake. In particular, 4 eruptions occurred inside the Denali's PA in the 30 years preceding the Denali earthquake; for Engano's PA, 31 eruptions occurred in the 30 years before the earthquake. The median of the distribution is the Θ value (on the x axis) corresponding to the cumulative value (on the y axis) of 0.5.

Table 6.3: List of the volcanoes in the PAs. The underlined volcanoes have already erupted after the Engano earthquake.

Event	Volcanoes
Denali earthquake	Spurr, Redoubt, Augustine, Wrangell
Engano earthquake	Marapi, Kerinci, Dempo, Tandikat, Talang, Sumbing, Kaba, Besar, Suoh, Krakatau, Talakmau, Sorik-Gajah, Hutapanjang, Kunyit, Pendan, Beyrang-Beriti, Daun-Bukit, Patah, Lumut Balai, Ranau, Sekincau Belirang, Hulubelu, Rajabasa, Danau Complex, Karang

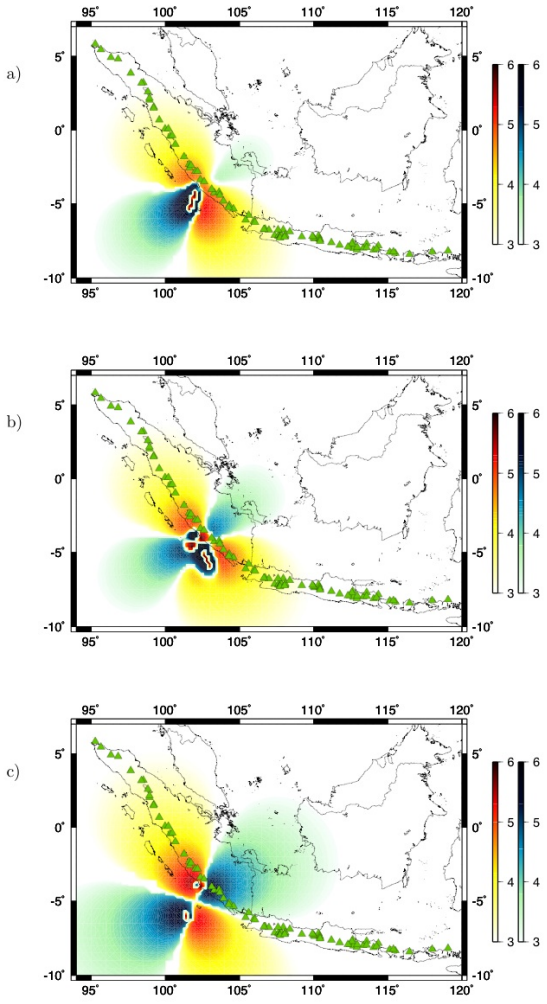

Figure 6.4: I_1 for the Engano earthquake just after the earthquake (t = 1 hr) at the depth of 10 Km; a) with the CMT source model, b) with the *Abercrombie et al* (2003) model, and c) with the *Zhou et al* (2002) model. The scales report the $\mathrm{Log}(I_1)$, where I_1 is measured in [Pa]. Hot colors mean positive values, while cold colors mean negative values.

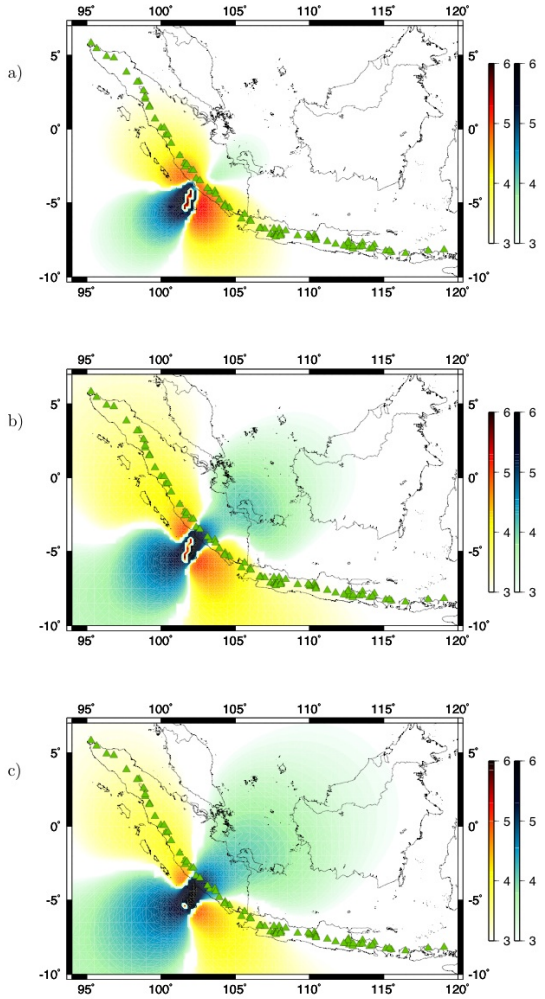

Figure 6.5: I_1 (depth of 10 Km) for the Engano earthquake at different times: a) just after the earthquake (t = 1 hr), b) 10 yr after, and c) 50 yr after. The scales report the Log(I_1), where I_1 is measured in [Pa]. Hot colors mean positive values, while cold colors mean negative values.

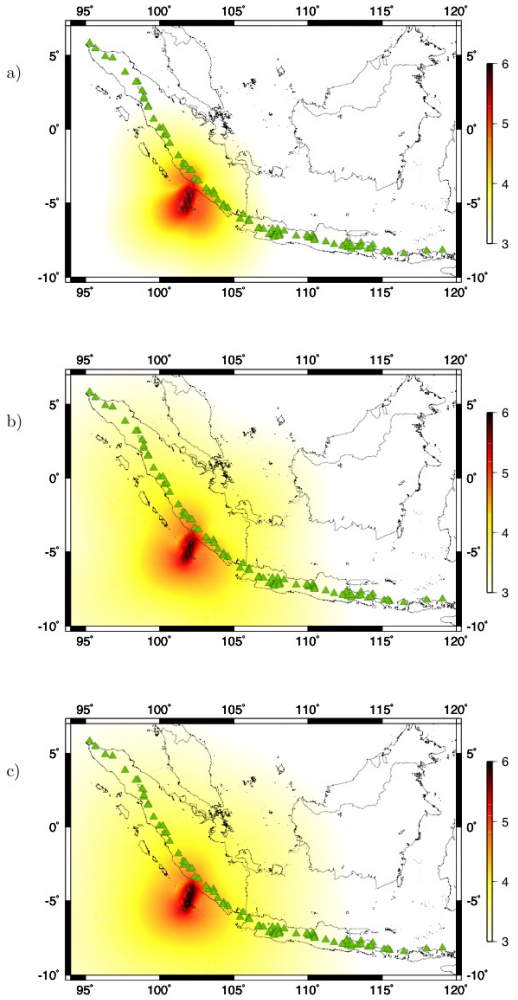

Figure 6.6: As for figure 6.5 but relative to J_2. The scale reports the Log($\sqrt{J_2}$), where $\sqrt{J_2}$ is measured in [Pa].

For the sake of example, we report in the same figure also a preliminary plot of the cumulative of Θ^a for the Engano earthquake. After the Denali earthquake none of the volcanoes in its PA has erupted yet; in the 3 years following the Engano earthquake, 5 eruptions occurred in PA. Obviously, taking into account the philosophy of the study (i.e., to provide a forward test), the null hypothesis of equal medians can be tested only in the future.

6.5 Final remarks

The main goal of this chapter has been to set up a formal quantitative procedure to verify the causal relationship between large earthquakes and following volcanic eruptions through a forward statistical test. We remark that this is the most objective procedure to verify such a kind of hypothesis, because it rules out any possible unconscious retrospective readjustment of the parameters of the model. The test consists of comparing the spatio-temporal distribution of eruptive events after and before the occurrence of a large earthquake, where each eruption is weighted with the stress perturbation induced by the earthquake at the volcano at the time of eruption. The stress perturbations are estimated through a spherical, layered, viscoelastic and auto-gravitating Earth model.

Finally, for the sake of example, we have shown the application of the forward test to two recent earthquakes occurred in Sumatra (Engano earthquake, June 2000), and Alaska (Denali earthquake, November 2002).

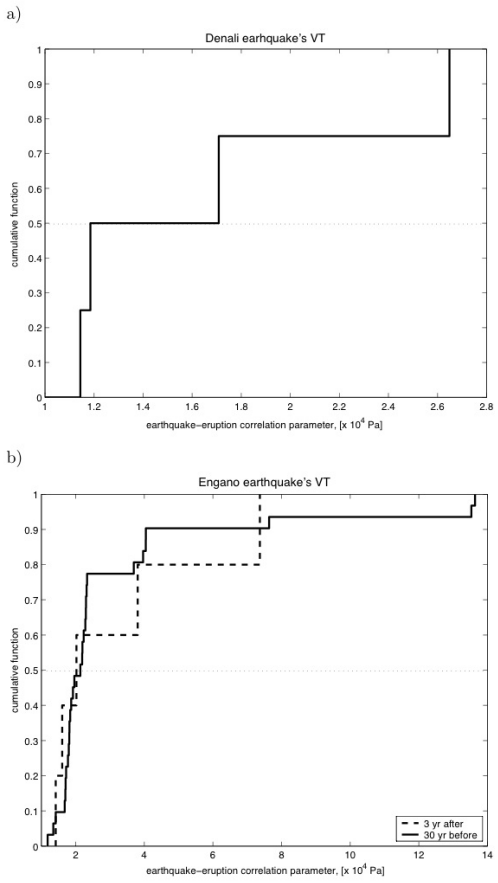

Figure 6.7: Cumulative distributions of the earthquake-eruption correlation parameters: a) Θ^b for the Denali earthquake (solid line), and b) Θ^b (solid line) and $\Theta^a_{\Delta t \leq 3yr}$ (dashed line) for the Engano earthquake.

References

Abercrombie, R.E., M. Antolik, and G. Ekstrom. The June 2000 M_w7.9 earthquakes south Sumatra: Deformation in India-Australia Plate. *J. Geophys. Res.*, 108, NO. B1, 2018, doi:10.1029/2001JB000474, 2003.

Bebbington, M.S., and C.D. Lai. Statistical analysis of New Zealand volcanic occurrence data. *J. Volcanol. Geotherm. Res.*, 74, 101-110, 1996.

Casarotti, E., A. Piersanti, F.P. Lucente, and E. Boschi. Global postseismic stress diffusion and fault interaction at long distances. *Earth Planet. Sci. Lett.*, 191, 75-84, 2001.

CMT Catalog, available at http://www.seismology.harvard.edu/projects/CMT/ . Denali earthquake: event 110302J. Engano earthquake: event 060400D.

Dziewonsky, A.M., and D.L. Anderson. Preliminary reference Earth model (PREM). *Phys. Earth Planet. Inter.*, 25, 297-356, 1981.

Dziewonski, A.M., and J.H. Woodhouse. An experiment in systematic study of global seismicity: Centroid-moment tensor solutions for 201 moderate and large earthquakes of 1981. *J. Geophys. Res. 88*, 3247-3271, 1983.

Eberhart-Phillips, D., et al. The 2002 Denali Fault Earthquake, Alaska: A Large Magnitude, Slip-Partitioned Event. *Science*, 300, 1113- 1118, 2003.

Fung, Y.C. Foundations of Solid Mechanics. *Prentice-Hall*, Old Tappan, N.J., 1965.

Gibbons, J.D., Nonparametric Statistical Inference. *McGraw-Hill*, 1971.

Gusev, A.A., V.V. Ponomareva, O.A. Braitseva, I.V. Melekestsev. Great explosive eruptions on Kamchatka during the last 10,000 years: self similar irregularity of the output of volcanic

products. *J. Geophys. Res.*, 108, B2, 2126, doi:10.1029/2001JB000312, 2003.

Hill, D.P., P.A. Reasenberg, A. Michael, W.J. Arabaz, G. Beroza, D. Brumbaugh, J.N. Brune, R. Castro, S. Davis, D. dePolo, W.L. Ellsworth, J. Gomberg, S. Harmsen, L. House, S.M. Jackson, M.J.S. Johnston, L. Jones, R. Keller, S. Malone, L. Munguia, S. Nava, J.C. Pechmann, A. Sanford, R.W. Simpson, R.B. Smith, M. Stark, M. Stickney, A. Vidal, S. Walter, V. Wong, and J. Zollweg. Seismicity remotely triggered by the magnitude 7.3 Landers, California, earthquake. *Science* 260, 1617-1623, 1993.

Hill, D.P., F. Pollitz, and C. Newhall, Earthquake-volcano interactions. *Physics Today*, 55 (11), 41-47, 2002.

Kenner, S.J., and P. Segall, Postseismic deformation following the 1906 San Francisco earthquake. *J. Geophys. Res.*, 105, 13,195-13,209, 2000.

Kikuchi M. and Y. Yamanaka, Source rupture processes of the central Alaska earthquake of the Mov. 3, 2002, inferred from teleseismic body waves (+ the 10/23 M6.7 event). *EIC Seismological Note No. 129, revised 5 November 2002.* Available from the Earthquake Information Center, University of Tokyo, at
http//www.eic.eri.u-tokyo.ac.jp/EIC/EIC_News/021103AL-e.html.

King G.C.P., R.S. Stein, and J. Lin, Static stress changes and the triggering of earthquakes. *Bull. Seismol. Soc. Am.*, 84, 935-953, 1994.

Linde, A.T., and I.S. Sacks, Triggering of volcanic eruptions. *Nature*, 395, 888-890, 1998.

Marzocchi, W., R. Scandone, and F. Mulargia, The tectonic setting of Mount Vesuvius and the correlation between its eruptions and the earthquakes of the southern Apennines. *J. Volcanol. Geotherm. Res.*, 58, 27-41, 1993.

Marzocchi, W., Remote seismic influence on large explosive eruptions. *J. Geophys. Res.*, VOL. 107, NO. B1, 10.1029/2001JB000307, 2002.

Marzocchi, W., E. Casarotti, and A. Piersanti, Modeling the stress variations induced by great earthquakes on largest volcanic eruptions of the 20th century. *J. Geophys. Res.*, 107, B11, 2320, doi:10.1029/2001JB001391, 2002.

Marzocchi W., L. Zaccarelli, and E. Boschi. Phenomenological evidence in favor of a remote seismic coupling for large volcanic eruptions. *Geophys. Res. Lett.*, VOL. 31, L04601, doi:10.1029/2003GL018709, 2004.

Melini, D., E. Casarotti, A. Piersanti and E. Boschi, New insights on long distance fault interaction. *Earth Planet. Sci. Lett.*, 204, 3-4, 363-372, 2002.

Miller, T.P., R.G. McGimsey, D.H. Richter, J.R. Riehle, C.J. Nye, M.E. Yount, andJ.A. Dumoulin, Catalog of the historically active volcanoes of Alaska. USGS Open File Report 98-582, 1998.

Nakamura, K., Volcano structure and possible mechanical correlation between volcanic eruptions and earthquakes. *Bull. Volcanol. Soc. Jpn.*, 20, 229-240, 1975.

Nostro, C., R.S. Stein, M. Cocco, M.E. Belardinelli, and W. Marzocchi, Two-way coupling between Vesuvius eruptions and southern Apennine earthquakes, Italy, by elastic stress transfer, *J. Geophys. Res.*, 103, 24,487-24,424, 1998.

Piersanti, A., G. Spada, R. Sabadini, and M. Bonafede, Global postseismic deformation. *Geophys. J. Int.*, 120, 544-566, 1995.

Piersanti, A., G. Spada, and R. Sabadini, Global postseismic rebound of a viscoelastic Earth: Theory for finite faults and application to the 1964 Alaska earthquake. *J. Geophys. Res.*, 102, 477-492, 1997.

Piersanti, A., Postseismic deformation in Chile: constraints on the asthenospheric viscosity. *Geophys. Res. Lett.*, 26, 3157-3160, 1999.

Pollitz, F.F., R. Burgmann, and B. Romanovwicz, Viscosity of oceanic astenosphere inferred from remote triggering of earthquakes. *Science*, 280, 1245-1249, 1998.

Simkin, T., and L. Siebert. *Volcanoes of the World.* Geoscieces, Tucson, 2003.

Sokolnikoff, I.S., Mathematical Theory of Elasticity. McGraw-Hill, New York, 1956.

Stein, R.S., G.C.P. King, and J. Lin, Change in failure stress on the southern San Andreas fault system caused by the 1992 magnitude = 7.4 Landers earthquake. *Science*, 258, 1328-1332, 1992.

Stein, R.S., G.C.P. King, and J. Lin, Stress triggering of the 1994 M = 6.7 Northridge, California, earthquake by its predecessors. *Science*, 265, 1432-1435, 1994.

Thatcher, W., Nonlinear buildup and earthquake cycle on the San Andreas fault. *J. Geophys. Res.*, 88, 5893-5902, 1983.

V.O.T.W. catalog, Volcanoes of the World catalog, available at http://www.volcano.si.edu/ .

Yokoyama, I., Volcanic eruptions triggered by tectonic earthquakes. *Geophys. Bull. Hokkaido Univ.*, 25, 129-139, 1971.

Zhou Y.H., L.S. Xu, and Y.T. Chen, Source process of the 4 June 2000 Southern Sumatra, Indonesia, Earthquake. *Bull. Seismol. Soc. Am.*, 92, No. 5, 2027-2035, 2002.

Appendix A

Nonparametric Estimation of the PF

Given a set of data points $x_i (i = 1, ..., N)$, we want to estimate the form of the probability function $F(x)$ from which they are drawn (the parent distribution). A first (rough) guess of such function is given by

$$y_i = \frac{i}{N+1} \approx F(x_{(i)}) \tag{A.1}$$

where $x_{(i)}$ represents the vector x_i sorted in increasing order. In equation A.1 the denominator is taken to be $N+1$ instead of N, because $x_{(N)}$ usually does not represent the maximum possible value for the random variable x. For the sake of simplicity, let us assume that the maximum value for the random variable is equal to 1. In practice, this can be easily achieved by dividing the original data x_i by x_{max}, where x_{max} represents an estimate of the largest expected values, i.e., $1 - F(x_{max}) \approx 0$.

The error associated with y_i in equation A.1 can be estimated by recalling that $F(x_i)$ is the probability of drawing a new sample below x_i, and that $NF(x_i)$ is the expected number of such data in a dataset of N points. If we assume Gaussian errors then the variance around the mean is

$NF(x_i)[1 - F(x_i)]$. Hence, the standard deviation of y_i (see equation A.1) is

$$\sigma_i = \frac{1}{N+1}\{NF(x_i)[1-F(x_i)]\}^{1/2} \tag{A.2}$$

$$\approx \frac{1}{N+1}\Big\{N\frac{i}{N+1}\Big[1-\frac{i}{N+1}\Big]\Big\}^{1/2} \tag{A.3}$$

Note that the standard deviation vanishes at the boundaries as it should where we know that $F(0) = 0$ and $F(1) = 1$. A more satisfactory estimation of $F(x)$ can be obtained by means of a convenient parameterization

$$\hat{F}(x) = x + \sum_{m=1}^{M} a_m \sin(m\pi x) \tag{A.4}$$

which enforces the boundary conditions $F(0) = 0$ and $F(1) = 1$ regardless of the values of the coefficients a_m. Here, $\hat{F}(x_i)$ is the empirical estimation of the real probability function $F(x_i)$.

The coefficients a_m can be estimated from the data, by imposing some conditions on the expected behavior of $\hat{F}(x)$. The first one is that the nearby points should behave similarly; this can be achieved by minimizing the integral square curvature of $\hat{F}(x)$

$$I_0 = \int_0^1 \Big(\frac{d^2\hat{F}}{dx^2}\Big)^2 dx \tag{A.5}$$

The second condition is that the expected mismatch given by

$$I_1 = \frac{1}{N}\sum_{j=1}^{N}\Big[\frac{\hat{F}(x_j) - y_j}{\sigma_j}\Big]^2 \tag{A.6}$$

is equal to 1. In fact, we do not want to minimize it because passing exactly through the data is a very unlikely event

given the uncertainty. Therefore we can solve the problem by introducing a Lagrange multiplier in a variational sum

$$I = I_0 + \lambda I_1 \tag{A.7}$$

and solving

$$\frac{\partial I}{\partial a_m} = 0 \tag{A.8}$$

Equation A.8 gives all the coefficients a_m as a function of the parameter λ, that can be estimated by substituting them in equation A.6.

As a final practical thought, we emphasize that the *a priori* choice of the number of coefficients M is not critical for a very large range of possible values. In fact, even when there are as many coefficients as data points, the regularization insures that the resulting cumulative function does not overfit the data.

Appendix B

The Wilcoxon Test

The Wilcoxon test is the nonparametric equivalent of the T-test. It tests the hypothesis of equal central values, i.e., medians, of two populations $X_i, i = 1, .., N_x$ and $Y_i, i = 1, ..., N_y$, under the assumption of equal distribution.

The Wilcoxon test statistic W_N is a function of ranks in the combined ordered sample composed by Xs an Ys. In other words,

$$W_N = \sum_{i=1}^{N} iZ_i \tag{B.1}$$

where $N = N_x + N_y$, and Z_i are called indicator random variables, and are defined as follows: $Z_i = 1$ if in the combined ordered sample the i-th random variable is an X, and $Z_i = 0$ if it is an Y.

The null hypothesis of equal medians of the two samples Xs and Ys can be tested through the W_N statistic. If W_N is too large, the median of Xs population exceeds the one of Ys population; if W_N is too small, the median of Ys population exceeds the one of Xs population; therefore, the hypothesis of equal medians can be rejected if W_N is either too large or too small.

Under the assumption of equal distributions for Xs and

Ys, the exact mean and variance of W_N are [see *Gibbons*, 1971]

$$E(W_N) = \frac{N_x(N+1)}{2} \tag{B.2}$$

$$\mathrm{v}ar(W_N) = \frac{N_x N_y(N+1)}{12} \tag{B.3}$$

Tables of critical values for $N \leq 20$ are given, for instance, in *Wilcoxon* [1947]. For greater N, the normal approximation for W_N can be used because of the asymptotic normality of the general linear rank statistic [see *Gibbons*, 1971]; in other words, the variable

$$z = \frac{W_N - E(W_N)}{[\mathrm{v}ar(W_N)]^{1/2}} \tag{B.4}$$

has a standardized $N(0,1)$ distribution.

References

Gibbons, J.D., *Non–parametric Statistical Inference*, McGraw–Hill, New York, 306 pp, 1971.

Wilcoxon, F., Probability Tables for Individual Comparisons by Rancking Methods, *Biometrics 3*, 119-122, 1947.

Appendix C

CPKS: a change point hunting method through changes in distributions

The search for change points in a time series [*Mulargia and Tinti*, 1985; *Mulargia et al.*, 1987] is performed through an approach based on Kolmogorov-Smirnov two-sample non-parametric statistics defined as

$$J3 = \left(\frac{mn}{d}\right) \max_{-\infty<x<\infty} |G_n(x) - F_m(x)| \qquad N = n + m \quad \text{(C.1)}$$

where m is the number of units in the segment 1 (before the change point), n the number of units in segment 2 (after the change point), d the maximum common divisor of m and n, and $F(x)$ and $G(x)$ are the empirical distribution functions of segment 1 and segment 2. The $J3$ statistic is related to the significance level α at which the samples 1 and 2 have a different distribution function i.e.

$$H_0 : P(X < a) = P(Y < a) \quad , \quad -\infty < a < \infty \qquad \text{(C.2)}$$

The critical values $J3\ (\alpha, m, n)$ for m, $n \geq 30$, rewritten as

$$J'3 = J3 \frac{d}{[(mn)(m+n)]^{\frac{1}{2}}} \qquad \text{(C.3)}$$

$$J'3 = \left(\frac{mn}{m+n}\right)^{\frac{1}{2}} \max_{-\infty<a<\infty} |F_m(a) - G_n(a)| \qquad \text{(C.4)}$$

are well approximated by the distribution

$$P(J'3 < \lambda) = \sum_{j=-\infty}^{\infty} (-1)^j e^{-2j^2\lambda^2} \quad ; \quad \lambda > 0 \qquad \text{(C.5)}$$

which is tabulated in a number of textbooks [see e.g. *Fisz*, 1963]. Also critical values for small n, m can be quite easily found in the literature (see e.g. Hollander and Wolfe, 1973). Subsets down to size 1 can in principle be treated (i.e. change points after the first or before the last element), but common sense suggests excluding sets smaller than 3 elements.

Assuming that a single change point is present in a given set of N (unordered) data, let us scan the data assuming a change point corresponding to datum $i = 3$, then to datum $i = 4, 5, \ldots, N-3$, and obtain the vector $J'3(i), i = 3, 4, \ldots, N-3$. The change point i relative to the maximum $J'3$ component

$$i : \max\{J'3(i)\} \qquad \text{(C.6)}$$

yields therefore the most likely position for the scan-point and the corresponding $J'3$ gives a direct measure of the confidence level $\tilde{\alpha}$ at which H_0 can be rejected, i.e., a measure of how significant is the inference attributing two different distributions to the segments before and after the change point i. Since the change point is found through a multiple application of the test, $\tilde{\alpha}$ cannot be considered as the significance level of the whole change point analysis; this issue is still an open problem in change point hunting methods, because the many statistical tests performed cannot be considered as independent. Nevertheless, the significance level of the change point is constrained to be greater then $\tilde{\alpha}$; thus, given

a threshold for rejecting the null hypothesis of no change points in the data s_{max}, the condition $\tilde{\alpha} \leq s_{max}$ is necessary, but not sufficient, to the acceptance of the change point.

References

Mulargia, F., and S. Tinti, Seismic sample areas defined from incomplete catalogs: an application to the italian territory, *Phys. Earth. Planet. Int. 40*, 273-300, 1985.

Mulargia, F., P. Gasperini, and S. Tinti, Identifying different regimes in eruptive activity: an application to Etna volcano, *J. Volanol. Geotherm. Res. 34*, 89-106, 1987.

Fisz, M., Probability Theory and Mathematical Statistics, *John Wiley & Sons*, New York, London, 1963

Appendix D

CPW: a change point hunting method through changes in medians

CPW searches for change points in a time series using a strategy similar to the one proposed in *Mulargia and Tinti* [1985] and *Mulargia et al.* [1987], where the Wilcoxon test replaces the two-sample Kolmogorov-Smirnov test.

The Wilcoxon test is the nonparametric equivalent of the T-test. It tests the hypothesis of equal central values, i.e., medians, of two populations $X_i, i = 1, .., N_x$ and $Y_i, i = 1, ..., N_y$, under the assumption of equal distribution.

The Wilcoxon test statistic W_N is a function of ranks in the combined ordered sample composed by Xs an Ys. In other words,

$$W_N = \sum_{i=1}^{N} iZ_i \tag{D.1}$$

where $N = N_x + N_y$, and Z_i are called indicator random variables, and are defined as follows: $Z_i = 1$ if in the combined ordered sample the i-th random variable is an X, and $Z_i = 0$ if it is an Y.

The null hypothesis of equal medians of the two samples

Xs and Ys can be tested through the W_N statistic. If W_N is too large, the median of Xs population exceeds the one of Ys population; if W_N is too small, the median of Ys population exceeds the one of Xs population; therefore, the hypothesis of equal medians can be rejected if W_N is either too large or too small.

Under the assumption of equal distributions for Xs and Ys, the exact mean and variance of W_N are [see *Gibbons*, 1971]

$$E(W_N) = \frac{N_x(N+1)}{2} \tag{D.2}$$

$$\mathrm{v}ar(W_N) = \frac{N_x N_y(N+1)}{12} \tag{D.3}$$

Tables of critical values for $N \leq 20$ are given, for instance, in *Wilcoxon* [1947]. For greater N, the normal approximation for W_N can be used because of the asymptotic normality of the general linear rank statistic [see *Gibbons*, 1971]; in other words, the variable

$$z = \frac{W_N - E(W_N)}{[\mathrm{v}ar(W_N)]^{1/2}} \tag{D.4}$$

has a standardized $N(0,1)$ distribution.

Event though critical values for small N_x, N_Y can be found, common sense suggests excluding sets smaller than 3 elements.

Assuming that a single change point is present in a given set of N (unordered) data, let us scan the data assuming a change point corresponding to datum $i = 3$, then to datum $i = 4, 5, \ldots, N-3$, and obtain the vector $W_N(i), i = 3, 4, \ldots, N-3$, and the relative significance level vector $\alpha(i), i = 3, 4, \ldots, N-3$. The change point i relative to the minimum α

$$i : \min\{\alpha(i)\} \tag{D.5}$$

yields therefore the most likely position for the scan-point. The corresponding $\tilde{\alpha} = \alpha(i)$ gives a direct measure of the confidence level at which the null hypothesis of equal medians can be rejected, i.e., a measure of how significant is the inference attributing two different distributions to the segments before and after the change point i. Since the change point is found through a multiple application of the test, $\tilde{\alpha}$ cannot be considered as the significance level of the whole change point analysis; this issue is still an open problem in change point hunting methods, because the many statistical tests performed cannot be considered as independent. Nevertheless, the significance level of the change point is constrained to be greater then $\tilde{\alpha}$; thus, given a threshold for rejecting the null hypothesis of no change points in the data s_{max}, the condition $\tilde{\alpha} \leq s_{max}$ is necessary, but not sufficient, to the acceptance of the change point.

References

Gibbons, J.D., *Non–parametric Statistical Inference*, McGraw–Hill, New York, 306 pp, 1971.

Mulargia, F., and S. Tinti, Seismic sample areas defined from incomplete catalogs: an application to the italian territory, *Phys. Earth. Planet. Int. 40*, 273-300, 1985.

Mulargia, F., P. Gasperini, and S. Tinti, Identifying different regimes in eruptive activity: an application to Etna volcano, *J. Volanol. Geotherm. Res. 34*, 89-106, 1987.

Wilcoxon, F., Probability Tables for Individual Comparisons by Rancking Methods, *Biometrics 3*, 119-122, 1947.